DEVELOPMENT AND CHARACTERIZATION OF GAS ELECTRON MULTIPLIER CHAMBERS FOR A DIGITAL HADRON CALORIMETER IN THE INTERNATIONAL LINEAR COLLIDER

by

JACOB RUSSELL SMITH

Presented to the Faculty of the Graduate School of
The University of Texas at Arlington in Partial Fulfillment
of the Requirements
for the Degree of

MASTER OF SCIENCE IN PHYSICS

THE UNIVERSITY OF TEXAS AT ARLINGTON

May 2009

ACKNOWLEDGEMENTS

I owe much of the progress and success of this thesis to the hard work and contributions of many people. The most influential person that has contributed to my work is my advisor, Dr. Jaehoon Yu. From my introduction to the work as an undergraduate to today he has continued to motivate, encourage and challenged me to pursue and achieve excellence. Additionally, I am especially appreciative of my committee members Dr. Andrew White and Dr. Amir Farbin. Among other faculty at UTA who have contributed to this work are Dr. Kaushik De, Dr. Mark Sosebee, Dr. Barry Spurlock and all my classroom professors. Among the professors who have especially contributed to my understanding of particle physics in the classroom are Dr. Andrew Brandt, Dr. Amir Farbin, Dr. Andrew White and Dr. Jaehoon Yu. The software used to collect data with prototype GEM chambers was originally written by Dr. De and his team. Dr. Sosebee and Dr. Spurlock have generously made themselves available to provide advice and assistance throughout many points of this work.

I would not have been able to survive in graduate school if it were not for support and encouragement from the UTA Physics Department Office Staff including but not limited to Jean Hanlon, Margie Jackymack, Amy Osborn and Fran Smith. To them I am especially thankful. The students who I have had the pleasure and honor to work with on this project are Heather Brown, David Jenkins, Carlos Medina, Dr. Venkat Kaushik, Soomin Kim and Akihiro Nozawa. From Stanford Linear Accelerator Center, I would like to thank Martin Breidenbach, Dietrich Freytag, Ryan Herbst and the rest of their team for developing KPiX electronics for use with GEM detectors. From Korea I would like to thank Dr. Chang-hie Hahn, Dr. Sang-nyeon Kim, Dr. Kwon-pyo Hong, Dr. Won-jeong Kim and Dr. Seongtae Park. They have each uniquely contributed to my success as a graduate student and the progress of GEM detectors.

Among all those involved with this project, Dr. Jia Li’s contributions were unmatched. Every GEM chamber discussed in this thesis was designed and constructed by Dr. Li. Just prior

to his tragic death in 2008 he completed the assembly of the latest GEM chamber integrated with version 7 KPiX readout board (also designed according to his specifications). Every measurement, result, and conclusion made in this thesis is due to Dr. Jia Li's contributions. These few sentences are hardly adequate to describe his effect on me, the GEM team, UTA and the physics community.

My parents, family, friends and local church continue to work behind the scenes in support of my endeavors. Their involvement in my career as a student is priceless.

April 14, 2009

ABSTRACT

DEVELOPMENT AND CHARACTERIZATION OF GAS ELECTRON MULTIPLIER CHAMBERS FOR A DIGITAL HADRON CALORIMETER IN THE INTERNATIONAL LINEAR COLLIDER

Jacob Smith, M.S.

The University of Texas at Arlington, 2009

Supervising Professor: Jaehoon Yu

Gas Electron Multiplier, or GEM, technology provides an attractive option for high precision jet energy measurements for future high energy physics experiments at the International Linear Collider. High voltage settings and gas mixture ratios are determined to optimize double GEM chamber gain and efficiency performance. Electronics readout using QPAO2 chipset and the analog KPiX system developed by Stanford Linear Accelerator Center are used at different stages of the development and characterization of double GEM chambers. The results presented in this thesis are performed primarily at UTA using radioactive sources and cosmic ray particles but also include results from test beam studies using 120 GeV protons at Fermi National Accelerator Laboratory. Plans for the development of GEM technology as a future digital hadron calorimeter and possible medical imaging device are also discussed.

TABLE OF CONTENTS

APPENDIX

LIST OF ILLUSTRATIONS

LIST OF TABLES

Table Page

CHAPTER 1

INTRODUCTION

1.1.Motivation

High Energy Physics, HEP, is the study of physical principles of fundamental particles and fields at the frontier of increasingly available energies. This thesis presents the development and characterization of novel technologies useful for measuring resulting energies of HEP experiments. Specifically, Gas Electron Multiplier [1], or GEM, technology provides an attractive option for novel detection methods in future high energy physics experiments such as the International Linear Collider [2, 3] . This research is done in conjunction with the CALICE [4], Calorimeter for the Linear Collider Experiment, collaboration. Similar to current high energy physics experiments, a lepton-based linear collider also consists of sub-detection systems necessary for a complete account of the collision of high energy particles [5]. GEM detector chambers fall within a subgroup for the digital-based hadron calorimeter section [6] and useful with implementation with Particle Flow Algorithms (PFA) [7, 8] .

A thorough program for the development and characterization for GEM consists of understanding the basic detector technology, developing possible data acquisition systems, testing possible electronics systems and configurations, characterizing basic performance with cosmic rays and approximating realistic collider environments through test beam experiments. Through experiments performed at UTA, Stanford Linear Accelerator Center (SLAC) [9], and Fermi National Accelerator Laboratory (FNAL or Fermilab) [10] this work presents optimized chamber gas mixture and high voltage settings, developed analysis tools, Monte Carlo simulated electronics effects, developed and tested data acquisition electronics, responses to cosmic muons and test beam protons and measure chamber efficiency and gains. Considerable advancement and progress for the development of GEM as a possible digital hadron calorimeter have been achieved as a result of this work. Further characterization remains for GEM technology in order to utilize it within a network of sub-detector systems and for a complete physics program of a future linear collider.

1.2.The Standard Model of Particle Physics

Experiments in HEP measure the properties of potentials, forces, and fields predicted by the Standard Model [11-14]. A short description of the Standard Model is given by Das and Ferbel. "The Standard Model incorporates all the known fundamental particles, namely the quarks, leptons, and the gauge bosons, and it provides a theory describing three of the basic forces of nature – the strong, the weak, and the electromagnetic" [15].

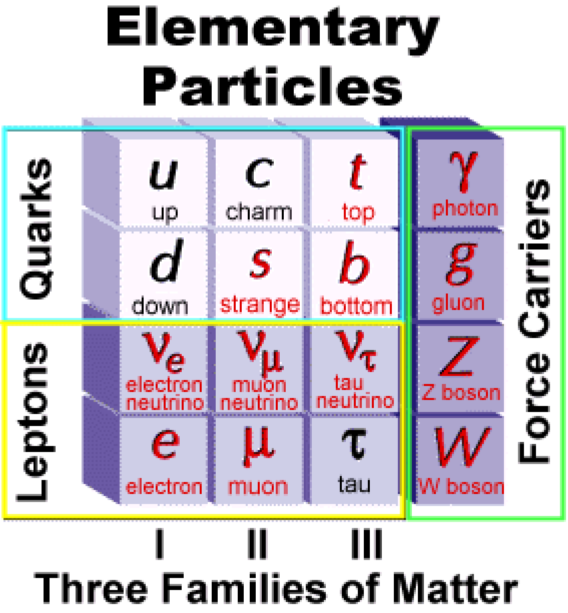

Figure 1.1 Table of fundamental particles predicted by the Standard Model and observed through experiment.

The goals of High Energy Physics are to investigate the existence of fundamental constituents of matter and the interactions between them. An organization of the fundamental particles predicted by the Standard Model is represented in Figure 1.1. Three sets of particles constitute its organization. They consist of quarks, leptons and force carriers. The Standard Model also predicts the existence of a Higgs particle. This particle remains to be discovered and is theorized to provide mass to the other particles.

The quarks and leptons are subdivided into three families or generations [15]. The first generation of lepton contains the electron and its associated neutrino while the two lightest quarks are the up and down. In the second generation are the charm and strange for quarks and the muon and its neutrino for the leptons. The third generation contains the heaviest of the quarks and leptons. The two quarks are the top and bottom and the two leptons are the tau and its associated neutrino. In all cases the masses of the particles increase with increasing generation. Quarks and leptons also have charge. Leptons have unit charge and quarks have a either 1/3 or 2/3 charge. Electrons, muons and taus have negative charge. Up, Charm and Top quarks have positive 2/3 charge and Down, Strange and Bottom have -1/3 charge.

The force carriers for the weak, strong and electromagnetic forces consist of the bosons, gluons and photons, respectively. The photon is the force carrier of the electromagnetic force and there is only one type. There are two types of bosons for the weak force, W and Z. Furthermore there is a neutral W and Z boson and a positive and negative W boson. Together the photon and W and Z bosons make up the electroweak force carriers. There are 8 different gluons for the strong force. These 8 gluons are arranged by combinations of three different colors, red, green and blue. An illustration of the interaction between the Standard Model particles is shown in Figure 1.2.

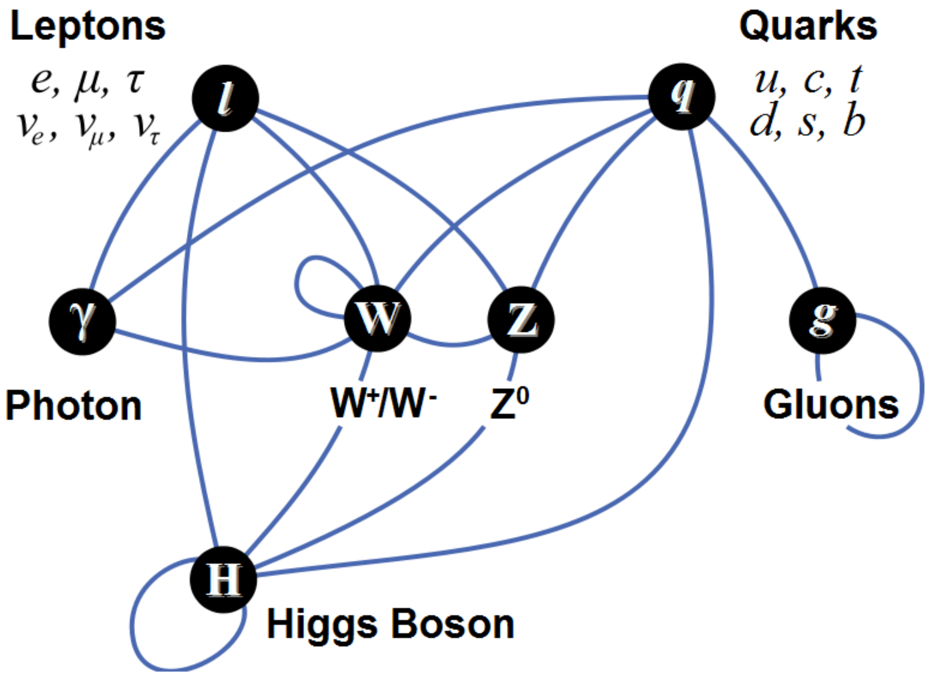

Figure 1.2 An illustration of the interaction relationships between the Standard Model particles. The black balls represent the group of particles and the connecting blue lines illustrate the interactions between them.

It is an understatement to say that the Standard Model is successful in predicting these constituents. In his well known textbook on Particle Physics, Griffiths hints to the beauty of the Standard Model, “Since 1978, when the Standard Model achieved the status of “orthodoxy”, it has met every experimental test” [16]. It has, moreover, and attractive aesthetic feature: in the Standard Model all of the fundamental interactions derive from a single general principle, the requirement of local gauge invariance” [13]. Figure 1.3 [17] shows the consistency of measured physical observables and their theoretical fit values. The bar chart shows the difference between measurement and fit as function of standard deviation. Further experiments are needed because this model predicts the masses of neutrinos as zero [18] but current experiments show otherwise [19].

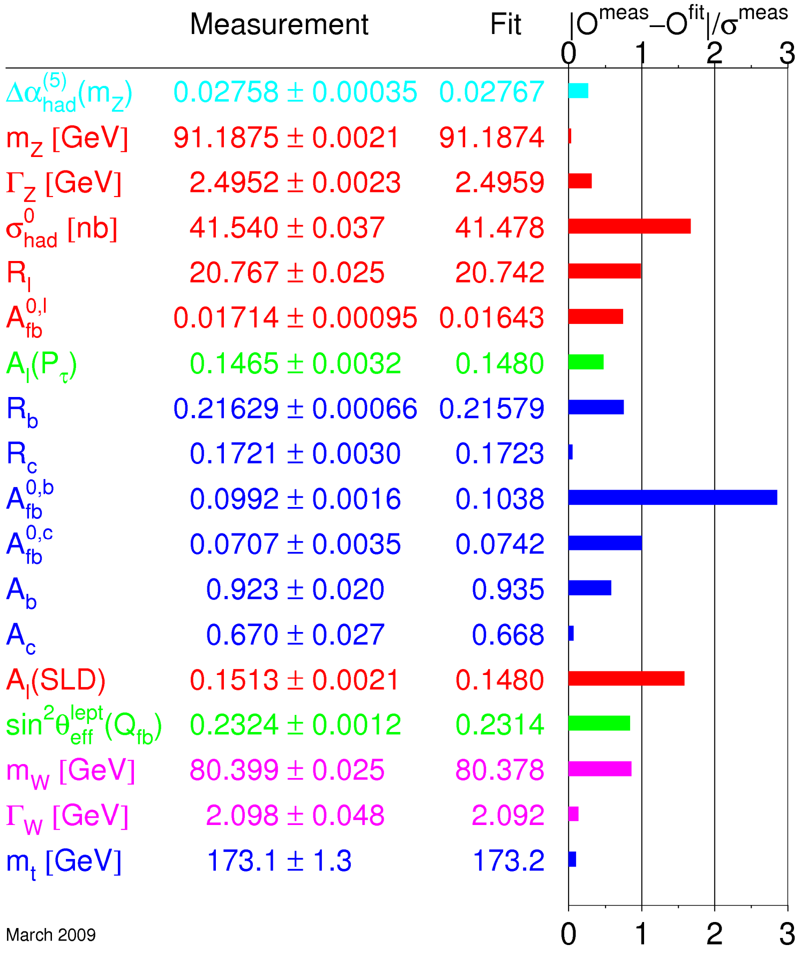

Figure 1.3 A measure of the consistency of the standard model fits to currently available high energy electroweak data as of March 2009.

A driving force motivating the work presented in this thesis is the Standard Model and the questions it presents. How many flavors of neutrinos exist in nature? What are the actual masses of neutrino mass Eigen states? What are the configurations of neutrino masses? The Standard Model predicts the existence of the Higgs field [18]. Higgs is a boson assumed to be responsible for the existence of mass of weak vector bosons, leptons, and quarks.

1.3.Detector Development and Characterization for High Energy Physics

The University of Texas at Arlington's High Energy Physics group and its collaborators are working on the development and characterization of double GEM chambers for use in a digital hadron calorimeter (DHCAL) for International Linear Collider, an electron-positron collider. In particular the digital hadron calorimeter is part of the Silicon Detector [20], or SiD, design. Collaborators working with UTA include a group at Argonne National Laboratory (ANL), SLAC, FNAL, the Center for European Nuclear Research (CERN), University of Washington and some Korean institutes such as Changwon National University (CNU) [21] and Korean Atomic Energy Research Institute (KAERI) [22]. The group at ANL is involved with the development of a competing detector technology using Resistive Plate Chambers and digital readout electronics [23-25] . The group at SLAC designed the KPiX electronics readout specifically for the Si/W electromagnetic calorimeter [26-29] for SiD but also useful for GEM chamber electronic readout. FNAL hosts the 120 GeV proton test beam facilities [30] used for the test beam studies presented in this thesis and are currently developing digital readout chip with ANL. GEM technology was invented and developed by the Gas Detector Development, or GDD, [31] Group at CERN [32]. Physics groups at University of Washington also played a role in the detector development of early UTA GEM chambers. Test beam studies, not presented here, of a 30 x 30 cm^2 GEM chamber were performed at KAERI while professors from CNU worked closely with the UTA group at all levels for detector development and data analysis.

Gas Electron Multiplier technology is an attractive solution for a digital calorimeter concept for linear colliders. In particular double GEMs studied at UTA are under development with use in a Digital Hadron Calorimeter for the International Linear Collider. Physics goals for a SiD based ILC include precision measurement of Higgs boson properties, gauge boson scattering, effects of the existence of extra dimensions, supersymmetric particles and top quark properties [33]. GEM detector integration in a linear collider is especially attractive for use with Particle Flow Algorithm (PFA). PFAs provide a way to attain the necessary energy resolutions required by the SiD physics program [33]. One of the detector requirements for a PFA that meets these energy resolution goals is a high granularity similar to that which GEM detectors can provide.

A GEM-based digital hadron calorimeter is advantageous due to many practical design qualities. The flexibility of GEM detectors allows anode cell size on the order of 1 cm x 1 cm or smaller, providing a desirable high granularity. Previous tests at KAERI [34] have shown GEM to be robust surviving 10^{12} paricles/mm^2 without performance degradation. GEM detectors are also fast since it collects electrons down to a 50ns pulse width. Advantageous to large complex detector systems is the simple Argon Carbon Dioxide gas mixture and relatively low operating voltage of 2 kV per double GEM chamber.

1.4. Thesis Outline

In this thesis the process for developing GEM as a technology for digital hadron calorimetry and the study of its related characteristic properties are presented. The first chapter gives an introduction to this thesis and GEM’s usefulness as a digital hadronic calorimeter as part of a larger high energy physics experiment detector for linear colliders. Chapter 2 introduces the technology of GEM foils and their arrangement in a gas chamber for the detection of charged particles. A description of the characteristic measurements taken from various GEM chambers discussed in this thesis is given in Chapter 3. There are three main prototypes under consideration, a small 10 x 10 cm^2 multi-channel double GEM prototype using simple preamp based data acquisition, a larger double GEM using the same electronics and a 30 x 30 cm^2 GEM using modern novel high intensity data acquisition systems. These designs and their corresponding read-out electronics and presented in Chapter 4. Chapter 5 andChapter 6 present the operational settings and gas flow determinations, respectively. The KPiX electronics and associated GEM chambers’ characterizations are given in Chapter 7. A description of test beam studies and results is provided in Chapter 8 and finally conclusions and future prospects for GEM are presented in Chapter 9.

CHAPTER 2

THE GAS ELECTRON MULTIPLIER TECHNOLOGY

Gas Electron Multiplier chambers rely on a GEM foil arranged between a high voltage and ground dispersed in an ionizing gas. The details concerning the technology of GEM foils as a detector of charged particles and its potential usefulness as a digital hadron calorimeter are introduced in this chapter. One advantage of GEM technology is that the foil is physically separated from the read-out anode allowing for fast response. Multiple GEM foils can be arranged within a chamber to produce higher gains of the ionization electrons. GEM chambers introduced in this chapter and discussed throughout this thesis use a series of two foils, or a double GEM arrangement. Finally, a concept of utilizing multiple GEM chambers for a digital sampling calorimeter is discussed.

2.1.GEM Foils

The Gas Electron Multiplier technology was invented by Fabio Sauli at CERN[1]. It is in a class of detectors known as micro-pattern gas detectors [35]. These type of detectors are characterized by a high granularity, high amplification and fast response. An example of a GEM foils is shown in Figure 2.1. and the electric field lines on a GEM foil are shown in Figure 2.2. A high electric field exists between the holes because a potential difference is maintained between the top and bottom copper layers covering about 50 μm. In particular, to create the regions of large magnitude electric fields between the holes, a potential difference of approximately 400 V is applied between the top and bottom layers of a single foil.

Figure 2.1 A photograph of a large 3M-UTA GEM foil developed for 30 x 30 cm2 prototype double GEM chambers.

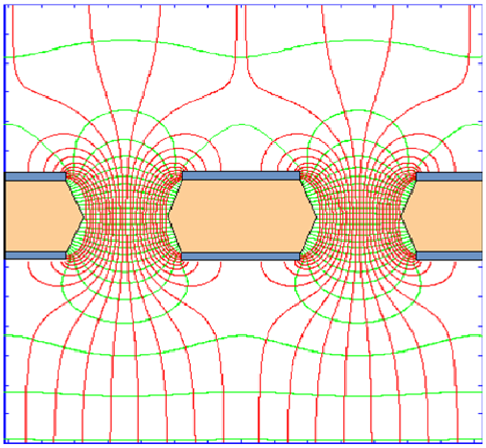

Figure 2.2 GEM foil electric field distribution across the holes in a GEM foil that accelerates electrons through the holes creating an avalanche of electrons.

GEM foils presented in this thesis are a copper clad kapton sheet. GEM foils contain micron sized holes throughout. Foils used in chambers described in this thesis are manufactured at CERN or 3M. The holes are etched out using chemical methods specific to the manufacturer. A micro-photo of a GEM foil manufactured at CERN is shown in Figure 2.3 [36]. The diameter of these holes is 70 μm and the space between the center of two adjacent holes, i.e. pitch is 140 μm. The thickness of the kapton is about 50 μm and the total thickness including the copper layers is about 65 μm. GEM foils constructed by 3M also use this geometry. Particular double GEM chamber structures and electric field orientations are discussed in section 2.2.

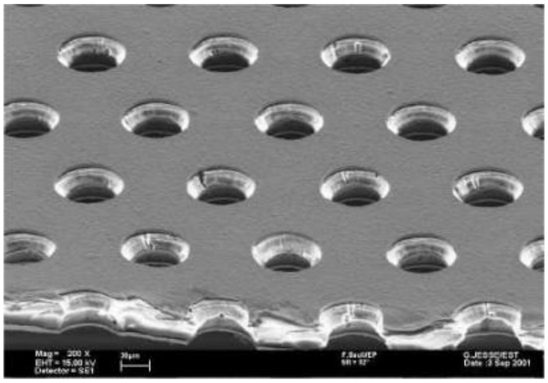

Figure 2.3 A micro-photo of a single GEM foil manufactured at CERN showing 70 µm diameter holes with a 140 µm holes.

2.2. Double GEM Chambers and Its Use in DHCAL

A schematic diagram of a double GEM chamber is shown in Figure 2.4 [37]. The standard components of double GEM chambers are a cathode, two GEM foils and an anode. A high voltage is applied between the cathode and anode where the cathode is at a negative voltage, and the anode is usually at ground, or 0 V. A resistor network is responsible for distributing the potential differences to each region and across GEM foils. The potential difference and depth for each region and thickness of each GEM foil set up electric fields within the chamber. Typically, a -2.1 kV potential is applied to the cathode and the anode is connected to ground at 0 V. The resistors can create a voltage drop of 400 V in the ionization gap, the transfer region, the induction region and across each foil. When a charged particle traverses the chamber it ionizes electrons in the ionization region. The ionization electrons drift toward the first foil where they accelerate through the holes across the large electric field and into the transfer region. Then this group of electrons are amplified a second time in the second foil where they accelerate again. Then the pulse from final ionization electrons arrives on a pad and is read out by the DAQ system. Once a resistor network and HV is set, the depth, or perpendicular distance from one layer to the next, of each region determines the associated electric field strength. The ionization region, for the UTA prototype chambers discussed in this thesis, is approximately 3 mm while the transfer and induction regions are typically 1 or 2 mm [38]. It is observed that these and similar separation depths and associated electric fields can achieve a maximum gain performance. Two arrangements of separation depths are presented in this thesis. 3:1:1 refers to the ionization, transfer and induction depths in units of mm, respectively. 3:2:2 follows the same definition except with 2mm in the transfer and induction gaps.

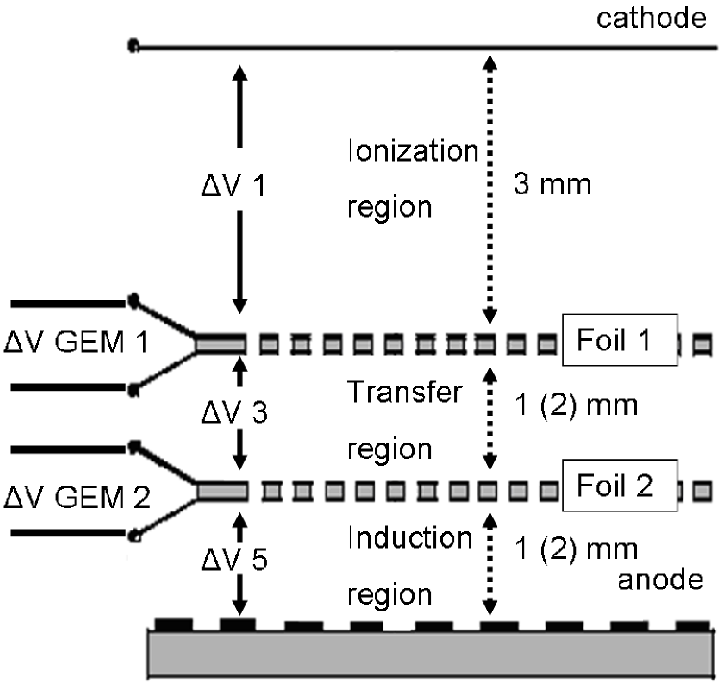

Figure 2.4 Double GEM structure. The cathode is the top layer, the GEM foils are represented by the dashed layers and the bottom is the anode and readout pads. The left side shows the nodes where the resistors are connected to create the potential differences for each layer. The ionization region, typically ~3mm, is the first layer after the cathode. The transfer region, typically 1-2 mm, is between the two foils. The induction region, also 1-2 mm, lies between the bottom foil and the anode pad.

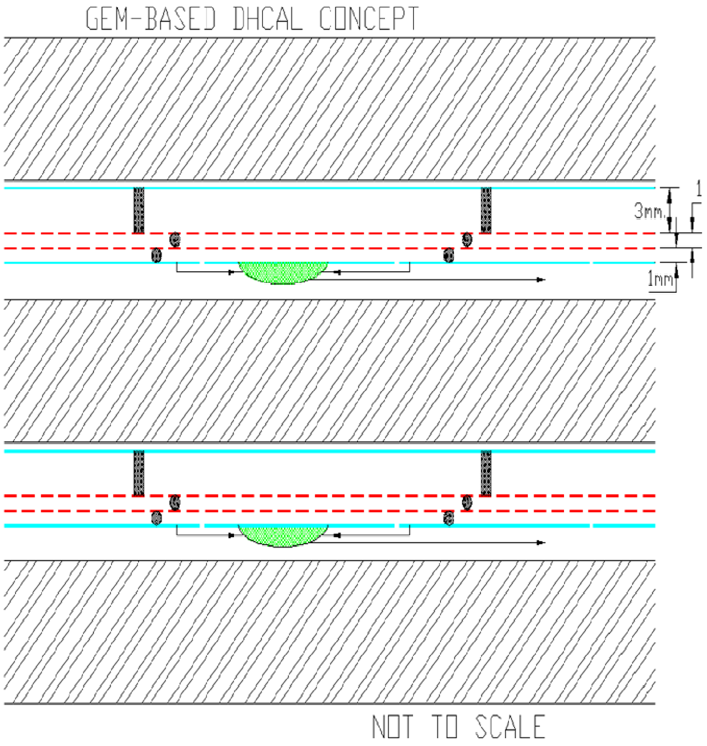

Figure 2.5 Double GEM implementation sampling calorimeter concept into a digital hadron calorimeter.

Figure 2.5 is a conceptual drawing of the implementation of double GEM into a digital hadron calorimeter. The shaded regions are a dense passive material that traversing particles lose energy through nuclear interactions creating showers of secondary particles. The secondary showers from these nuclear interactions ionize gas in the active GEM regions. Between the dense passive material are the active double GEM chambers. A system of active and passive layers covers the complete azimuthal range surrounding the collisions. This concept serves as a GEM-based DHCAL concept for the ILC in combination with PFAs and energy sampling.

CHAPTER 3

CHARACTERISTIC GEM MEASUREMENT DESCRIPTION

In order to develop GEM technology as a viable digital hadron calorimeter it is important to characterize GEM chambers with specific measurements. The measurements used to characterize GEM chambers are presented in this chapter. Signal and noise as it relates to GEM chambers is defined. The basic measurements of gain and efficiency are then described. The chapter is concluded with operational HV, gas mixture and gas flow rates.

3.1. Minimum Ionizing Particle Response

3.1.1. Definition of Signal

Signal is the intentional result from the design of the detector. Noise is the result of other processes and is discussed in further detail in section 3.2. Both are due to a current of electrons but their definition depends on the source of electrons. Signal in GEM chambers is a particular collection of electrons with a particular charge associated with the ionization from the incident charged particle. To determine the characteristic properties of the double GEM prototype chambers discussed in this thesis, minimum ionizing particles are used as the source of incident charged particles. Every data set derives from these particles as a source of the ionization on the interior of a GEM chamber. The typical signal produced by the detector are fast pulses 50-250 ns wide coming from direct charge collection on the anodes of the chamber. The widths of a pulse depends on the depth of the chamber through the various layers such that thinner chambers have faster pulses than thicker chambers. A distribution of signals from a minimum ionizing particle, or MIP, results in a Landau probability distribution as shown in Figure 3.1. This shape is characterized by a sharp peak toward the low end of the x-axis followed by a long tail. The peak of the Landau is called the Most Probable Value, or MPV, and is used for gain calculations. Gain is described in more detail in Section 3.3.

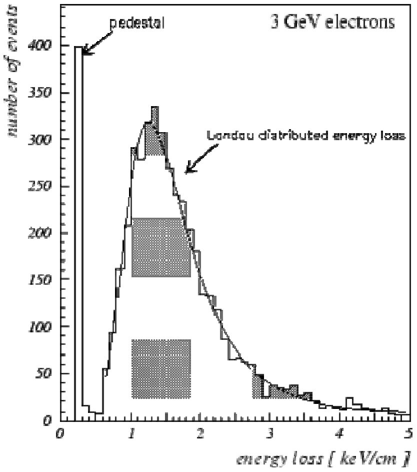

Figure 3.1 Simulation data of energy loss of 3 GeV electrons fit with a Landau probability distribution function. Data from GEM chambers are expected to have a Landau shape.

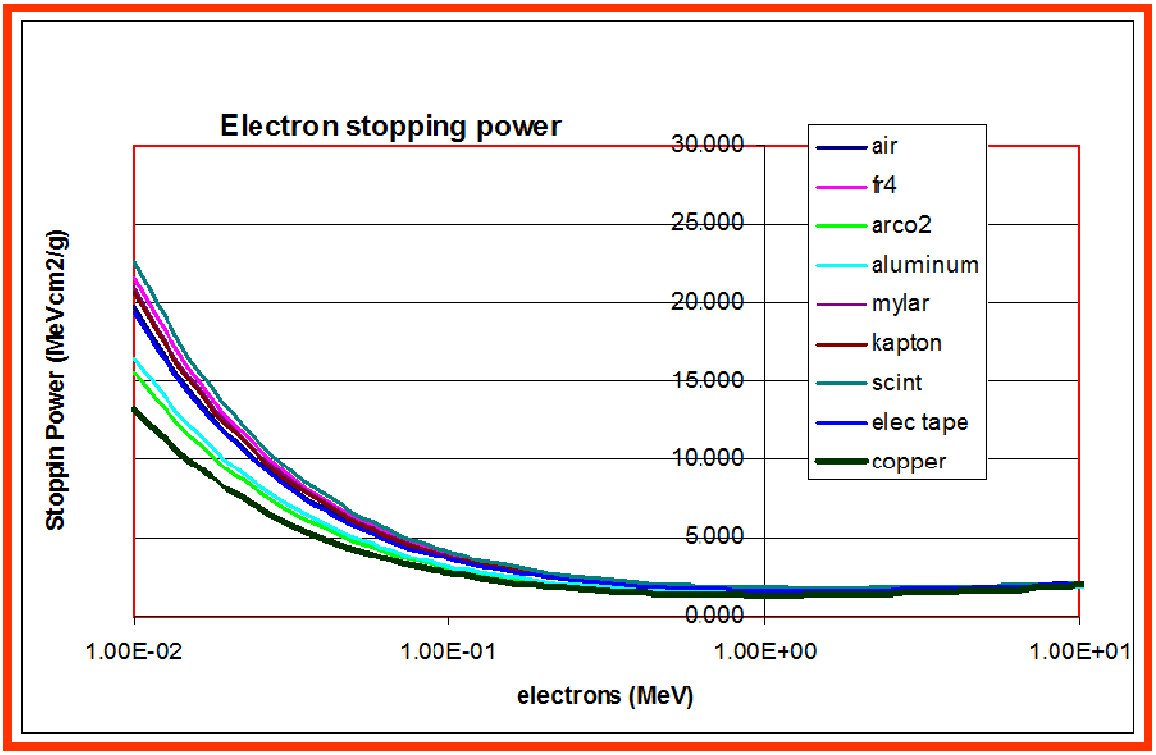

Figure 3.2 This graph represents energy loss through a material as a function of incident particle energy. A minimum ionizing particle is one such that a minimum energy loss occurs. In this example this range is most likely between 0.5 and 500 MeV.

Figure 3.2 [39] shows the stopping power of electrons through the different materials that make up a typical GEM chamber. A MIP is characterized as an electron or muon with a minimum stopping power in a corresponding material. So for beta-decay from Sr-90, a MIP has energy between 0.5 MeV and 10 MeV. As the ionizing particle traverses material in the chamber it loses energy according to its energy and the material it is traveling through. In ionization, MIPs produce a number of electron-ion pairs proportional to the length traversed by the particle through the gas and in passing through a gas mixture of 80% Argon and 20% Carbon Dioxide in double GEM chambers MIPs produce about 30 electrons in the 3-1-1 double GEM structure and more electrons in the 4-2-2 configuration [38].

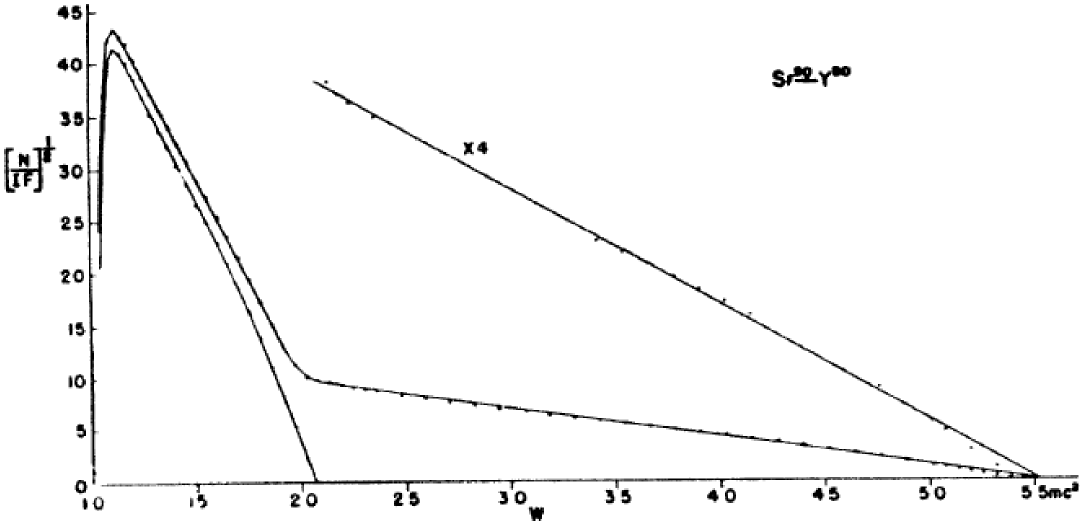

Figure 3.3 Kurie plot of intensity vs energy of beta-spectrum of a Sr-90 source. The x-axis is in units of energy mc^2 where 2.05 mc^2 = 0.53 MeV and 5.37 mc^2 = 2.23 MeV corresponding to the respective upper limits of beta-energy for the SR90 based beta and the Y90 based beta respectively.

The energy range of beta-decay from the Sr-90 radiation source is shown in Figure 3.3 [40]. Starting from the left, the first curve that ends at 2.05 W corresponds to the intensity from Sr-90 beta-decay and the second curve that ends at 5.37 W corresponds to the intensity from Y-90 decay associated with the Sr-90. Here W is a unit of energy. 2.05 W is equivalent to 0.53 MeV, the end-point energy of Sr-90 beta-decay, and 5.37 W is equivalent to 2.23 MeV, the end-point energy from Y-90 beta-decay. The Sr-90 source has an emission probability of 100% that emits a beta-decay and a Y-90 with an associated beta-decay. Therefore every decay consists of two beta-decays each with a unique end-point energy but there is only one possible MIP. Also, most of the decays from Sr-90 are not a MIP. The area below the curve between 2.05 W and 5.37 W represents the probability of MIP decays from a Sr-90 source. For cosmic rays, the average muon flux at the surface is approximately 1 $cm^{-2}min^{-1}$ for muons close to 3GeV for all angles [41]. All of these behave as MIPs in double GEM chambers.

3.1.2. Chamber Signal Collection

The collection of chamber signals depends on the detector, electronics and DAQ system. The computer is used to store and analyze collected signal distributions. The means of extracting signals to the DAQ computer various between chamber designs. Specific chamber designs are discussed in Chapter 4. Data used in this thesis are taken using two main signal collection systems, QPAO2 [42] electronics and KPiX analog electronics.

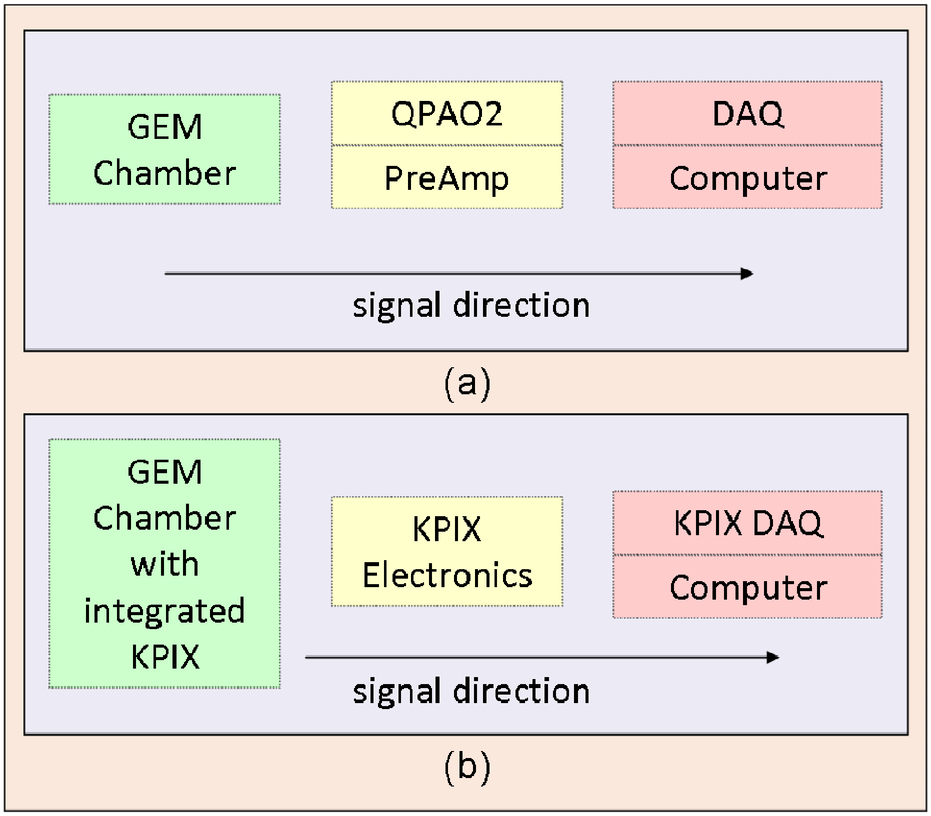

Figure 3.4 Generalized flow diagram for signal collection using QPAO2 (a) and KPiX (b). For QPAO2, Signal starts in the GEM chamber, moves through the QPAO2 electronics and finally arrives to the DAQ computer. For KPiX, signal also starts in the GEM chamber but is embedded with the anode board. It is initially processed by the embedded KPiX electronics, moves to the supportive electronics systems and finally arrives to the DAQ computer.

3.1.3. Signal Rate

The typical signal coming directly from the double GEM detector to any electronics in the data acquisition system are fast pulses 50-250 ns wide, depending the depth of the chamber, and come from direct charge collection on the anodes interior to GEM. Signal duration, i.e. pulse width, depends on the depth of each region. Figure 3.5 is a photo from an oscilloscope display of a signal after the pre-amp showing what a collection of electrons/charges, or signal, looks like. Limitations on signal rate are initially due to the time it takes for ionization charge, in the form of fast pulses, to be collected on the anode pads. This is the intrinsic time resolution of the chamber. For instance, if it takes 100 ns for the charge from a single event to deposit on the anode pad then the maximum signal rate is 10 MHz. Beyond this, one events cannot be distinguished from another. An event occurs when a charged particle traverses the chamber and charge is collected on a read-out pad. Discussed later, inefficiency occurs when a charged particle traverses the chamber but little or no charge is collected on a read-out pad because either electrons are not ionized in the gas or the GEM foils did not adequately amplify ionization electrons. Therefore, in general, an event occurs whenever a particle capable of producing signal passes through the GEM chamber. The possibility then exists that two charged particles traverse the chamber within 20 ns but charge is collected together so that the two events are considered as one.

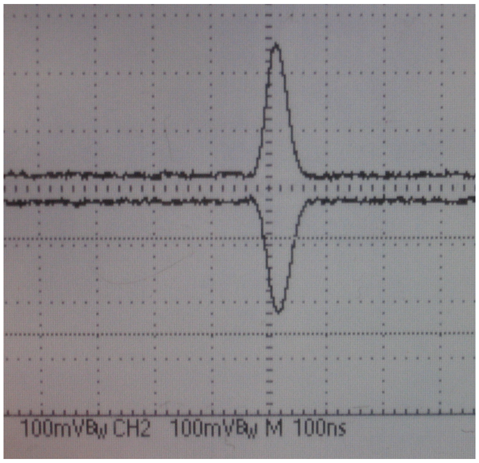

Figure 3.5 A photo of output signal after pre-amp on an oscilloscope. The positive pulse is from the positive output and the negative pulse is from the negative output of the QPAO2 preamp card.

The effective signal rates of data taken also depend on the readout electronics. Many data acquisition (DAQ) systems are discussed in later sections but it is important to introduce its effects. Simple charge pre-amplifiers take about 50 ns to convert charge to readable signals.

3.2.Definition of Noise

In general, noise refers to the aspect of an electronic system different from the desired characteristic signal. Characteristic signals, in the case of GEM detector studies in this thesis, are observed as pulses of a particular time and voltage or charge and occur with a frequency that depends on the source of charged particles. Characteristic signals have a unique source of origin due to physical ionization process within the GEM chamber. Noise is usually characterized by a baseline flat signal as observed by an oscilloscope such as shown in Figure 3.5 other than the pulse.

There are two main types of noise. Intrinsic electronics noise and environmental noise. Intrinsic noise is a basic irreducible type of electronics noise characteristic of the chamber and its associated electronics. This electronics noise is irreducible assuming chamber design and associated electronics has been optimized for minimum noise. Besides this there are no additional actions to reduce this noise. Since GEM output, whether noise or signal, is observable with an oscilloscope, the intrinsic noise is always affected by environmental noise. Environmental noise is often characterized by a particular frequency especially if it has a source of origin like florescent lights in the lab room or radio waves. Environmental noise is not directly associated with the chamber and is reducible through various grounding or shielding techniques. The combination of intrinsic electronic noise, environmental noise and chamber noise is the operational noise.

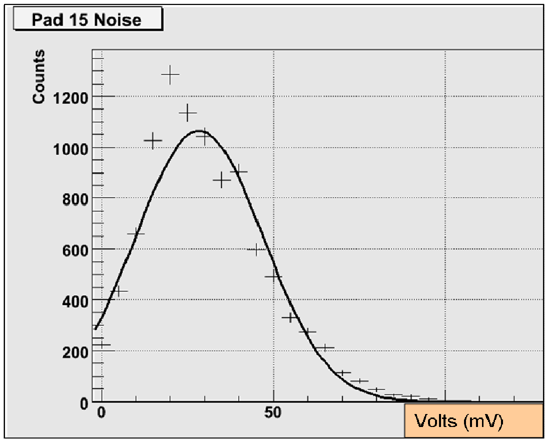

Figure 3.6 Example of pedestal (noise) distribution from a double GEM chamber.

Noise signals have a different pulse height distribution than data signals. Figure 3.6 is an example of a histogram of noise signals, or pedestal, fit with a Gaussian probability distribution. Pedestal is a distribution of pulse heights from operational noise. The mean value of the Gaussian distribution is the minimum level and represents the baseline for signal. The width, or sigma, of the Gaussian distribution represents the fluctuation of the noise. So typically, a MIP generated signal follows a Landau distribution but noise follows a Gaussian probability distribution. Figure 3.7 shows a comparison of noise to signal pulse height distributions from a double GEM chamber. Notice that the lower peak closer to zero is separate from the second peak with a long tail. The best case is that the MPV and pedestal are sufficiently separated in order to distinguish noise from signal. The details of the sufficiency of separation is discussed further throughout this thesis as it corresponds to chamber design, experiment and data analysis techniques.

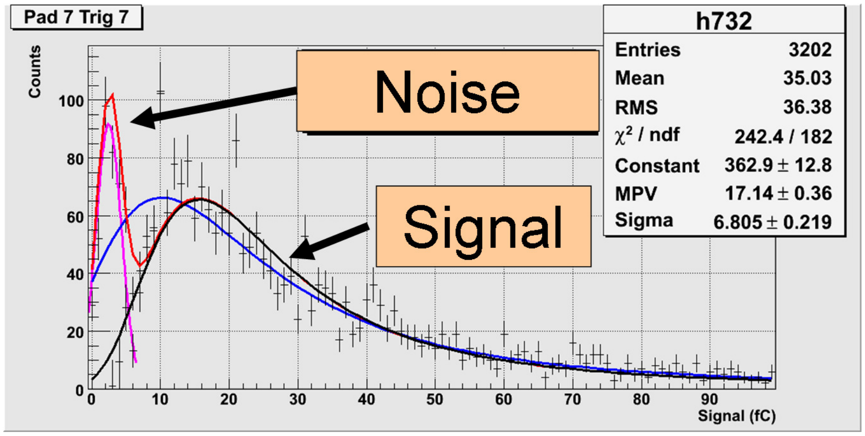

Figure 3.7 An example pulse height distribution from a double GEM chamber. The lower peak is from noise while the Landau shaped peak is from signal.

Elements that contribute to intrinsic irreducible electronics noise are readout electronics associated with the DAQ system, HV to the chamber, soldering and construction of electronic components for the GEM chamber, and power associated with the DAQ system. The number of sources and contributors to this electronic noise is as varied as the available DAQ systems. For GEM detectors discussed in this thesis further details about the specific electronics noise in the various DAQ environments are provided in later sections.

Another source of noise comes from the surrounding environment. Radio waves, experiments from other labs within the building, shielding enclosures and even room lights can supply environmental noise. Furthermore, various electronics components associated with the complete detector system can pick up environmental noise. In general these are uncontrollable noise sources that are manageable and reducible. Proper grounding and shielding can help to manage and alleviate the effects of environmental noise. For example, double GEM chambers using KPiX are enclosed in an aluminum box and grounded with the building ground to manage environmental noise.

3.3.Gain

Gain is the ratio of output charge divided by input charge. The input charge comes from ionization in the drift region and provides electrons for the GEM foils to amplify. The output charge is due to the collection of electrons on the anode pad in the chamber.

On average, MIPs produce about 33 electrons/cm, or 3.3 electrons/mm from ionization in 80:20 Ar:CO_2 gas. Then in a 3mm drift region, vertical MIPs produce an average of 10 electrons. In a double GEM chamber secondary ionization increases this by a factor of 3 resulting in about 30 electrons. This is the number of electrons considered as the input charge where 1 fC equals 6240 electrons. The number of electrons produced through ionization fluctuates according to a Landau probability distribution. The peak of this distribution is the most probable value, or MPV and does not fluctuate for a given chamber structure. Therefore, gain is considered a constant measurable characteristic for a given double GEM chamber.

Although the charge deposited on the anode pad is the output charge of the chamber, this value is not measured directly. The signal read is usually in units of volts or mV. This value must be converted back to charge according to the electronics gains inherit in the DAQ system. Usually this is done by testing the readout electronics separately to determine the proportion of mV to charge.

In order to measure gain, the chamber output pulse height distribution produced by MIPs, cosmic-ray muons or radiation source, is collected and fit with a Landau function. Then, all electronics gains are applied to convert the MPV to units of charge, typically fC. Finally this output charge is divided by the input charge to determine the gain of the double GEM chamber.

3.4.Efficiency

Efficiency is a measure of the detector's ability to accurately record the entire output charge of each event from all MIPs. Inefficiency occurs when a MIP goes through the detector, triggers the DAQ, and little or no corresponding charge is recorded. In other words it is when a signal is counted as noise. The most accurate way to measure the efficiency is to have accurate unbiased knowledge of the incoming MIPs. For example, each triggered event stores pulse height information from the chamber output to a histogram on the DAQ computer. The number of events contained in the histogram reflects the number of times charge from the chamber is recorded to the computer. It does not reflect the number of MIPs traversing the chamber expected to produce ionization and subsequently signal. One unbiased method of triggering the chamber (and counting passing MIPs) uses plastic scintillation counters that cover an area less than the active region of a GEM chamber.

Another way to measure efficiency in the case of a biased trigger and high energy mips is through an inference method. This method relies on an assumption that there are no missed MIPS that produce signals above a threshold. The output histogram is fit with a Landau probability distribution. This fit extends below the threshold and estimates MIP signals that contribute to inefficiency.

3.5.Operational HV

GEM detectors function based on the electric fields between the different regions of the detector. The regions are between the cathode and first GEM foil, each GEM foil, first and second GEM foil, and between second foil and anode. The voltages at these sections are set according to a chain of resistors between the high voltage and ground. The HV first connects to the cathode and then to the subsequent sections through a resistor.

There is a particular HV that contributes to optimal chamber performance. This is the operational high voltage. This can be determined by comparing the gain from data at different high voltages with a radiation source or cosmic ray muons as the ionizing particle. The HV value that results in maximum gain and maintains reliable stability is the operational HV.

Stability refers to the absence of discharges that occur within the chamber. If the HV is too high then sparks can occur between the copper layers of a GEM foil. Considering the extremely large electric field this can permanently damage the GEM foils. It is also possible for a discharge to cause carbon buildup between the holes of a GEM foil and a short to develop. If this occurs then that particular foil may become non-functional and severely reduce the gain of the chamber. A minimum amount of discharge is required. One key aspect of GEM is its robustness and stable operation under high radiation environments similar to large detector environments near HEP accelerators.

3.6.Operational Gas Mixture

There is also an optimal operational proportion of gas mixture. A simple mixture of Argon and Carbon Dioxide completely fills the volume of the chamber. In addition to HV, an optimal gas ratio also contributes to optimal gain. Characterization tests using Ar:CO_2 mixtures of 70:30, 80:20, and 85:15 were performed to find that the optimum mixture is 80:20. Although gain increases with increasing argon ratio, increased discharges are observed with a reduction of CO_2. Therefore, Ar:CO_2 80:20 was observed to discharge with a similar rate to gas mixtures containing lower ratios of Argon. Chapter 5 contains detailed information on experiments performed to determine operational HV and gas mixture ratios.

3.7.Operational Gas Flow Rate

In order to provide GEM chambers with a constant source of gas for ionization, gas is continuously supplied to the chamber from an external source. The resulting flow of gas through the chamber effects performance. Since cosmic-ray muons or electrons from a radiation source continuously pass through the chamber the internal gas is continuously ionized. Ionization of the gas is how signal is generated. Therefore, a constant supply of fresh gas is needed and the chamber must perform consistently over time. Since chamber performance depends on the gas mixture ratio it is also important to know the time it takes for GEM gas to replace any air inside the chamber. In the development stage of detector design a chamber may be disassembled and reassembled many times. As a result, air enters the chamber and must be purged. Therefore, it is necessary to understand and optimize the rate that gas flows through the chamber and the time to completely fill the chamber with the desired gas mixture.

An optimal gas flow rate does not inhibit the performance of the chamber. A gas flow rate that permits maximum signal rate is preferred. Turn-on time is defined as the time to achieve maximum gain for a given configuration. A minimum turn-on time uses less gas thereby reducing operational cost. Another advantage to a minimum turn-on time is that there is less time to begin taking data between startups. This is most advantageous during detector development and in testing various chamber configurations. The method used to reduce turn-on time for tests presented in this thesis is to initially fill the chamber with gas at a high rate and then reduce the flow to an operational level.

CHAPTER 4

CHAMBER DESIGNS AND ELECTRONICS SYSTEMS

4.1.Introduction

There have been various DAQ systems employed by UTA's prototype double GEM detectors to read signals. A complete DAQ system is the entire ensemble of readout and data taking electronics. All DAQ systems described in this thesis are based on either the FNAL charge preamp QPAO2 or the SLAC designed KPiX system. Both QPAO2 and KPiX are used as a preamp and front-end readout chips that serve a central role in their associated DAQ systems. The 32-channel FNAL charge preamp card, or simply preamp, is based on the QPAO2 chip. KPiX is different in that it is an imbedded application specific integrated circuit that is controlled by a field programmable gate array, or FPGA. The KPiX system integrates the GEM chamber, supportive electronics and computer as a complete DAQ system whereas the QPAO2 based preamp is a stand-alone preamp card.

4.2.QPAO2 Chip Based Preamp

4.2.1. Introduction

Since previous experiments [43] observe double GEM chambers to have gains on the order of 10k and MIPs produce about 30 electrons per crossing, the expected GEM charge pulses input to the preamp are about 30k electrons or 4.8 fC. Therefore, GEM signals are too small to be distinguished from noise without an initial stage of amplification. One of the data acquisition systems used for GEM chamber readout is based on the QPAO2 charge amplifier chip. This is used in combination with an AD811 ADC (analog-to-digital converter), CAMAC system and a computer to record data or oscilloscope to observe GEM chamber signals before arriving to the ADC. This section discusses the QPAO2 based 32 channel preamplifier card, AD811, and other DAQ components.

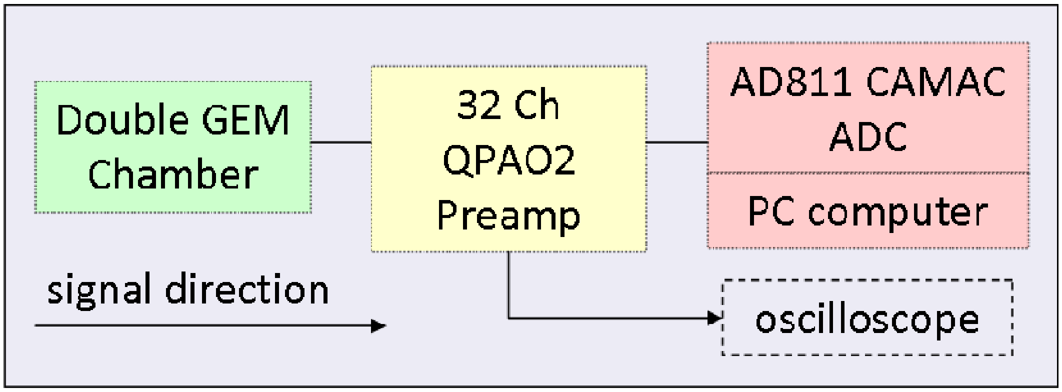

Figure 4.1 Flow diagram for preamp certification tests

4.2.2. QPAO2 32 Channel Preamplifier

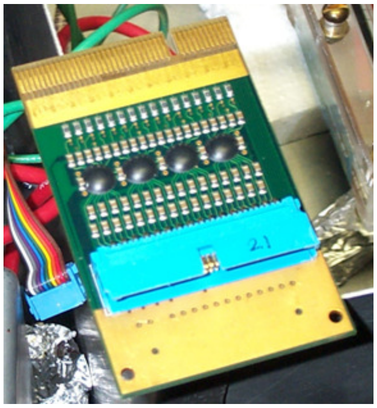

Figure 4.2 A photo of the 32 channel QPAO2 preamplifier.

Preamplifier stage readout for GEM chamber is a 32 channel amplifier card utilizing the QPAO2 amplifier seen in Figure 4.2. The QPAO2 is a high speed bipolar transimpedance amplifier utilizing a Tektronix "Quickchip 2S" semicustom linear array that converts an impulse of charge to a fast voltage pulse [42]. Each preamp card has 32 channels capability and separates each channel into a positive and negative output. An example of simultaneous output of the preamp is shown in Figure 3.5 as a photograph from an oscilloscope connected to the negative and positive output of a preamp card with GEM as the input. Experiments using a QPAO2 based DAQ use the negative signal as a trigger signal and the positive signal is used as the data signal.

The average gain for most QPAO2 preamp card channels is measured to be between 8 and 10 mV/fC per channel. This means that incoming charge pulses from a GEM chamber are converted from charge to potential. The AD811 CAMAC ADC is then able to convert GEM signals to a digital signal for storage on a computer.

4.2.3. AD811 CAMAC ADC

After the preamp, signal goes to the AD811 ADC. The ADC is part of a CAMAC based DAQ that connects to a PC via an ISA, industry standard architechture, interface card[44]. Together this DAQ system is capable of reading up to 8 channels simultaneously.

The software on the DAQ PC is adaptable to match the number of channels of the AD811. This is the same system as used for the preamp certification measurement described in section 4.3. The program runs under the DOS shell operating system and is written using the FORTRAN programming language. The user can select the number of channels, up to 8. Additionally, the user can also pause during any data run to examine histograms from the collected data.

4.3. Preamp Certification Measurement

The main goal of preamp certification is to determine the electronics gain in units of mV/fC for each channel on each 32-channel card. This provides the effective gain of the preamp for each channel and uncertainties. This measurement is useful for determining the electronics gain and ultimately to correct these gains to obtain actual chamber gains.

4.3.1. Experimental Setup

The goal is to measure the gain in units of mV/fC of the preamp. As a part of GEM chambers, the preamp will receive an amount of charge contained in a single pulse as produced by a charge particle in the chamber.

In order to measure the gain of the preamp we must provide an input signal using a known amount of charge. In order to reliably inject a known amount of charge an interface card was built. This interface card attenuates and distributes the pulse generator signal using a voltage divider and an array of thirty-two 5pF capacitors for each channel. The pulse generator provides a periodic square wave signal of 500 mV as illustrated in Figure 4.3. First the voltage divider attenuates the signal to 18.5 mV to the 32 capacitors. According to the relationship between charge and voltage, $Q = CV$, the input charge to each channel is determined by the total capacitance on the input side. The preamp has a 10 pF capacitor on the input side of each channel so that it is in series with the 5 pF capacitor on the interface card thus making a total 3.33 pF capacitance. Then the capacitors provide about 60 fC to each preamp channel. This is about 12 times greater than most signals created in a GEM chamber by a MIP. After the preamp amplifies the signal, an 8 channel output card distributes the signal to the ADC. In this way up to 8 channels of each preamp card is simultaneously tested for gain. The flow of signals for preamp certification is illustrated in Figure 4.4.

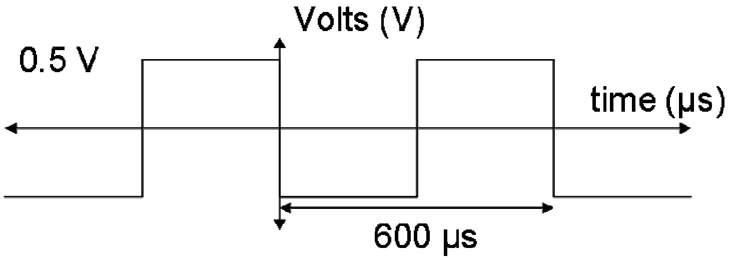

Figure 4.3 Input signals to preamp certification circuit are square waves with amplitude of 500 mV and periods of 600 us.

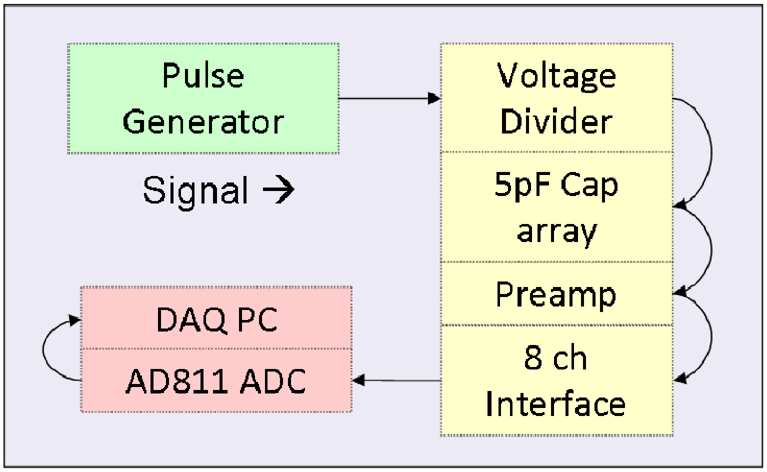

Figure 4.4 Flow chart of the signal path for preamp certification measurements. The signal starts at the pulse generator, moves through the voltage divider and 5 pF capacitor array on the interface card, goes through each channel of the preamp, 8 channels are read out to the ADC and then finally DAQ PC.

4.3.2. Preamp Gain Measurement Procedure

The first step in this measurement is to make all the necessary connections. The voltage divider card connect to the preamp card, the power lines are connected to the preamp card, the $\overline{\text{OUTPUT}}$ from the pulse generator connects to the input on the voltage divider card, and all the necessary ground points are connected. Set pulse generator (PG) to -490 mV for Vlow and +490 for Vhigh. If testing positive signal connect the trigger output (PG) to discriminator. If testing the negative signal connect the OUTPUT (on PG) to discriminator. The output card of the preamp that interfaces with the ADC can only measure 8 channels at a time so the desired channels are connected at this time. Data is then recorded using the gemtest7 DAQ software on the heppc34 computer allowing the program to collect data for approximately 30,000 iterations. The power connections for the preamp card and the input connections for the voltage divider card are shown in Figure 4.5.

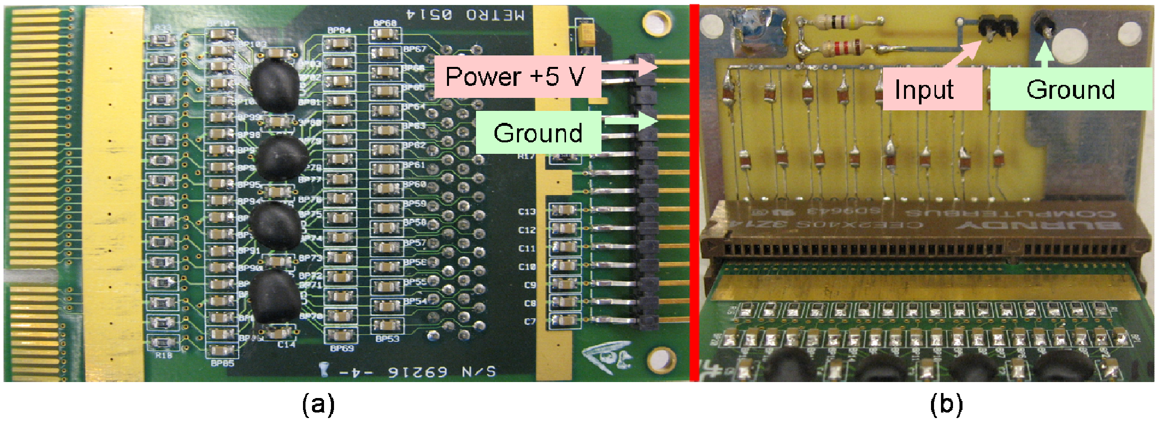

Figure 4.5 Bottom view of preamp showing power connections (a). The red wire is for the positive 5 volts and the black wire is for the ground connection. Photo of voltage divider card (b) used to connect an input from the pulse generator to the all channels of the preamp card. The remaining 16 capacitors are placed on the other side (not shown) of the interface card.

4.3.3. Data

Thirteen QPAO2 32 channel preamplifier cards are certified during the time of this testing. A well performing card has large and consistent gain values. A gain is large compared to the average of all cards tested. Consistency means that for a given card the gain values don't fluctuate too much around a mean value. Cards showing the largest and gain values are chosen to be used with GEM detectors. All the cards are labeled with a unique arbitrary number between 0 and 20. It is assumed the numbering of the cards is arbitrarily. Since the delivery of preamp cards to UTA, various cards are used for different experiments and measurements.

Despite the bipolar output of the preamplifier cards, each polarity is tested individually to uniquely identify gain of each polarity and channel. Therefore there are a total of 64 outputs of each card with a unique gain. Preamp cards are tested individually with only 8 channels tested simultaneously due to the channel quantity restriction of the AD811. Therefore each card requires 8 iterations of testing to determine the unique gain values for each polarity of output for each channel. The complete number of test iteration is multiplied by 11 to account for all cards resulting in 88 unique gain measurements.

As previously mentioned, each test accumulates 30k triggers from the pulse generator and the output is saved in ASCII format where the software creates a histogram at the end of the run fitting it with a Gaussian distribution. The mean and sigma values for each test are recorded. Therefore there are a total of 88*2 = 176 unique units of data available for analysis. It should be noted that 30k*88 data is contained in all histograms for all cards, channels, and polarities. An example of the gain values in all channels for a given card and polarity is depicted in Figure 4.6.

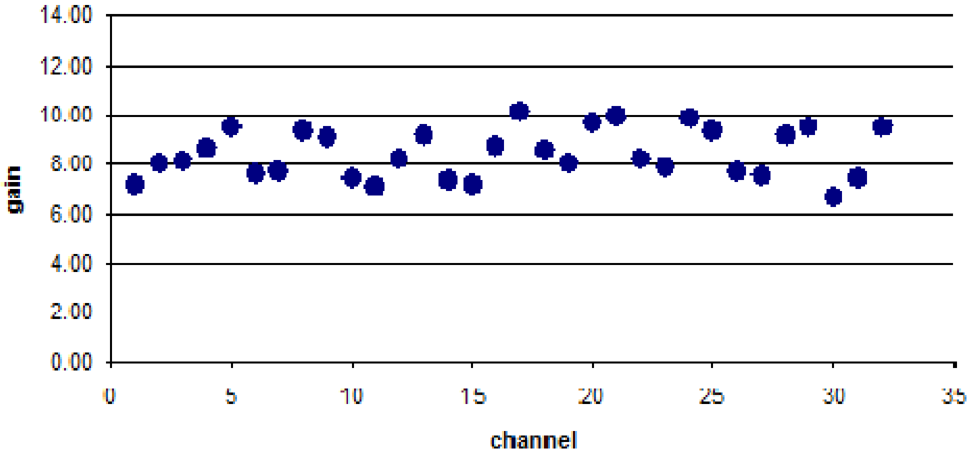

Figure 4.6 Gain vs. Channel # is shown in this figure. It contains all gain values for all channels of card 10's negative polarity output. The uncertainties of each point are the size of the markers.

The most important information from these preamp tests is the gain from each channel for the positive polarity. Once the best card is decided and integrated into the DAQ for a particular GEM chamber the gain of any channel used can be referenced by this data. Recall that positive polarity is used to record data from GEM while negative is used to self-trigger such as the case for radiation source runs. The average gain for all cards is important as well since it provides a benchmark to weigh the performance of the cards.

4.3.4. Results

Data is collected for all available preamplifier cards 6, and 9 – 18. Graphs are made for each card and polarity. These graphs are similar to Figure 4.6. In addition to these graphs the average mean value for all channels of a particular card for both polarities is calculated. The uncertainty to the mean is calculated as the standard deviation. It is expected that the gains from channel to channel do not fluctuate so the standard deviation is an overestimation, at best, of the uncertainty. Then the average gain for each card is graphed with respect to card number for each polarity as seen in Figure 4.7 and Figure 4.8, respectively. Each point represents the average gain for all 32 channels on a single card.

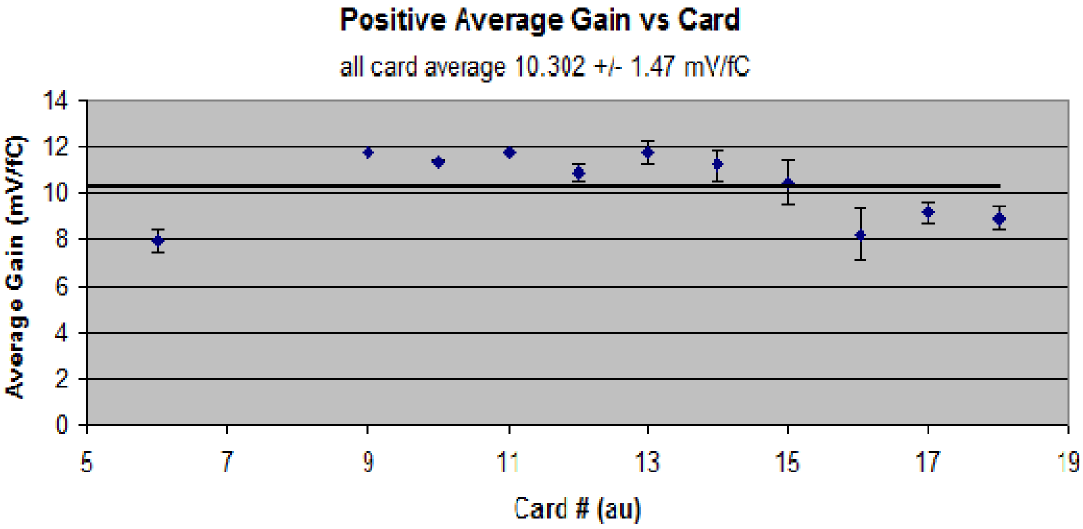

Figure 4.7 Graph of average gain from each card. The average value of all cards is represented by the black line. The units for the x-axis are arbitrary units corresponding to the label of the card.

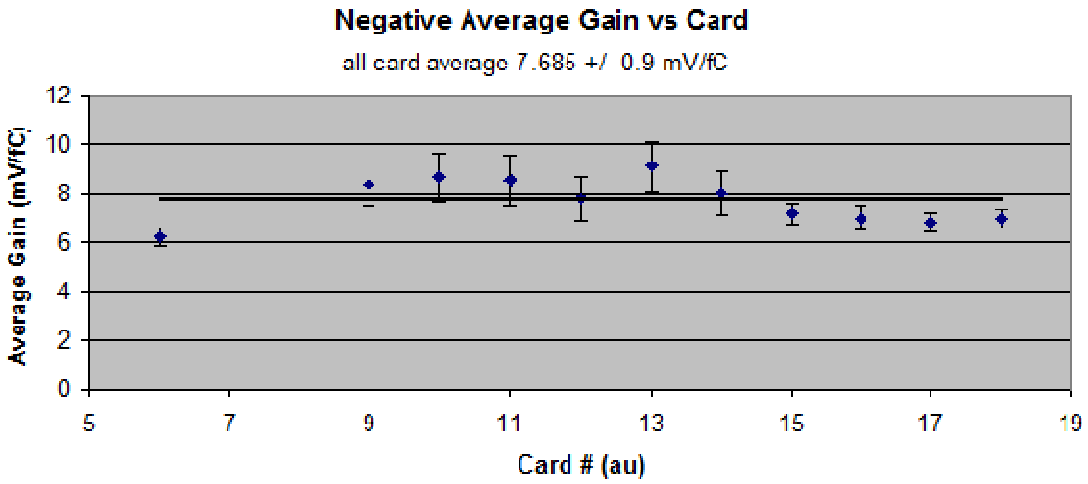

Figure 4.8 Graph of average gain from each card's negative output. Likewise, the average value of all cards is represented by the black line.

The uncertainty for each point is the standard deviation to the average of all channels for a particular card. The positive polarity of all cards has an average of 10.3 ± 1.5 mV/fC and the negative polarity shows an average of 7.7 ± 0.9 mV/fC. The average gain of the negative polarity is smaller than that of the positive polarity. Positive polarities are observed to have 25 % higher gain than negative polarities. Although the uncertainty bars in negative appear large, there is about 20% less fluctuation compared to positive standard deviations. In comparing the polarities, each uncertainty represents the accuracy of the average gain. Between cards there is a large fluctuation of gain in the positive output than in negative.

4.4.Prototype Multichannel GEM Chamber

This chamber, shown in Figure 4.9, is a 10 x 10 cm^2 double GEM chamber with a active area of 9 cm^2 using 9 centrally located 1cm^2 pads. The active pad region is arranged in a 3 x 3 square of 1cm^2 pixels. This prototype chamber is the first GEM chamber at UTA to employ multiple channel readout.

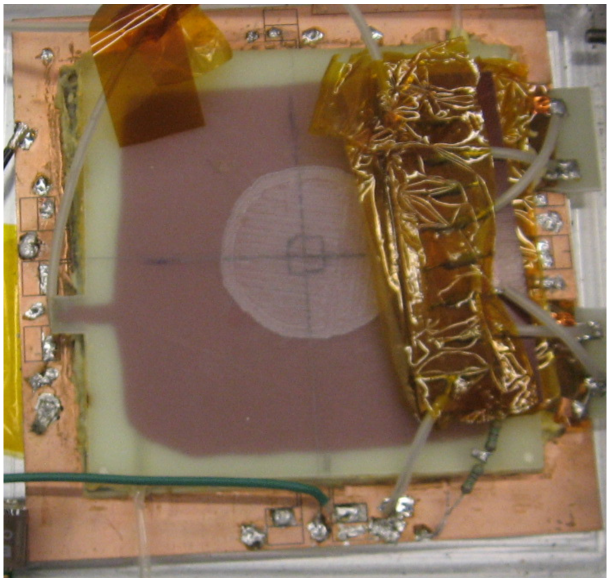

Figure 4.9 A top view photo of the prototype 9 channel double GEM chamber.

This prototype 9 channel GEM chamber utilizes the double GEM foil structure as shown in Figure 2.4. Each of the anode pads is connected to the input of the preamp whose first component is a large 100kΩ resistor to ground. Figure 2.4 shows the locations of the 5 unique regions of potential difference.

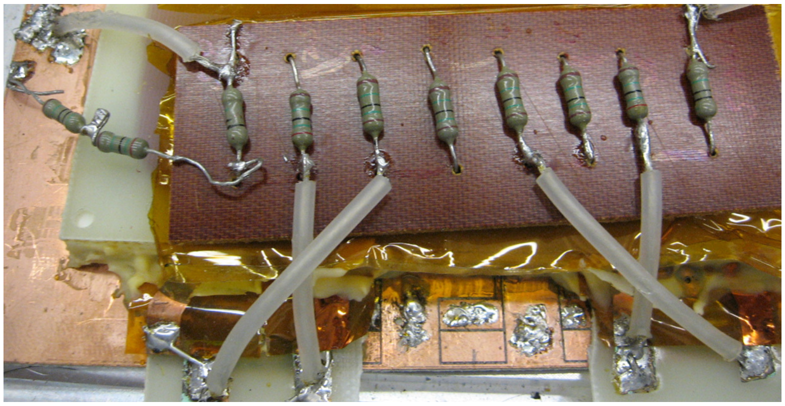

Figure 4.10 A photo of the resistor network creating the various potential differences across each region. There are a total of 10 resistors.

For this prototype 50 MΩ is in V1, 40 MΩ is in ΔV GEM 1, 30 MΩ is in V3, 40 MΩ is in ΔV GEM 2, and 30 MΩ in V5. A current between cathode and ground is observed at 10 μA when 2 kV is applied. The potential drop in each region is $\Delta V = I \bullet R$, where R refers to the resistance in the region. A HV of 2 kV provides a voltage across each GEM foil of 400 V.

Figure 4.11 shows a drawing of the anode board used for the prototype 9 channel chamber. The internal structure of GEM is the same as that described for the 3:1:1 structure in Figure 2.4. The board is a copper clad standard circuit board, in particular FR4, with copper etched out for the connections (not shown) and the central pads. The area surrounding the central 9 pads is the ground plane. Each pad in the center is connected to an accessible readout pad along the edge of the copper clad board. It is here that signal cables are soldered and read out to the preamp card.

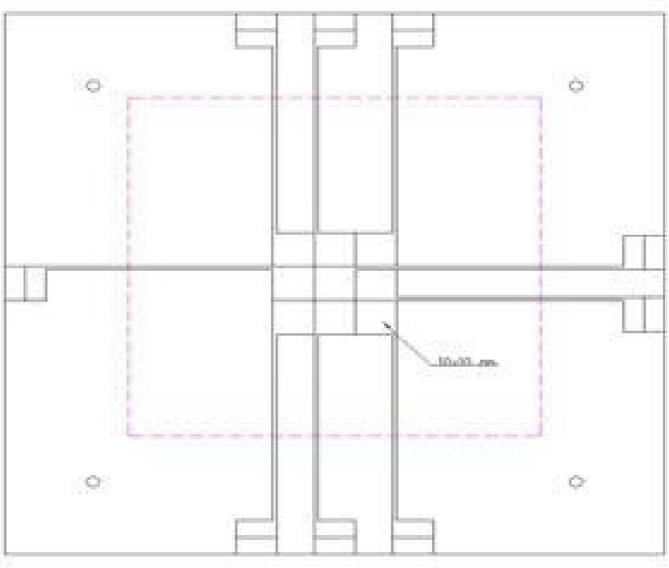

Figure 4.11 Drawing of 9 channel prototype chamber anode board. The board is a copper clad FR4 with copper etched out for the connections (not shown) and the central pads. The area surrounding the central 9 pads is the ground plane. Each channel is individually connected to another pad along the edge of the copper clad board.

4.5.30 cm x 30 cm Prototype Double GEM Chamber

UTA jointly developed 30 cm x 30 cm GEM foils with 3M Inc. to construct large scale GEM detectors as part of the development for a hadron calorimeter. The data acquisition system for the 30 x 30 cm^2 double GEM chamber is also based on the QPAO2 32 channel preamplifier. The total active area of this chamber is 30 cm x 30 cm covering a total of 900 anode pads. The entire available active region is not used in Fermilab test beam experiments due to limitations on the readout electronics.

Implementation of these large GEM chambers with QPAO2 and later KPiX uses the center 8 cm x 8 cm area of the GEM chamber. The large GEM foils used for these chambers are constructed using 12 separated high voltage strips surrounded with a ground plane as illustrated in Figure 4.12. Each strip has an area not laced with holes for soldering and attachment of resistors and can either be grounded or connected to HV. For the large GEM chambers discussed in this paper only the center 4 strips are used since there is no need to have the other strips connected to HV. These large GEM foils were constructed by 3M Inc. where as the 10 cm x 10 cm foils for the prototype 9 channel chamber were constructed at CERN.

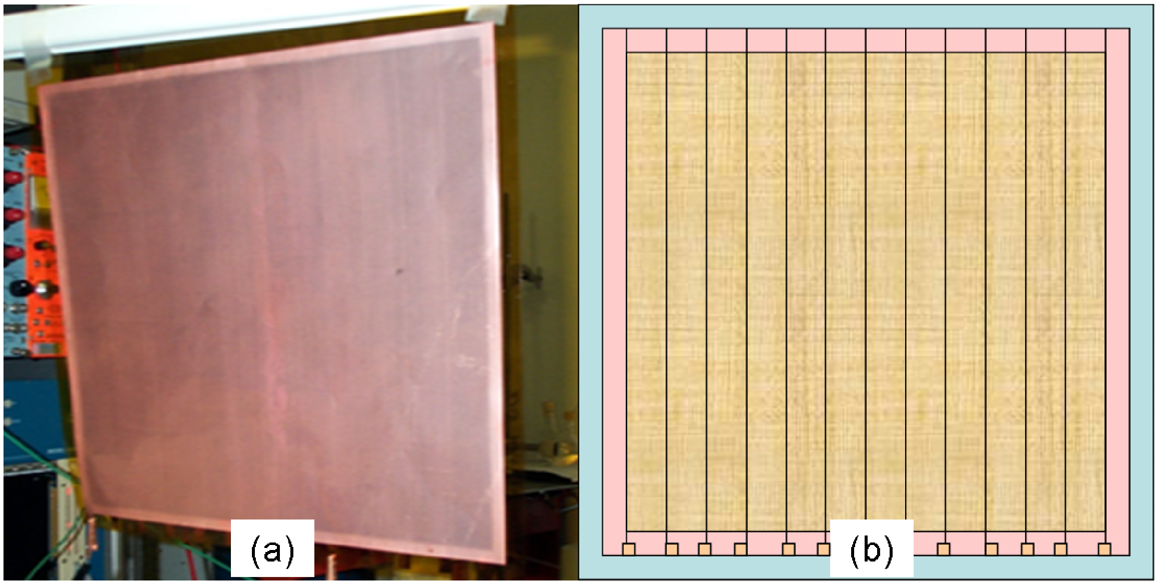

Figure 4.12 Large GEM foil for 30 cm x 30 cm chambers. Photo (a) shows a GEM foil and drawing (b) illustrates (not to scale) the division of foil into 12 HV sectors.

There are three factors to a complete DAQ system that limit the number of available channels to record data from a detector. The electronics must be able to match as closely as possible the performance of the detector. GEM detectors have a time resolution depending on the depth of the ionization, transfer and induction regions. For the 3:1:1 arrangement signal sizes are on the order of 50 – 100 ns. For the 3:2:2 arrangement pulses are on the order of 250 ns. Therefore GEM detectors cannot distinguish consecutive incident charged particles that traverse the chamber in less than 250 ns. A readout system should be able to also distinguish and record data from all channels with this resolution. A DAQ system is designed to match its detector performance as closely as possible. The strategy employed for GEM is to read signals from all channels at the same time. This means in parallel. This should be the case since the exact location of the ionizing particle is unknown and that the detector should be ready to record data from all channels.

One way the DAQ knows to record data is according the trigger signal. There are two options for the trigger signal. One is that there is a trigger signal for each channel. The advantage to this is that only a few channels are read at a time while the others do nothing. The disadvantage is the complexity of the electronics. Not only does each channel need a readout system, as is mandatory, but also a trigger system. This too may be impractical. Another option is that one trigger is used for all channels in the chamber. The advantage is an answer for the disadvantage for the first case. Only a single trigger is needed for any number of channels. Then an increase in granularity of the detector does not effect the trigger system. The disadvantage is that all channels must be recorded in parallel.

There are two ways to record information in parallel. One is to store the information in a type of short term memory while reading each channel serially. Although the data is being processed serially through the DAQ, storing it in cache allows the chamber to gather more signal. It does not turn off the chamber or ignore signals. An issue with this method is that the serial process must be quick enough and the cache is large so that information from all channels can be stored. If the processing is slow or the cache is small or has a short memory than this method will not work.

The other method, and the one used for parallel processing is to process each channel in parallel completely through the entire system to the point of recording information to disk. The advantage to this is that the chamber is ready to accumulate more data and there is no storage of information on chip. A disadvantage is that parallel processing requires each channel to have a processing signal and the associated electronics to control a high level of parallel processing. This is the preferred method and most closely matches the performance of the detector than the others.

Multiple channel readout of 30 cm x 30 cm GEM chambers requires 900 channel readout if all 1 x 1 cm^2 pads are used. A computer based 96-channel ADC card is used to accommodate a large number of channels. Although this does not allow readout of the entire system it does provide a benchmark for the analysis of data. It is also a good point to start testing the large multiple channel nature of GEM detectors.

The AD811 CAMAC ADC is replaced by the ADLINK DAQ-2208 96-channel PCI Express ADC with Labview software [45]. This ADC is also PC based entirely house within the computer except an interface adapter where the signal is fed in. This allows for up to 96 channel readout in series. The initial QPAO2 preamplifier card remains as the initial stage for signal readout. Besides 96 channels, this ADC provides the same functionality as the AD811 in that it converts the analog signal to a digital signal for the DAQ PC. One disadvantage is that as the number of input increase the sampling rate decreases. This means that the incoming signals must last longer so that the ADC can accurately sample the peaks of pulse heights.

4.6.KPiX DAQ Electronics

Double GEM detector's usefulness as a viable option for a digital hadron calorimeter for linear colliders depends greatly on the capabilities and performance of their readout systems. KPiX, shown in Figure 4.13, is an attractive electronics system for multi-channel readout with these properties in mind. One advantage of KPiX is its integrated calibration operation.

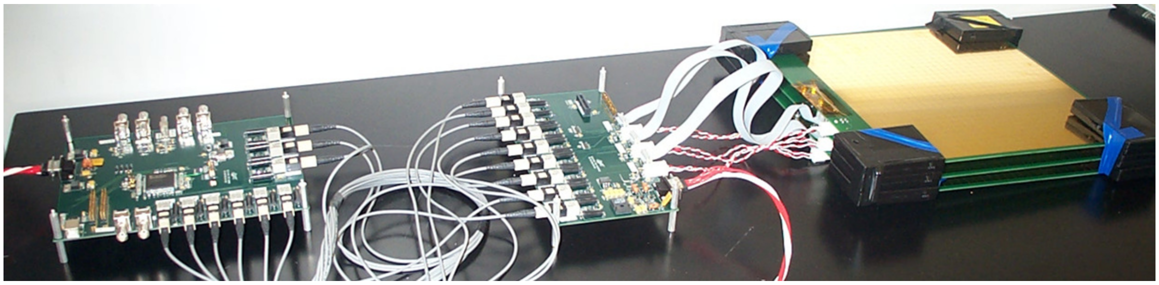

Figure 4.13 Photo of KPiX V4 showing (from right to left) anode board, interface board, and FPGA board.

The timing of the acquisition cycle for KPiX is represented in Figure 4.14. The rate often referred to is the rate of acquisition cycles. This is also the iteration count in the KPiX software. In every acquisition cycle KPiX has 2890 bunch trains corresponding to the current International Linear Collider beam structure [20]. The software keeps track of each acquisition cycle with an arbitrary serial number called Train Number. During an acquisition cycle there is a sample cycle where each bunch is given a corresponding value called Sample Time ranging from 0 to 2890. These are the available time slots for KPiX to accept a trigger and record data. If a trigger signal arrives during one of these times the charge information from the GEM chamber is recorded. The ratio of the sample cycle duration divided by acquisition cycle duration is the live time. Live time reflects the percentage of the acquisition cycle available to accept a trigger signal.

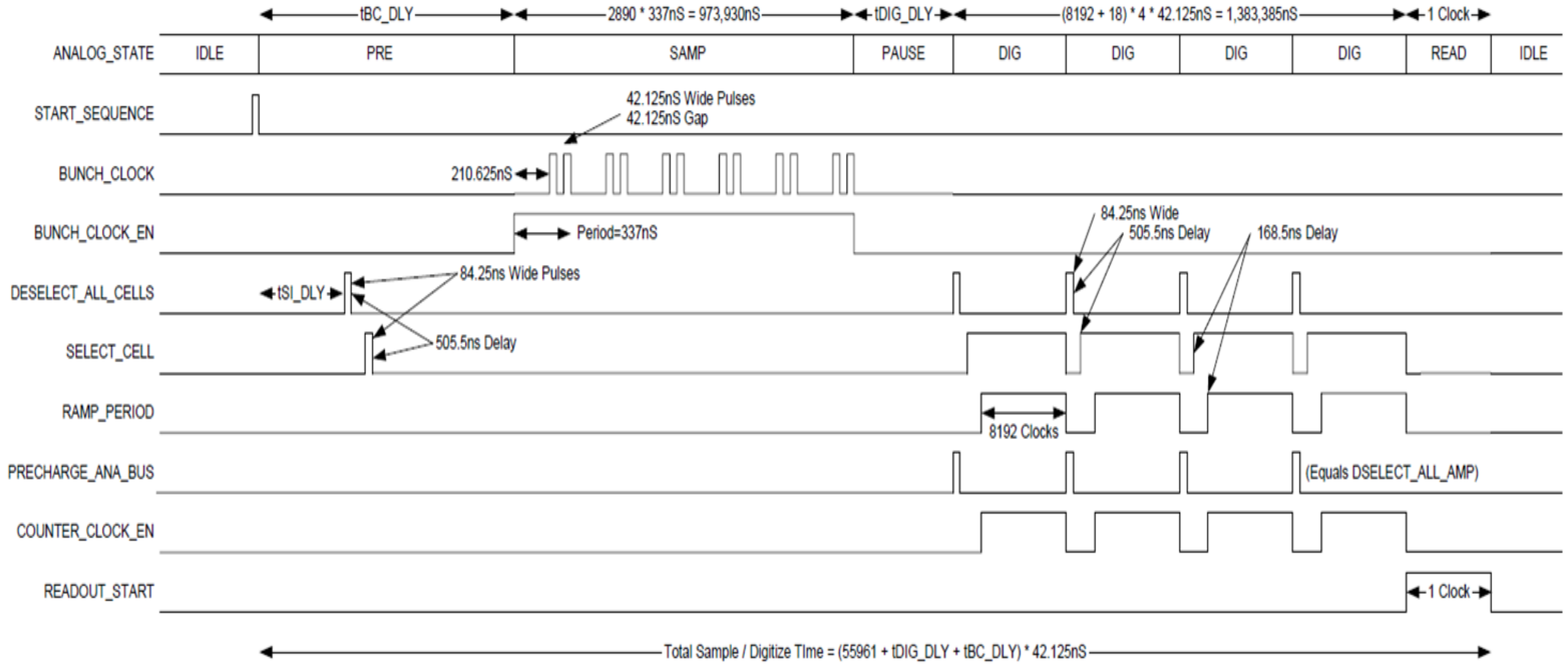

Figure 4.14 Timing chart of the digital signals during a KPiX acquisition cycle. The name for each signal is on the left. ANALOG_STATE describes what the digital signals are doing to the analog signal. The sample cycle is the duration of the BUNCH_CLOCK. The start of each acquisition cycle is initiated by the START_SEQUENCE signal. The time samples where triggers are accepted are initiated by the BUNCH_CLOCK signals that occur 2890 times.

KPiX electronics also have the capability to operate in different trigger and gains modes. Self trigger and force trigger are the two trigger modes. Normal, double, and low refer to the gains modes. Currently double GEM detectors at UTA use the Normal gain mode. Self trigger allows the KPiX to decide what ADC values to trigger a read. Force trigger only triggers a read depending on the source of the trigger. There is an internal trigger and external trigger option. Radiation sources are measured using the internal force trigger option while cosmic rays are measured using a scintillation counter coincidence as an external force trigger.

Self trigger and force trigger refer to the method that KPiX uses to determine the charge contained in the analog signal. Self trigger mode collects charge from the analog signal when a pulse exceeds a threshold. As part of a digital calorimeter system, this trigger method will eventually be used. For chamber development and characterization the force trigger method is used. This method allows KPiX to receive external triggers. This is useful when characterizing GEM chambers with cosmic-ray muons, radiation sources and at test beams. Force trigger may also come from internal circuits of KPiX. Initial radiation source measurements are performed using the internal calibration circuit as a force trigger. The advantage of using internal triggers is that the signal always occurs at the sample time and its behavior is most similar to calibration.

If KPiX is a viable option as the readout electronics for a GEM based ILC Digital Hadronic Calorimeter then it must be shown to reliably and consistently take data. Calibrations provide the means for testing these qualities as well as understanding GEM chambers. The calibration of KPiX electronics must make systematic measurements of various parameters to that reliable and consistent data can be taken and analyzed. Any fluctuation of the characteristic electronics noise behavior must be precisely measured and if possible investigated to minimize.

Internal circuits provide the means to self calibrate. A circuit diagram for one channel is shown in Figure 4.15. It consists of four capacitors controlled by a shift register. An external, from the circuit but within KPiX electronics, DAC supplies voltages to these capacitors. The calibration circuit also has its own trigger source that relates to the main reset and trigger logic. Together all four capacitors act as input just like that of the chamber input and assembled in such a way that

KPiX can inject known amounts of charge to the main input for each channel and each bucket triggering the system accordingly and provide electronic gain measurements.

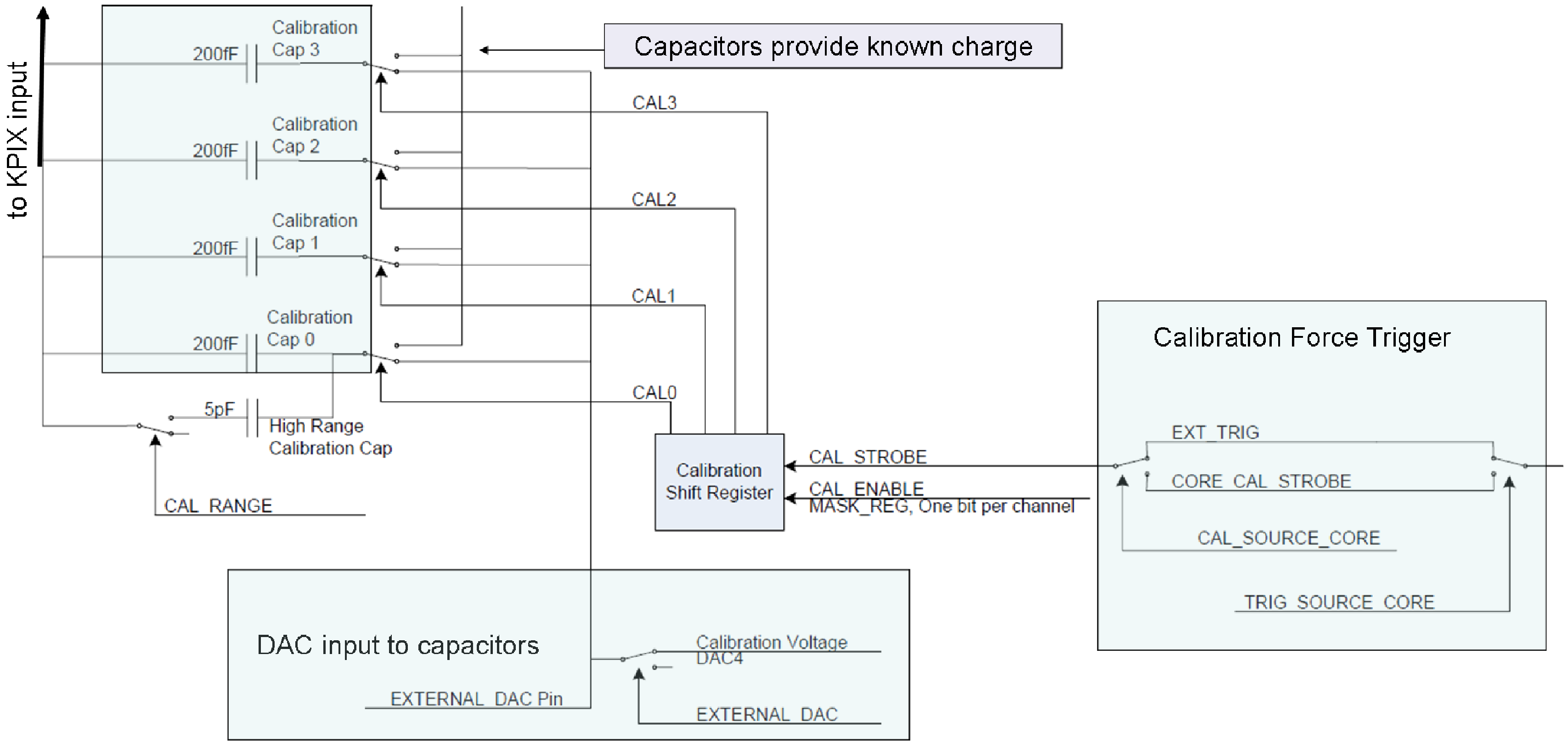

Figure 4.15 Schematic shows the calibration circuit for single KPiX channel. A digital to analog converter, or DAC, generates a voltage as in input to 4 available capacitors. Capacitors generate a known amount of charge as input to the KPiX. KPiX is triggered with a calibration force trigger synchronized to the KPiX acquisition cycle rate.

4.6.1. Calibrations

The KPiX system performs two tests within a single calibration measurement. One test is known as pedestal distribution and the other as gain calibration. The pedestal distribution determines the mean noise level of the system. This test records charge information from the analog signal 4000 times from each of the channels without any charge injected or incoming signals and histograms the associated ADC counts. The pedestal is the noise or reference level for all signals. In other words, it is the zero point. Due to the level of noise in the dense KPiX electronics there is an offset in ADC counts so that zero femto-Coulombs (fC) input is not equivalent to zero ADC counts. As a result, if calibrations are done correctly, the distribution should be Gaussian. Using tools in ROOT [46] (a data analysis framework), a gaussian function is fit to this distribution.

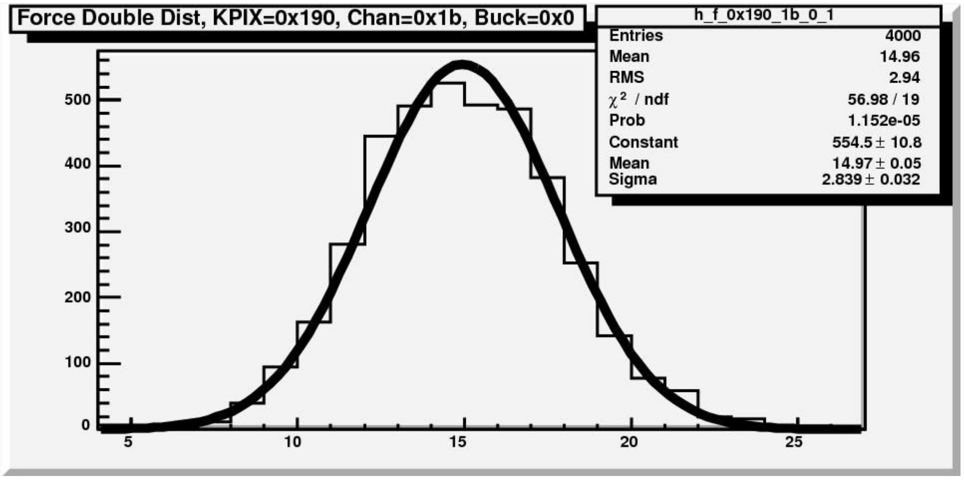

Figure 4.16 An example pedestal distribution form calibration. This particular calibration is performed in force trigger double gain mode on channel 27 (1b in hexidecimal)

Figure 4.16 shows the result of fitting a pedestal distribution with a gaussian function. The mean value from the gaussian fit represents the pedestal and width represents fluctuation of the noise. Gain is determined by injecting incremental amounts of known charge to the electronics input and plotting the resulting output ADC value. The slope of a graph, as shown in Figure 4.17, of ADC counts vs. injected charge in Coulombs represents the gain calibration constant. These calibrations can be performed for every available modes of operation.

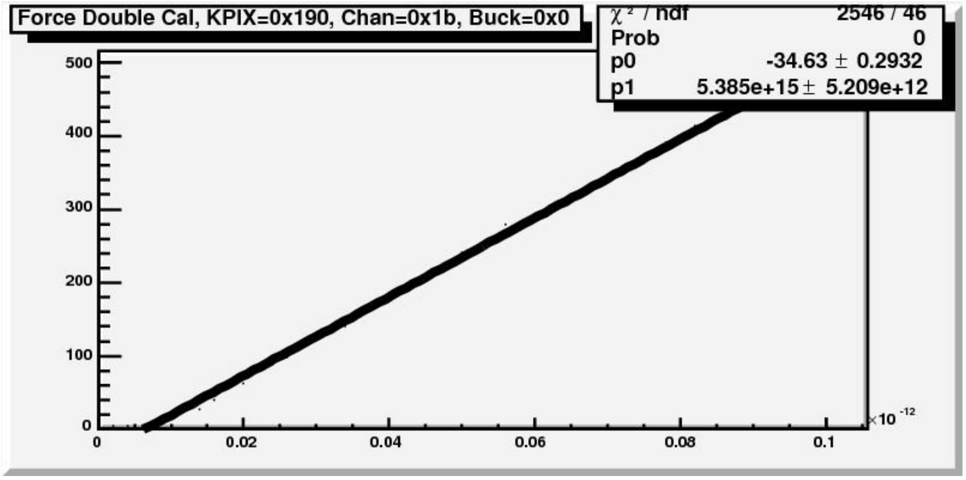

Figure 4.17 An example gain graph from calibration from force trigger double gain on the same channel as pedestal example directly above.

A calibration must determine the benchmark for all operational modes. Currently there are two working versions of KPiX, version 4 and version 7. The modes of operation include, trigger, gain, channel, and bucket. There are two trigger modes, three gain modes, 32 channels in version 4, 64 channels in version 7, 4 buckets, and 2 calibration tests consisting of 4 parameters. In total then for version 4 there are 3072 measureable parameters per calibration and in version 7 there are 6144. Furthermore, a complete calibration analysis requires more than a few calibration runs for each version. The book keeping is an analysis project on its own. The complexity of calibration and subsequent analysis is shown in Figure 4.18.

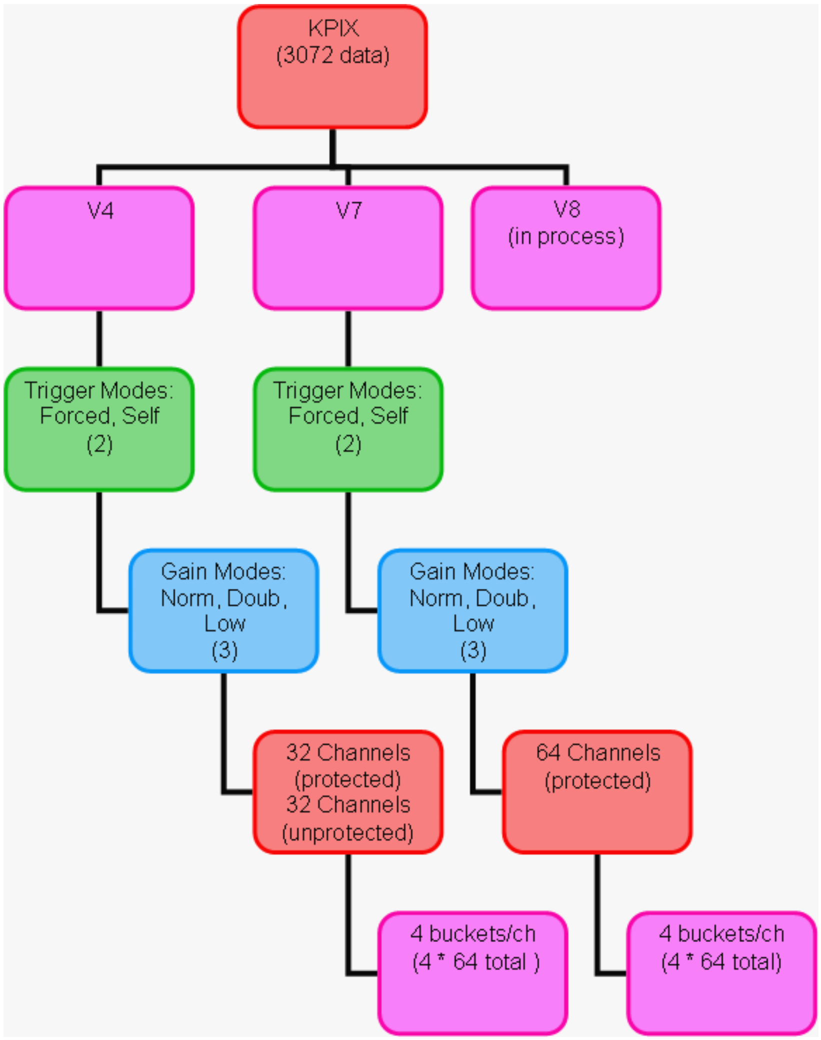

Figure 4.18 A diagram of the complexity of operational modes in KPiX version 4 and 7.

4.6.2. KPiX Version 4

Version 4 is the first working version of KPiX integrated with UTA prototype double GEM detectors. A majority of the version 4 analysis is completed on calibration data only employing a force trigger mode and normal and double gain modes for 32 protected channels. There is a circuit on the input side that protects KPiX electronics from discharges in the chamber. For the calibration and data analysis only the first bucket is considered. Part of the original data taking code developed by SLAC uses a single calibration run's pedestal and gain parameter to shift data distributions and convert ADC counts to fC. This is analogous to converting potential to charge as discussed in Chapter 4. An accurate calibration's application to data should successfully shift data distributions from its ADC offset to zero fC. On the contrary, this is not the case for the majority of data runs with radiation sources. This evidence suggests that pedestal measurements from calibrations fluctuate with time. The analysis of calibration data seeks to discover, understand and quantify fluctuations and inconsistencies. Calibration experiments and analysis are discussed in section 4.8.

4.6.3. KPiX Version 4 30 cm x 30 cm GEM Chamber

The first integration of KPiX with GEM chambers is version 4 with a 30 cm x 30 cm GEM Chamber. For this chamber the center 8x8 area of pads is connected to KPiX, 32 protected and 32 unprotected. One side of 4x8 pads is connected to 32 protected channels and the other side of 4x8 pads is connected to 32 unprotected channels of KPiX. The chamber is enclosed in a grounded aluminum box. The chamber itself is airtight and also uses Argon Carbon Dioxide 80:20 gas mixture.

4.7. KPiX Version 7 30 cm x 30 cm GEM Chamber

Version 7 is the second version of KPiX integrated with UTA double GEM chambers. The upgrades to version 7 include hardware and software. Version 7 refers to a different hardware setup and new software programs. The software upgrades to KPiX 7 include a new GUI program to take data and perform calibration tests and self trigger functionality with threshold determination programs. Hardware upgrades include self-trigger functionality, input protection circuits and a refined method of integrating analog signals.

The self trigger operation is available, all 64 channels are available for readout, a new anode board is in place, and the periodic reset has been replaced with a DC reset. An advantage of self trigger mode is that KPiX can take data with an asynchronous particle source. This is beneficial to experiments requiring test beams at Fermilab and a radiation source. KPiX is originally designed for use in the precise beam structure timing of a future International Linear Collider. The means that in order to take data as designed a timed beam must be provided to GEM. The option is extremely inconvenient and impossible for testing UTA double GEM chambers with currently available methods. Prior to the release of KPiX Version 7 SLAC closed its electron test beam user facility that can provide an ILC designed beam structure synchronous with KPiX.

The protection circuit now consists of two diodes between AVDD and AGND to protect the KPiX electronics from signals more positive than AVDD and less negative than AGND. Signals also must go through a resistor before coming to the KPiX electronics. Shown in Figure 4.19, the protection circuit consists of two zener diodes and a resistor.

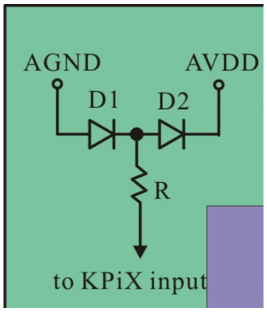

Figure 4.19 Circuit diagram of KPiX 7 protection circuit for each pad.

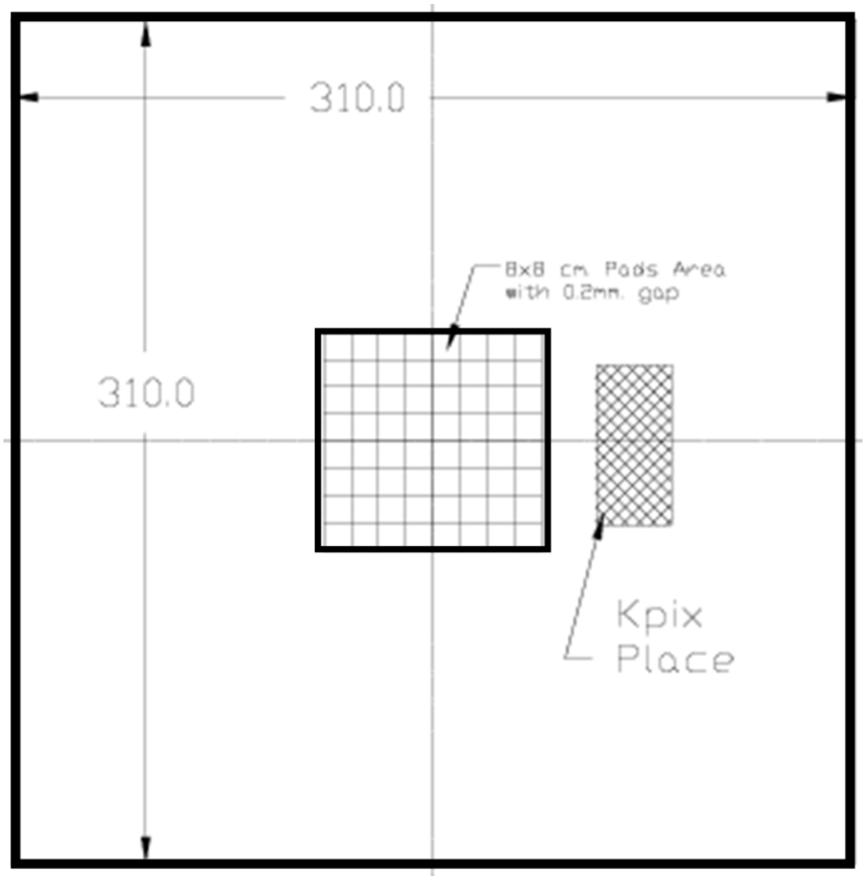

Figure 4.20 Schematic of chamber size references to integrated KPiX readout anode board. The actual size of complete chamber is 310 mm or 31.0 cm.

The second integration of KPiX with large GEM chambers uses version 7 of KPiX. This version is upgraded with a new protection circuit for all 64 channels. In version 4 the complete anode board was utilized for readout pads but in version 7 only the center 8 x 8 area of the anode board is equipped with 1cm^2 pads area and surrounded by bare FR4. A series of resistors is still used to distribute potential difference to each region. The resistor network to distribute voltage to the difference regions is shown in Figure 4.21.

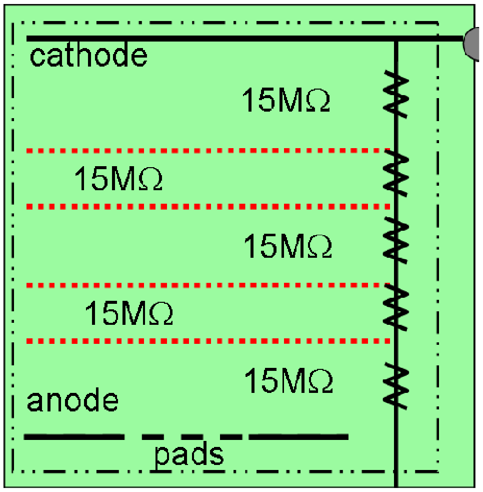

Figure 4.21 Resistor network of KPiX V7.

The spacing of the ionization, transfer and induction regions were all increased. The spacer consists of plastic fishing line 0.8 mm in diameter. The ionization region is now 3.8 mm, the transfer region is 1.6 mm and the induction region is 1.6 mm. As a result the path length for MIPs increases making pulses about 250 ns wide. Figure 4.22 shows the new spacing structure of the KPiX V7 based GEM chamber. The red lines represent the GEM foils, the blue circles represent the fishing lines, the bottom black line represents the anode board and the top structure is the white plastic frame with the recessed area covering the center 8 x 8 center area pads.

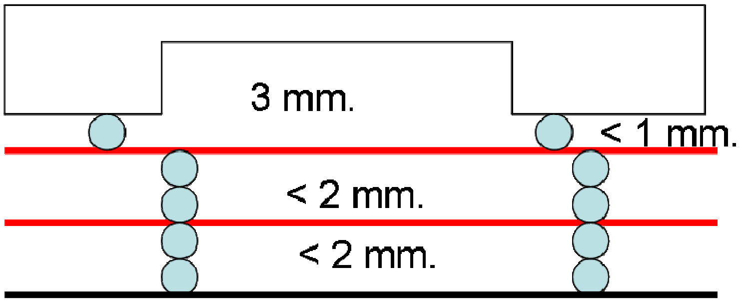

Figure 4.22 Side view of KPiX V7 GEM chamber showing spacing between foils, anode and cathode.

The chamber design was also modified for the new KPiX version 7. It uses a plastic frame that uses fishing line to separate GEM foils. It also has a built in hole in the center for radiation sources. The center 8 x 8 area of pad is used for readout and signal charge collection.

4.8.KPiX Calibration Studies

Calibrations are the source of operational parameters the KPiX software and user needs in order to make physical interpretations from digitized data. Physical interpretation of detector output are based on the data output and are useful to measurements such as chamber response, gain, and efficiency. Therefore, consistent and reliable calibrations are necessary aspects of the physics conclusions made about the detector. Not only do calibrations relate digital data to physical data but they also describe the performance of the detector electronics. A thorough study of the behavior of calibrations describes dependencies on time, chamber high voltage, electrical environments, functional fitting, and KPiX operational modes. Since the chamber and its associated electronics must perform consistently over time a study of calibration performance with respect to time is very important.

The main parameters for a calibration analysis are the mean and sigma values attained from fitting pedestal distributions with a Gaussian function and gain values from calibration's ADC vs. Injected Charge graphs. Each of these three calibration constants also has an associated uncertainty. They are called constants because they are provided as calibration values for data taking runs. A long list of questions must be answered about a new detector system. Calibrations provide a way to answer many of these questions. Here is a list of questions calibration studies in this thesis aim to answer.

- How well do the functional fits describe calibration data?
- What are the criteria to determine a “bad” channel?
- What experimental conditions would require a particular trigger and gain mode?
- How does ext trig cable effect calibration constants?
- Are there any other side effects of external connections to KPiX?
- How do the buckets in each channel relate to each other?
- How much do constants and their uncertainties fluctuate between channels?
- How do buckets in channels relate to other channels?
- How do the buckets fluctuate over time?
- How do the constants change over time?
- Do the buckets fluctuate over time?
- What is an “acceptable” amount of fluctuation for each constant?
- How do the fluctuations between KPiX version 7 and 4 compare?
- How do the allowable ranges of fluctuations compare between versions?
- Is KPiX a reliable and consistent DAQ system for Double GEM detectors?

4.8.1. KPiX Version 4

An accurate calibration’s application to data should successfully produce histograms in units of absolute charge. Absolute charge represents the charge produced in GEM chambers by ionization from MIPs only. This is done by subtracting each event in data by the pedestal and then dividing by the gain. Subtracting the calibration pedestal constant in this way removes effects from DC offset and allows gain to convert ADC values to absolute charge. The success of the first step, subtracting pedestal should move pedestal data from its offset to zero.

In order to study the behavior of KPiX electronics over time a set of two series calibrations are performed. Each series of measurements starts a calibration every hour. One set is a 19 hour multi-calibration and the other is for 24 hours. The 19 hour multi-cal took place over the weekend and in the middle of the night through morning. The 24 hour run took place during the week starting and ending in the morning at 8 am.

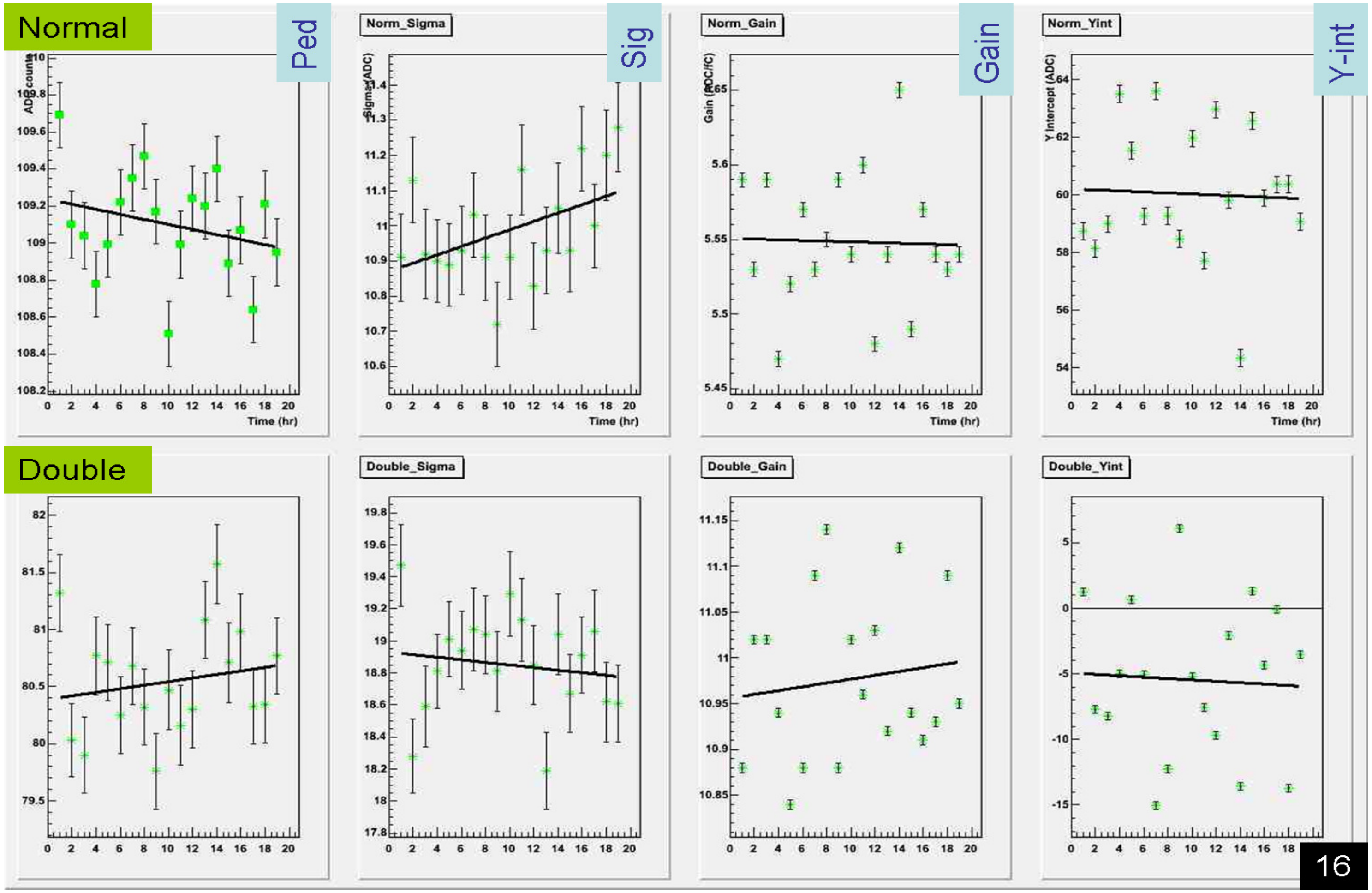

Figure 4.23 Calibration constant versus calibration iteration for 19 calibrations spread evenly over each hour. There are 8 graphs total, one for each constant and KPiX gain mode. The line shows the slope of each constant over time. Although the y-axis is not visible and the slope of the sigma constant for normal gain looks large it is almost zero.

The calibration constant values are plotted in a graph of Constant Value vs. Iteration (Time). Figure 4.23 shows a collection of results for channel 16 from the 19-hour series of calibrations. Each point is the calibration value pertaining to iteration of calibration recorded. For instance, each points the pedestal vs. iteration plot is the mean value taken from a gaussian fit of the pedestal distribution. Evidence of time dependence is suggested by the slope of each line and is called walking rate. To determine the slope, each of the graphs is fit with a first-order polynomial providing a slope and y-intercept. These fit parameters also provide the key characteristic information. If there is little or no slope then KPiX does not have any time dependence in the calibration. The amount of slope depends on the particular constant's effect on data analysis.

Figure 4.24, Figure 4.25, and Figure 4.26 all show the slopes of lines from Constant Value vs. Iteration graphs from the 19 hour calibration studies. The slope from these describes how each calibration constant walks over time. A large slope means that particular constant has a time dependence. A small slope means that calibration constants are constant in time and do not dramatically increase or decrease. This further means that a calibration performed on one day is useful for the next. As a side note, the extent of these time studies is 43 hours combined. A long term study, over many days, has not been thoroughly performed.

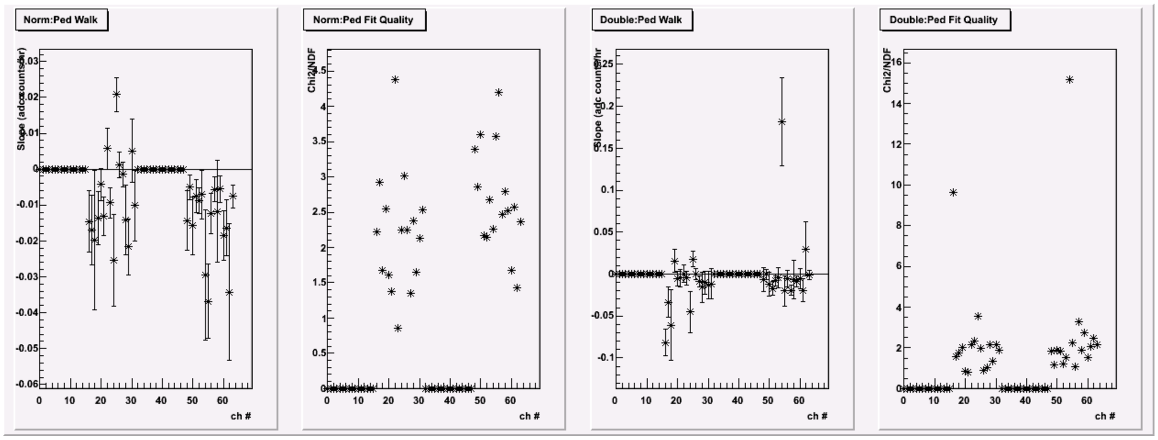

Figure 4.24 From left to right these are graphs of normal gain Pedestal Walk and Fit Quality and double gain Pedestal Walk and Fit Quality all as a function of channel number.

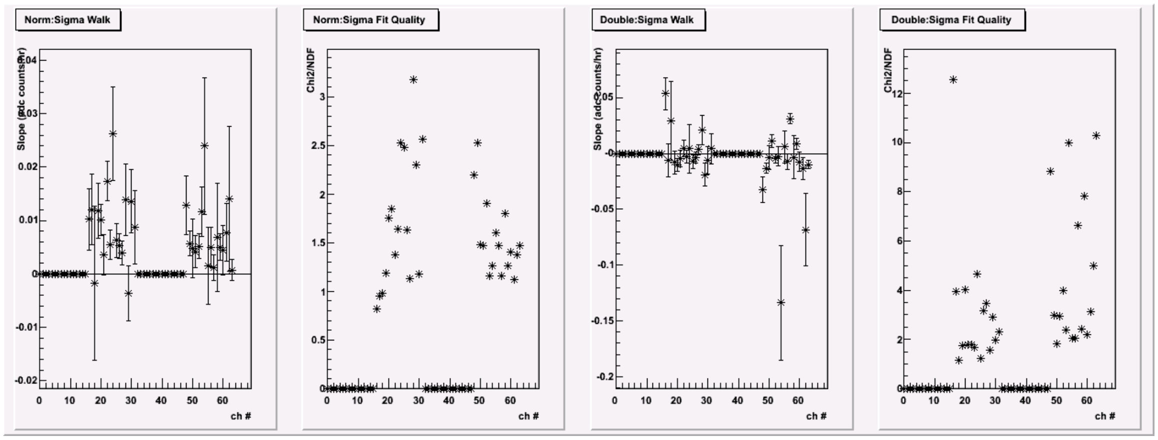

Figure 4.25 From left to right these are graphs of normal gain Sigma Walk and Fit Quality and double gain Sigma Walk and Fit Quality all as a function of channel number.

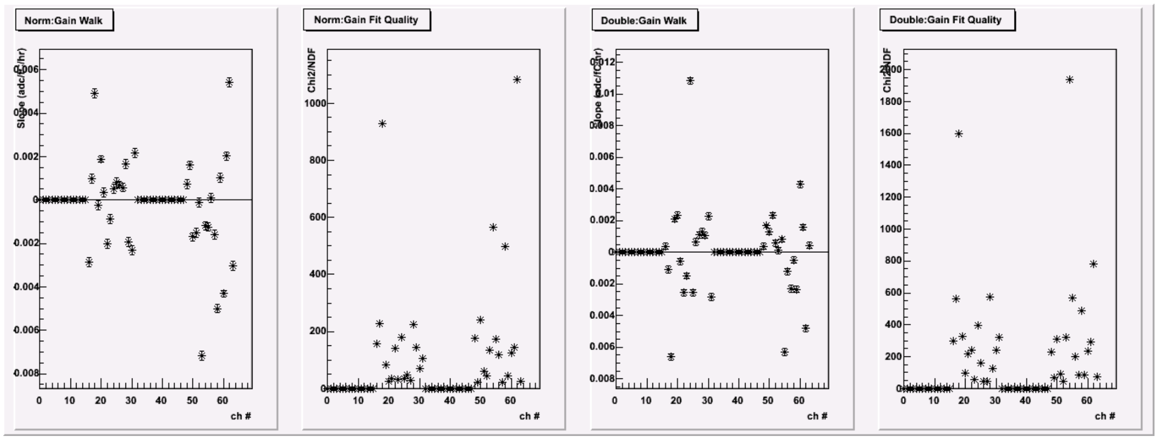

Figure 4.26 From left to right these are graphs of normal gain Gain Walk and Fit Quality and double gain Gain Walk and Fit Quality all as a function of channel number.

Since each of the Constant Value vs. Iteration graphs is fit with a first-order polynomial there is an associated fit quality. This fit quality must also be examined. The fit quality cannot be ignored because a line may not accurately describe the data. For instance if the slope is near zero but fluctuates heavily such that a line results in a poor fit quality then the slope does not describe the calibration dependence on time but rather on some other quantity.

Figure 4.24 refers to the mean value calibration constant. The center line is zero and the maximum point is less than 0.06. This means that the mean value does not fluctuate over a 19 hour period. The fit quality for normal gain mean values is also never more than 5. This is an acceptable value. Therefore, in a 19 hour period normal gain is consistent and reliable. Double gain also shows reliable behavior. There are two channels that do not behave properly. For double gain mode these channels can be classified as bad channels. Except for the two bad channels normal and double gain behave in a comparable manner.

Figure 4.25 refers to the sigma value calibration constant. This is a measure of the noise in each of the channels. In normal gain operation, sigma values performs much like the case of the pedestal mean values in that there is no considerable fluctuation or time dependence. This makes sense because both constants derive from the same histogram. There are about 6 bad channels in the double gain mode. These 6 bad channels are identified by the fit quality. Any fit above 6 is classified as a bad channel. In double gain mode there is an 82% acceptance.

Figure 4.26 shows the gain value calibration constant. This is the most meaningful and sensitive constant. It is alone responsible for converting ADC values to charge values in units of charge. A large fluctuation or uncertainty in this constant supports a high level of concern for the reliability and consistency of KPiX. All channels in normal and double gain mode have less than 0.12 slopes in the gain over time. Unfortunately, the fit quality is very poor. Naively, if fit quality is poor this means a line does not describe the gain values from calibrations.

Since it is determined from the first-order polynomial fits that calibration constants do not rise or fall with respect to time it can be assumed that there is a mean value for each constant. This study focuses on the average fluctuation of gain and pedestal from the mean over time. Figure 4.27 describes the time dependence considering all 43 hours of calibrations for a typical channel with a focus on the percent fluctuation from the mean. This figure shows that pedestals fluctuate less than 1.8% from the mean while gains fluctuate just over 3.3% from the mean in normal gain mode. For double gain mode there is a 4.5% fluctuation of the pedestal and a 2.5% fluctuation of the gain. Although the gain for double gain mode is more consistent than normal gain mode this behavior is less typical in the sense there are more non operational channels in double gain mode than in normal gain. Even still, a 3.3% fluctuation in gain is acceptable although a lower fluctuation is more desirable.

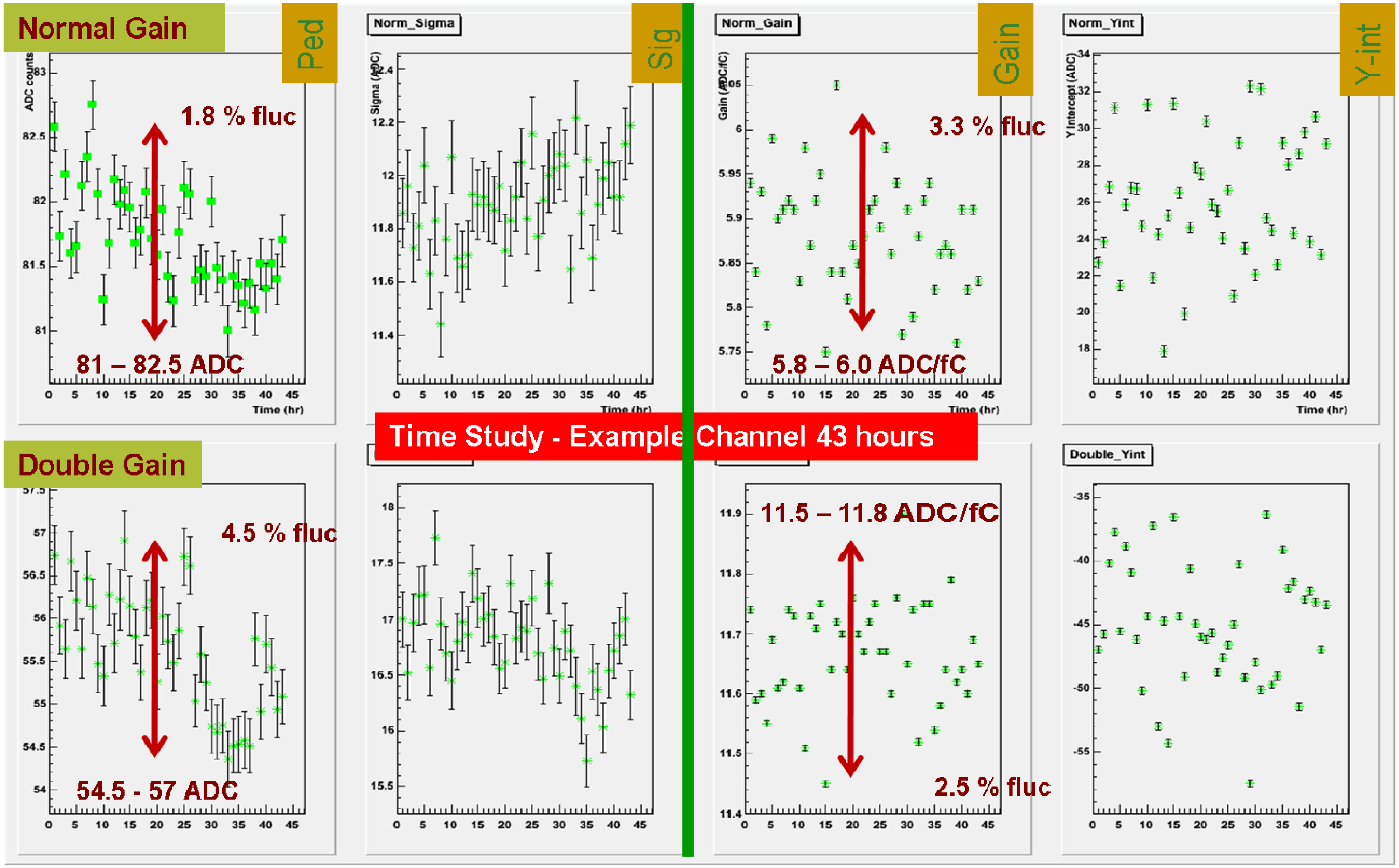

Figure 4.27 Time dependence graphs of calibration constants for normal and double gain mode in version 4. All graphs cover a total of 43 hours of calibrations.

The variation of pedestal and gain constants between the channels is also an important measurement. This characterization describes the consistency and percent acceptance of usable channels. Figure 4.28 shows the channel to channel variation for pedestal and gain. Pedestal values fluctuate between 20 to 130 ADC counts, more than a factor six variation. Gain values go from 5 to 20 ADC/fC, a factor 4 variation. Channel to channel variation of gain is a cause of concern because two adjacent pads with factor 4 gain variations effect the electronics' measurement of pulse height. Too much variation may adversely effect the quality of KPiX as part of a digital detector that uses a threshold based on pulse height.

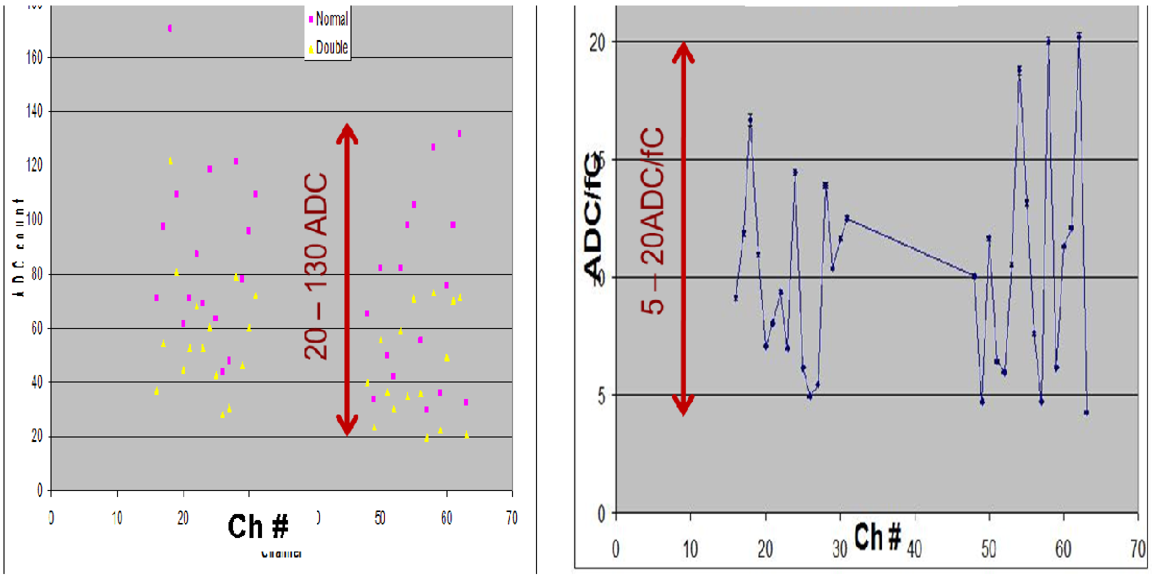

(a) (b)

Figure 4.28 Channel to channel variation of pedestal (a) and gain (b) for version 4. Graph (a) is the pedestal mean (ADC counts) for each channel in double and normal gain mode. Graph (b) is the gain (ADC/fC) for each channel in normal gain mode.

4.8.2. KPiX 7 Fit Range Study

In version 7 of the KPiX calibration software the user selects the appropriate range of injected charge to fit the gain calibrations. The range selected determines the gain value used and stored as a constant. Since the gain constant is such an important calibration constant an investigation of its determination criteria is important. The goal of this study is to determine the most accurate way of assigning the proper fit range for gain calibrations.

The user will perform a calibration and then, looking at the graph of ADC vs injected charge, choose the fit range and save the data. During this time the user can see on the screen how well the fit line describes the data points by observation only.

In order to study the effect of fit selection, fit ranges are selected in increments of 10 fC starting at 0 up to 200. (ie 0-10, 0-20,…0-190, 0-200). The gain value (ADC/fC) and pedestal value (fC) is then plotted for each range. Note, pedestal ADC value is converted to fC using gain value parameter. Based on the calibration graph 0-130 fC is chosen as the benchmark range and used to calculate the standard deviation, uncertainties, and average for all other range windows. This range is chosen because it is the maximum range that is conservatively within the average of most range selection options.

Figure 4.29 is a graph of the gain and pedestal value as a function of fit range for a given channel in normal gain mode. The x-axis represents the maximum value of the range selection. The minimum value is always 0. The y-axis is the gain and pedestal value resulting as a function of range. The pedestal is given in units of fC to observe the gain’s effective usage. This is important because the best range should be chosen that represents the pedestal linearly. Between 30 and 150 maximum range values there is no change in either gain or pedestal. Therefore, the fit selection method based on user observation is valid and provides a good determination of the KPiX electronics gain.

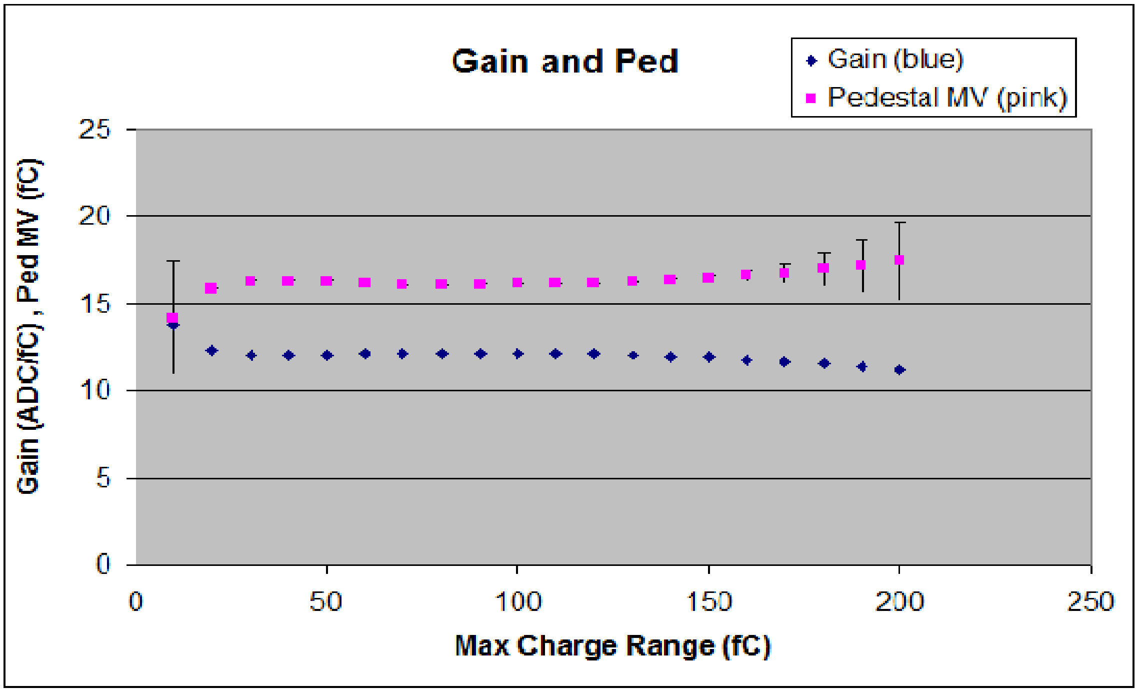

Figure 4.29 Fit Range selection graph showing gain and pedestal effects as a function of fit range selections. The x-axis is the upper end range and the y-axis is gain (blue) and pedestal (pink).

4.8.3. KPiX 7 Calibration Constant Comparison

A typical well behaved channel's pedestal calibration in version 7 of KPiX is represented in Figure 4.30. The distribution is fit with a Gaussian function by the ROOT analysis framework and the statistics are shown in the box on the right. This example shows Normal Gain value for Channel 30 in bucket 0. Based on correspondence with the SLAC KPiX designers normal gain is decided to be a sufficient operational mode for GEM-KPiX chambers at this time.

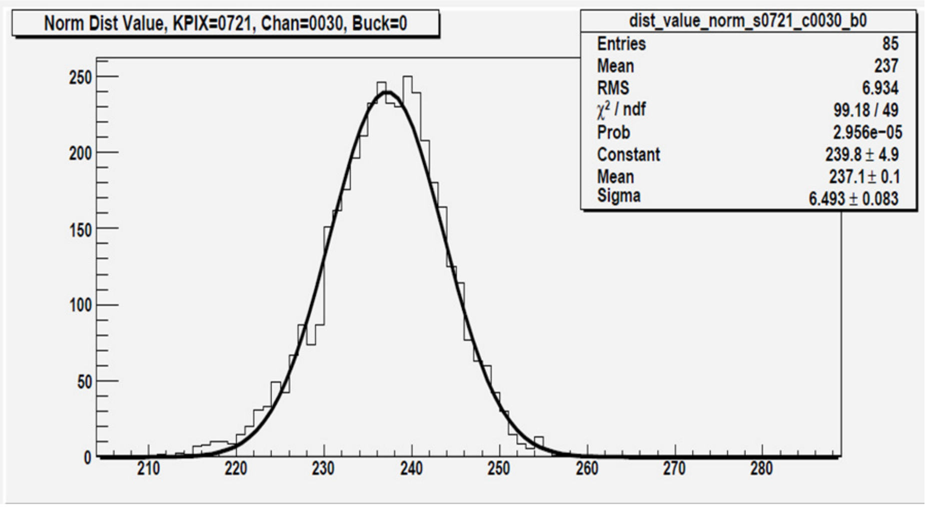

Figure 4.30 Typical behavior from pedestal calibration in KPiX version 7. The distribution is fit with a Gaussian function by the ROOT analysis framework and the statistics are shown in the box on the right. This example shows Normal Gain value for Channel 30 in bucket 0.

A typical gain calibration is shown in Figure 4.31. Figure 4.31 (a) is the main graph of ADC counts versus injected charge. The slope determines the gain. Part (b) shows the sample time that each charge was triggered. The calibration is set to trigger at the same time for all injected charges. In this example calibration the gain is 9.363 ADC/fC and triggered at a sample time of 2563.

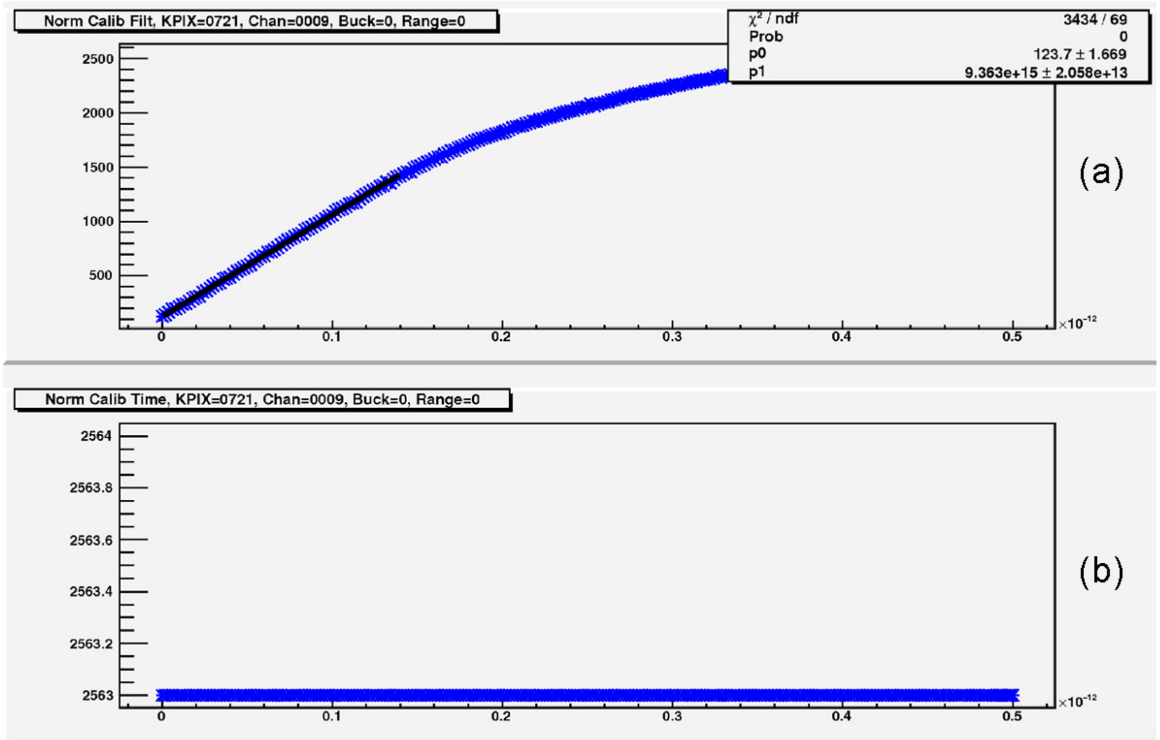

Figure 4.31 Typical calibration curves from gain calibration. Gain is the slope in (a) and the sample time for each point from (a) is plotted in (b) for the injected charge.

The initial measurements consist of performing calibrations and making observations to understand and characterize version 7 behaviors. It is expected to perform at least as well or better than version 4 but an increase in performance beyond extended functionality is desired.

The variation of pedestal and gain constants between the channels is also considered in version 7. This characterization describes the consistency and percent acceptance of usable channels. Figure 4.32 shows the channel to channel variation for pedestal and gain from version 7. Pedestal values fluctuate between 40 to 120 ADC counts, a factor 3 variation. Gain values go from 3.5 to 6.5 ADC/fC, a factor 2 variation. Recall from section 4.8.1 that version 4 saw a pedestal variation of factor 6 and gain variation factor 4. Therefore KPiX version 7 has a total factor 2 improvement in the channel to channel fluctuation of pedestal and gain calibration constants.

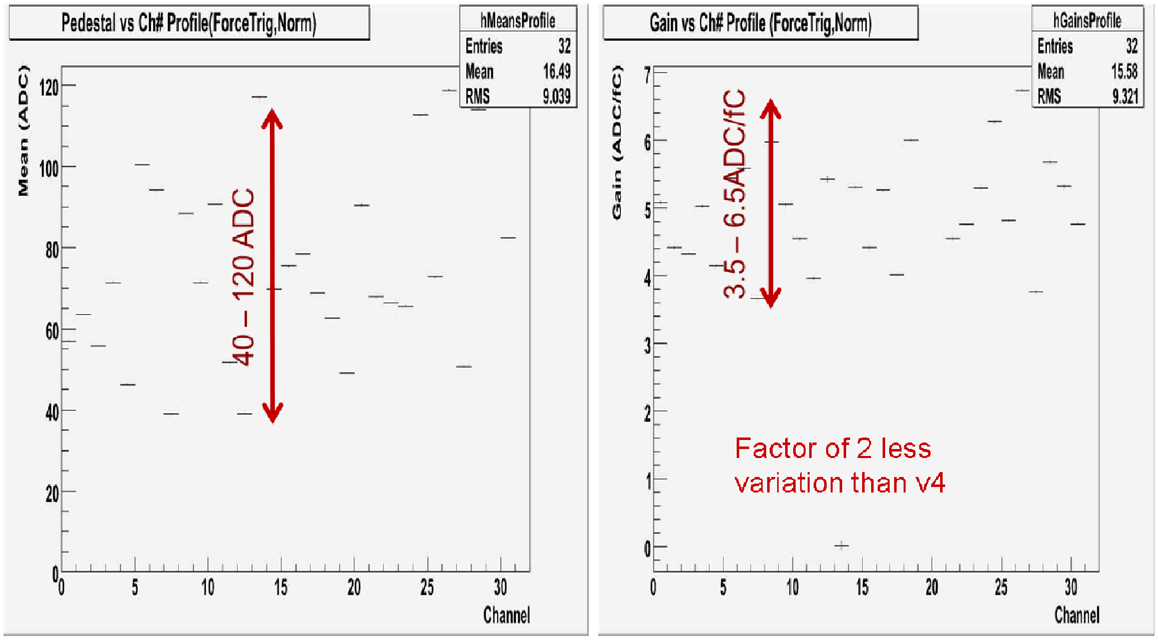

(a) (b)

Figure 4.32 Channel to channel variation of pedestal (a) and gain (b) for version 7.

CHAPTER 5

HIGH VOLTAGE AND GAS MIXTURE

5.1.Introduction

High voltage applied across the GEM chamber, the resistors connected between them and the GEM foils, and the spacing of all regions and GEM foils determines the electric field everywhere. The most important field region for the amplification of ionization electrons is between the top and bottom copper layer of each GEM foil. Therefore the optimum high voltage settings must be used in order to sustain the life of the chamber as well as produce the largest sustainable gain. This chapter describes the tests performed to determine operational HV and gas mixture for double GEM chambers.

The gain of the chamber is also sensitive to the mixture ratio of the gas that fills the inner volume. For all studies and measurement performed with GEM chambers at UTA some mixture of argon and carbon dioxide is used. There is an observable difference as much as a factor of 3 between different gas mixtures.

5.2.Experimental Setup

This section will discuss the experimental setup used to determine operational high voltage and gas mixture. Results for the optimum operation high voltage and gas mixture ration come from a single set of experiments. These experiments use the 10 x 10 cm2 prototype GEM chamber in combination with a radiation source as the source of incident charged particles. Two radiation sources, Sr-90 and Cs-137, are used to collect pulse height distributions from the GEM chamber. Readout electronics record pulse height distributions from the radiation sources using a self triggering mechanism.

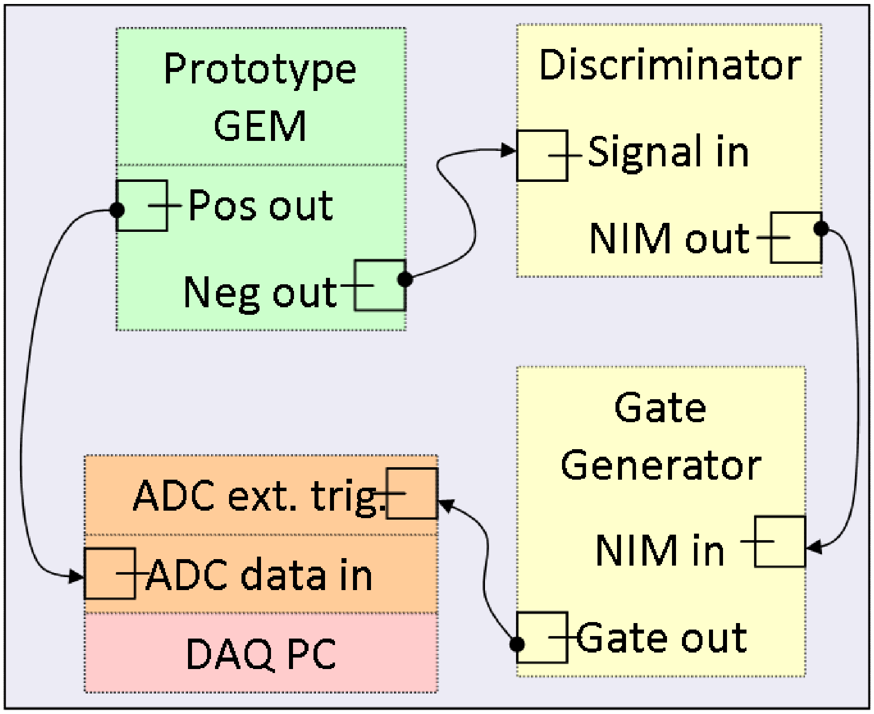

Figure 5.1 Flow chart of the electronic system used for HV and gas mixture. Signals are generated in the GEM chamber indicated in the green box. Preamp positive output is used to record data signals by the ADC. Preamp negative output is used for the trigger signal. A discriminator sends a NIM standard signal to a gate generator when the pulse height from the preamp's negative out is below -61.4 mV. The gate generator sends a variable width NIM standard signal to the ADC ext. trig to trigger the ADC to read from the input.

Figure 5.1 is a flow chart of the electronics setup of the experiments to determine the optimum operational HV. In this experiment we apply a high voltage (1800 to 2100 V) to the GEM chamber. The applied high voltage provides each GEM foil different potential difference depending on the HV to produce an avalanche of electrons. The resistor network remains constant throughout this experiment, providing a fixed proportion of the voltage drop across each gap in the detector. First, the analog signal from the GEM chamber is sent the preamp card. Then the positive signal goes to the AD811. The ADC converts the analog signal from the GEM chamber into a digital signal that is read and stored in histograms by the DAQ computer. The negative output of the preamp is used as the trigger source and is sent to a discriminator whose threshold is set to -61.4 mV. The discriminator sends a NIM standard to a gate generator producing a variable width NIM standard that is sent to the strobe input of the ADC (AD811) to finally trigger the ADC to record the positive polarity analog output from the GEM chamber's preamp card.

Each of the preamp's outputs leaves the preamp at the same time. The trigger signal takes longer than the data signal to arrive at the ADC. As a result, the ADC misses the data signal from the GEM chamber. To ensure the ADC does not miss the data signal a long NIM cable is used between the preamp's positive output and the ADC input. The length of this cable is such that the pulse arrives to the ADC at least 50 ns after the leading edge of the trigger signal. The length of the NIM cable is proportional to the time it takes for a signal to traverse the length of the cable. Therefore, the arrival of the data signal coincides with the arrival of the trigger signal and ADC reads the entire data signal.

5.3.Data

To determine operational high voltage and gas mixture ratio two radiation sources, three gas mixtures, and multiple high voltage settings are varied. The three mixtures of Ar:CO_2 gas used are 70:30, 80:20 and 85:15 where the first number is the argon percentage and the second number is the carbon dioxide percentage. The two radiation sources used Strontium-90 and Cesium-137.

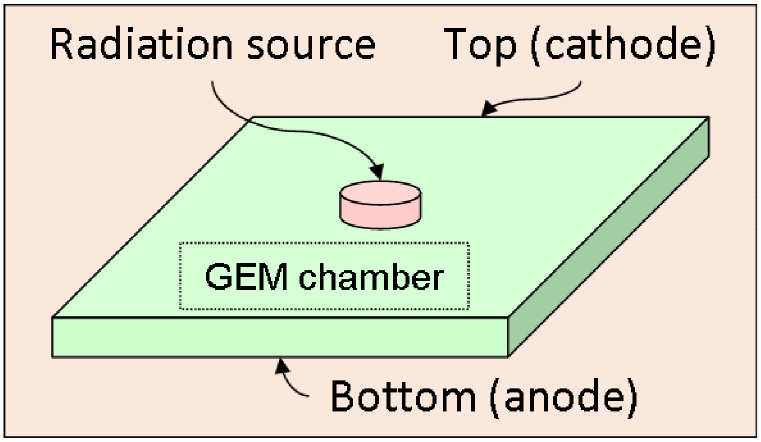

Figure 5.2 Representation of the orientation of the radiation source with GEM chamber. The radiation source is at the center and on top (cathode side) of the chamber providing incident charged particles.

One of the radiation sources is chosen and centrally placed outside the chamber on the cathode side as shown in Figure 5.2. The decay products from the source provide incident charged particles producing signals in the chamber. Since changing gas mixture ratio involves replacing a large heavy supply bottle, disconnecting and reconnecting associated gas supply lines, and purging the chamber of the previous mixture, the gas mixture ratio remains constant while the high voltage is varied for a particular radiation source. The high voltage is varied by adjusting a knob on the high voltage supply located in the NIM crate. The radiation source is replaced by opening the grounded aluminum GEM chamber enclosure and physically removing the previous source and placing the next source. The electronics settings for the trigger remain constant throughout the experiments.

Table 5.1 Energy emission probability for Cs-137 and Sr-90. Emission probability refers to the probability per decay of a given emission including possible cascades.

Source	**Electron Energy (MeV)**	**Photon Energy (MeV)**	**Emission Probability**
Cs-137		0.662	85%
	0.514		94%
	1.176		6%
Sr-90	0.546		100%
→Y-90	2.283		100%

The expectation for pulse height distributions using radiation sources are complex due to the statistical nature of the decays and the material of the GEM chamber. Table 5.1 [41] shows the end-point energy and emission probability of the decay products from Cs-137 and Sr-90. Cs-137 has three decay modes and Sr-90 has two. Emission probability refers to the probability per decay of a given emission including possible decays. End-point energy refers to the maximum available energy but does not represent the distribution for all energies. For every decay mode, most of the electron energy is below the MIP range for each chamber material. The rate of lower than MIP energy emissions is greatest and drops exponentially for larger energy decay products. Furthermore, there is enough energy loss through the chamber material between the source and the ionization region that their energies are no longer in the MIP range as they ionize gas in the chamber. This means that pulse height distributions will not follow a Landau distribution and gain is not directly measured.

5.4.Results

Results from Ar:CO_2 mixtures are shown in Figure 5.3, Figure 5.4 andFigure 5.5 for 70:30, 80:20 and 85:15 respectively using the Cs-137 radiation source for the various HV settings noted in the figure. Figure 5.6 shows the results of 85:15 gas with Sr-90. The maximum range of high voltage used for each gas mixture depends on the number of discharges within five minutes. If the number of discharges is more than zero then the high voltage is turned down until the number of discharges is zero. Previous work [47] with GEM detectors has shown that gain increases as voltage across each foil increases and as the Argon ratio increases. The x-axis for these graphs is in units of mV and represents the pulse heights of signals produced by charge particles incident from the radiation source. The location of the second peak along the x-axis is a representation of the chamber gain. Chamber gain increases this peak moves to the right along the x-axis. Also, a flattened distribution reflects the increased amount of ionization from non-MIP particles.

For the Cs-137 test there is a moving second peak and a third peak on the high end. The second peak moves with the increasing HV and argon ratio. This is because the potential difference between each layer also increases with HV increasing the gain. Increasing HV increases the electron avalanche through each foil. The lowest energy emission from Cs-137 is the 0.514 MeV electron and the 0.662 MeV photon. These are on the lower edge of the MIP range and as these traverse through the detector material between the radiation source and ionization region they lose energy. As a result, these particles are no longer in the MIP range for any of the Ar:CO^2 mixtures and ionize the gas more than MIPs. The Sr-90 test does not have the moving second peak because this source does not emit photons but only electrons. Therefore the first peak in Cs-137 and Sr-90 distributions is a result of the electron and the second peak in the Cs-137 distributions are due to the photon.

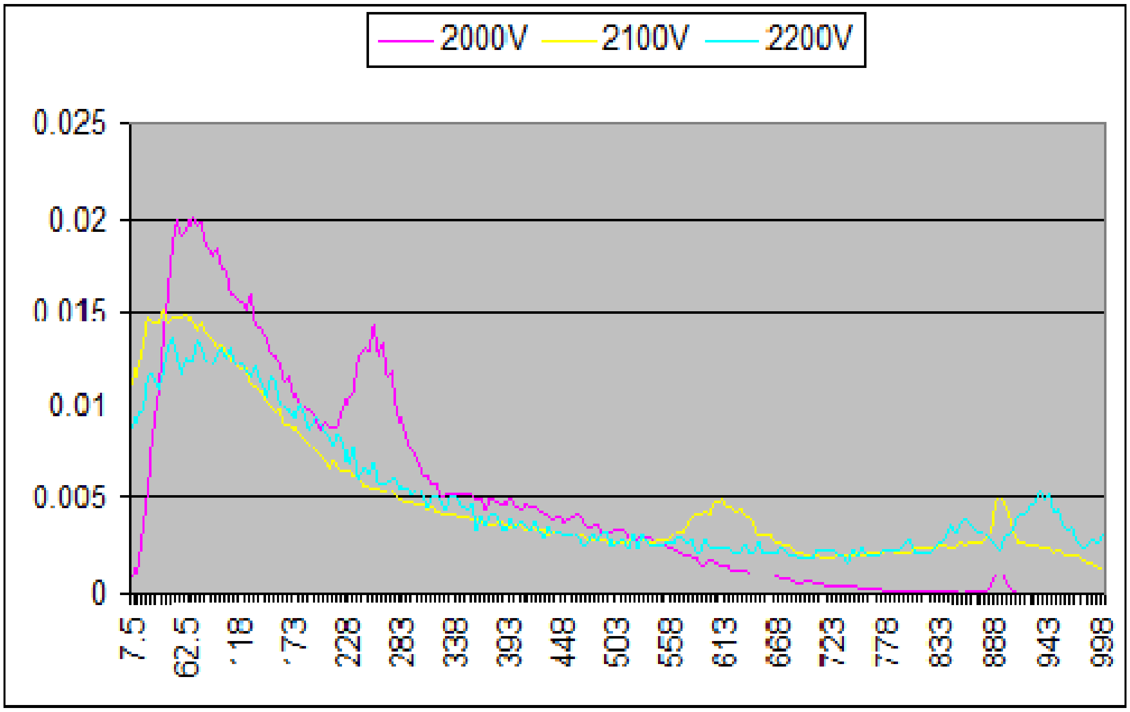

Figure 5.3 Cs-137 pulse height distribution with Ar:CO_2::70:30.

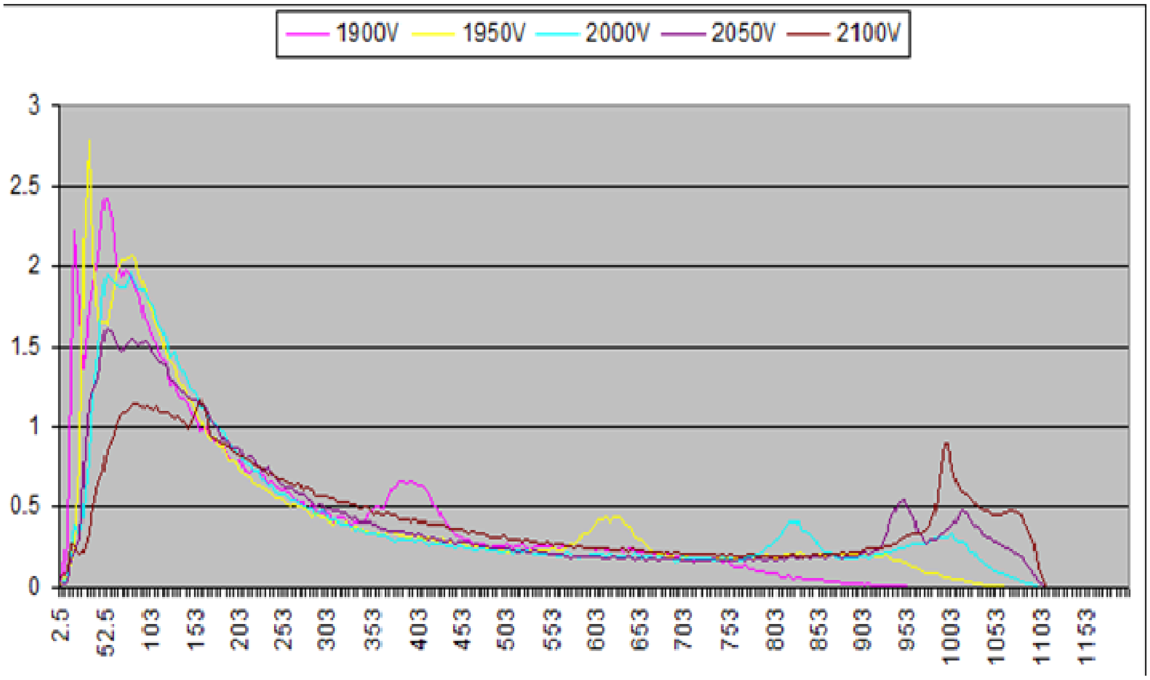

Figure 5.4 Cs-137 pulse height distribution with Ar:CO_2::80:20.

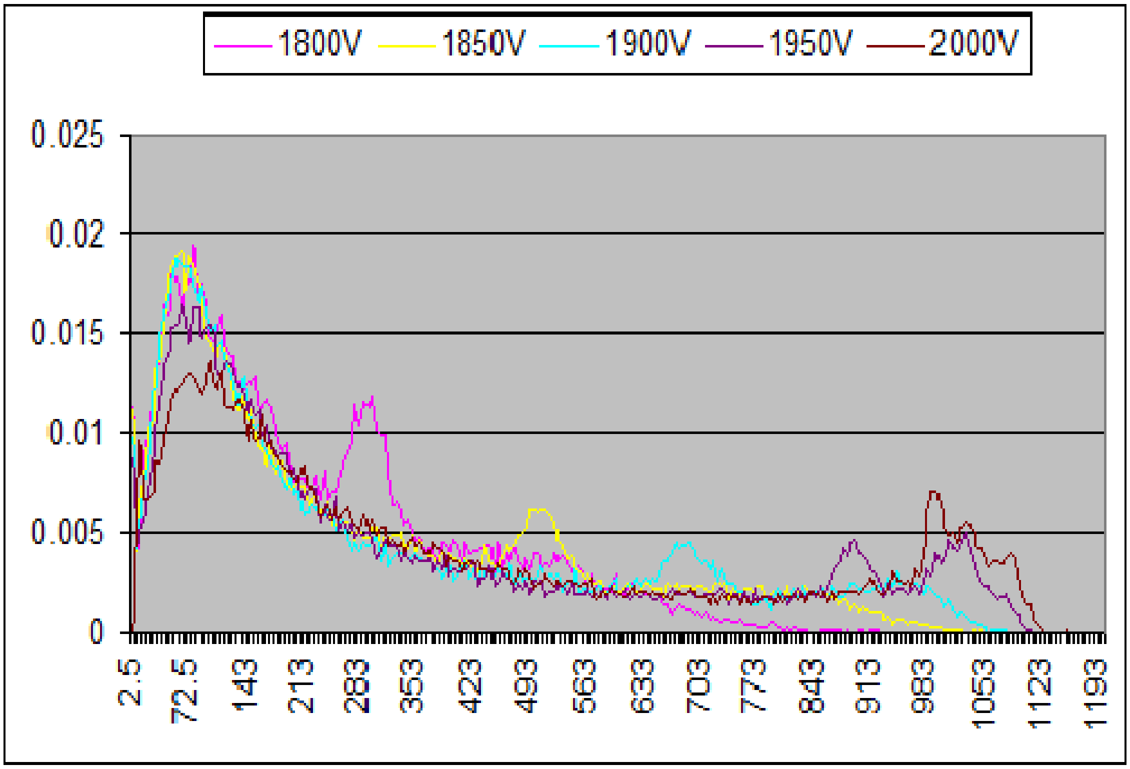

Figure 5.5 Cs-137 pulse height distribution with Ar:CO_2::85:15.

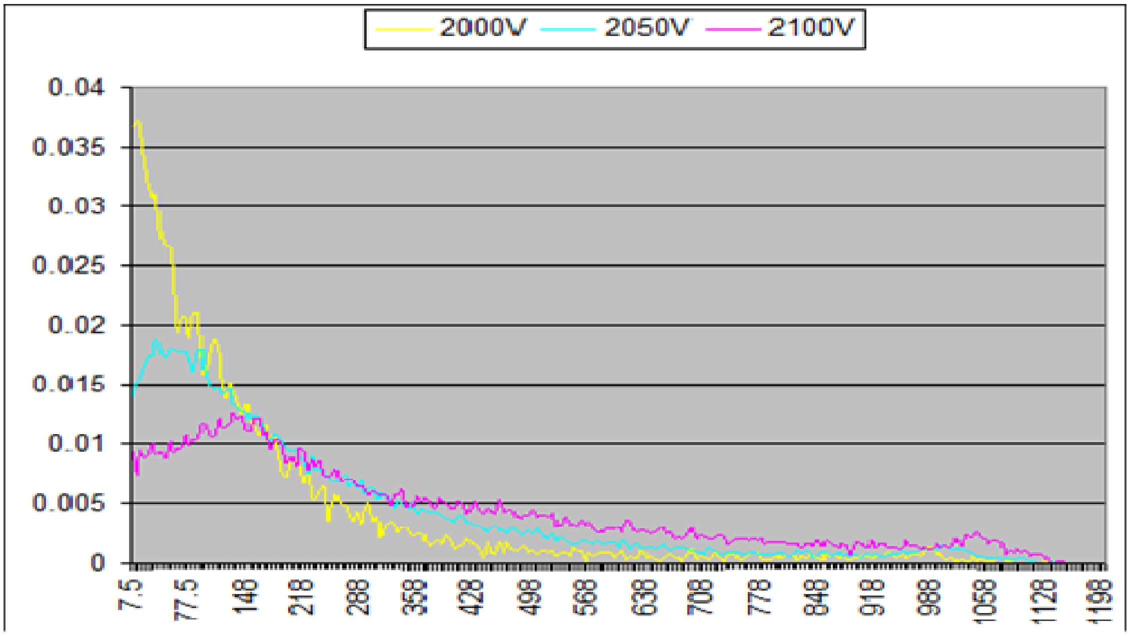

Figure 5.6 Sr-90 pulse height distribution with Ar:CO_2::85:15.

To determine the operational high voltage and gas mixture the ADC output, in units of mV, corresponding to center of the second peak is used. The voltage associated with the center of the second peak increases as HV is increased for each gas mixture. This means that the chamber gain increases as HV increases. Although the gain increases with increasing HV it is better to characterize gain as a function of voltage across the GEM foils. The goal of setting a particular HV is to achieve a desired voltage across GEM foils. It is the voltage across GEM foils that directly effect the electron avalanche in the holes. Recall from section 2.2 that the voltage across GEM is maintained by the particular resistor network. Many possible resistors may be used to distribute HV to each region. Therefore, the chamber gain should not directly depend on the particular resistor network used but rather the voltage across the GEM foils. Since Sr-90 does not produce a noticeable effect in relation to the voltage across GEM, it is not used to determine operational HV.

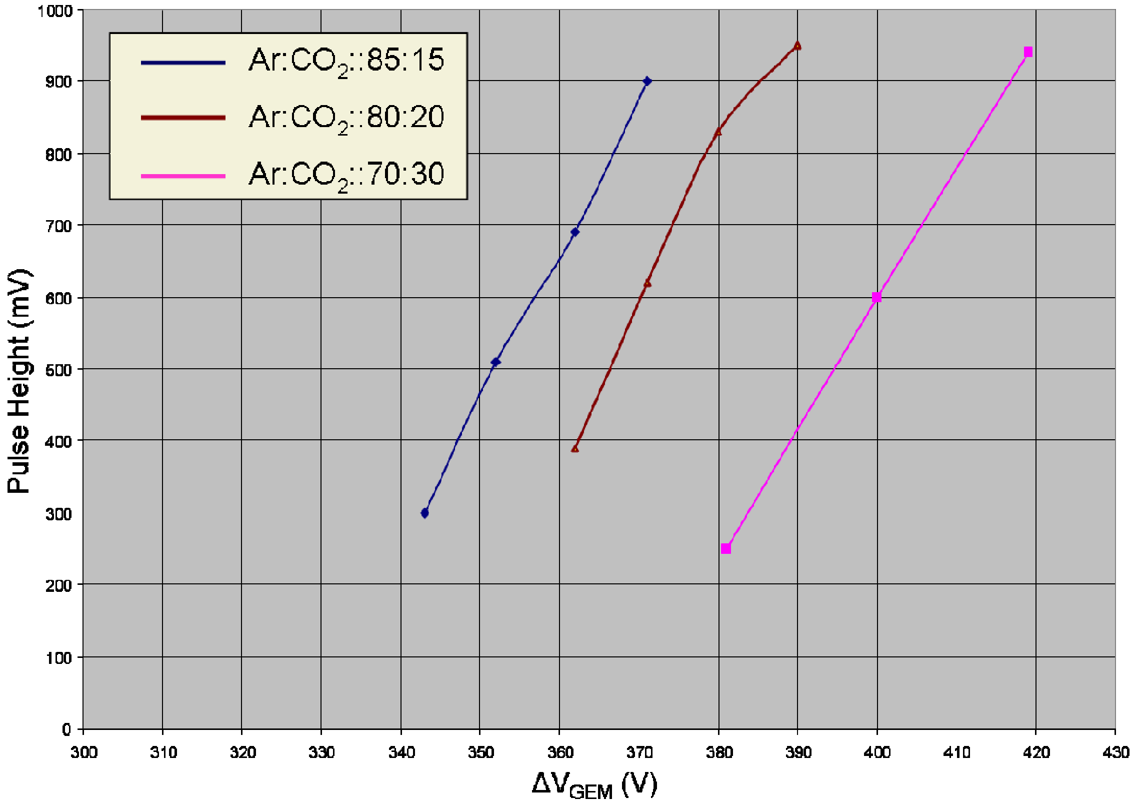

Figure 5.7 Chamber gain with Cs-137 source as a function of voltage across GEM foils and gas mixture.

The results are summarized in Figure 5.7. Each point represents the voltage corresponding to the second peak from each different gas mixtures and HV settings. The voltage across GEM foils and the gas that gives the most gain should be selected. The lowest Argon content, 70:30 gas mixture can sustain large voltage across GEM foils but does not show an increase in gain compared to 80:20 and 85:15 gases. Although 85:15 gas mixture achieves the same gain for lower voltages across GEM foils as 80:20 and 70:30, discharges are heard from the chamber. The 80:20 gas mixture is chosen because it has a factor of three increase in the gain for the same voltage across GEM as 70:30 gas and it shows no evidence of discharge for any HV settings. Since 80:20 can achieve the same gain as 70:30 for a lower voltage across GEM it is also safer.

CHAPTER 6

GAS FLOW MEASUREMENTS

6.1.Introduction

GEM chambers must be opened, closed, assembled and reassembled many times throughout the development and characterization stages. Every time a chamber is closed after being open all air must be purged and replaced with Ar:CO_2 gas. The goal of measuring gas flow is to determine when the gas has had enough time to completely purge any air and fill the chamber with the desired Ar:CO_2 and a maximum operational gain for a given setting is achieved. A chamber is considered off until the maximum operational gain is achieved. If the chamber is off then any data taken is not valid for measurements such as gain, efficiency, multiplicity and cross-talk. Knowledge of the start-up time is also important for high energy physics experiments in general. As the size and complexity of detectors in high energy physics experiments increases, knowledge of their sub-detector start-up times becomes very important. Measuring the signal rate, from a radiation source, as a function of time after closing a chamber and starting the gas flow provides a way of determining when maximum chamber gain is possible and therefore the turn-on time.

One important property of GEM chambers is an ability to prevent gas from leaking. Additionally, as more gas leaks more gas must be supplied to maintain positive pressure. Therefore leaky chambers not only take longer to turn on but they also waste gas and therefore financial resources. To ensure that only the desired gas mixture is present in the chamber a slight positive pressure is maintained. A commercially supplied pressurized bottle of pre-mixed Ar:CO_2 gas is the source of gas supply for the chamber. It is supplied to the chamber through a flexible tube directly into the ionization region. The exhaust exits on the opposite side of the ionization region in the chamber through another flexible tube of the same size to a bubbler containing mineral oil. The presence of bubbles in the bubbler on the exhaust side ensures the existence of a slight positive pressure in the chamber.

Measurements in this chapter seek to determine the optimal rate to fill GEM chambers with gas, the optimal rate to flow gas through GEM chambers during operation and the initial amount of time it takes for the GEM chamber to achieve its peak performance after opening and closing the chamber. The amount of time it takes for GEM chambers to achieve their peak performance is called the turn-on time. The turn-on time depends on the quality of chamber seals to prevent gas leakage and the rate gas flows through the chamber. The rate of signals from a Sr-90 radiation source above noise as a function of a threshold value is measured to determine the turn-on time. The rate of noise above threshold is measured as a control for the signal rate and shows the amount of time the chamber is not at its peak performance or that the chamber is considered off.

6.2.Noise Rate as a Function of Gas Flow

Before signal rate can be accurately measured the noise rate is measured because the output from the GEM chamber is considered as noise or signal depending on the pulse height. Noise rate tests assume pulse heights from GEM chambers are considered as noise without the presence of a radiation source. Noise rate tests effectively determine the baseline chamber output rate above threshold for the signal rate tests.

6.2.1. Description of Procedure and Quantities

Noise rate measurements are performed without the Sr-90 source to provide signal. The testing begins immediately after the HV is turned on. After flowing the gas at 30ccm for 15 minutes, gas flow rate was increased to 50 ccm as this is the initial flow rate used in signal rate tests discussed in section 6.3. After the second 15 minute period (i.e.30 total minutes elapsed) the noise rate increased by a factor of 2. Another 50 ccm measurement is made to confirm this factor 2 increase. The flow rate was then decreased to 25 ccm for the next two 15 minute measurements.

6.2.2. Results

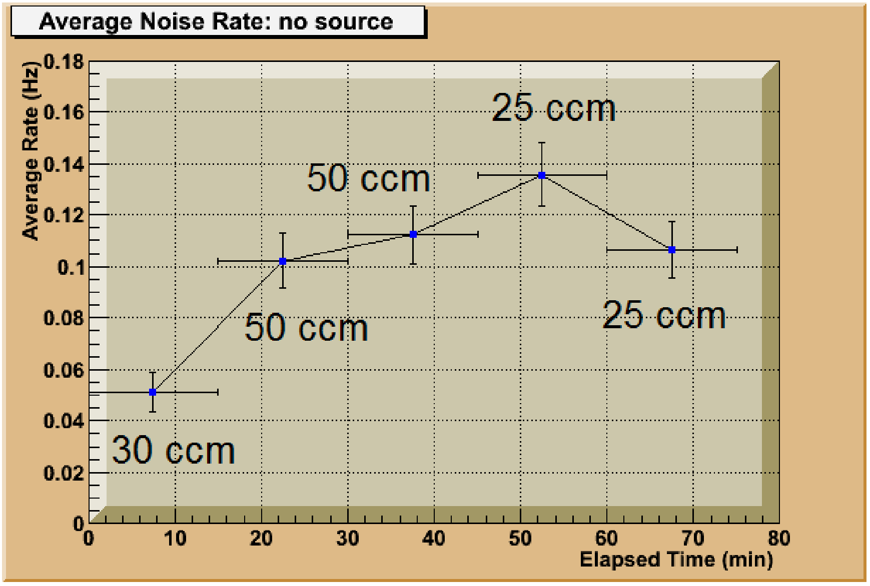

Figure 6.1 Average Rate of Noise after turning on HV. The numbers on the graph represent each point's gas flow rate. Each point represents the average noise rate (Hz) measured in a 15 minute time interval.

The result of noise rate measurements is shown in Figure 6.1. The time for these measurements starts immediately after HV turn on. Each point represents the average rate without a radioactive source in a 15 minute period. There is an increase in the noise rate after the first 15 minute interval that seems to suggest that the electronics warm up during the first 15 minutes. After the first 15 minute interval the noise rate does not significantly increase or decrease. The measured noise rates during the time intervals with a 25 ccm gas flow rate suggest that the noise rate does not depend on the purity of gas in the chamber. The increase in the noise rate between the first 15 minute interval measurement and the second 15 minute interval measurement suggest that the noise rate increases with gas flow rate. If this is true then the noise rate should decrease when the gas flow rate decreases but this is not observed as is shown by the noise rates during the 25ccm measurements. This measurement does not provide the lowest noise level conditions but does show the time to raise the system to its operational noise levels for a given electronics environment. Therefore, prior to starting any measurement with this GEM chamber all electronics must be on for at least 30 minutes before operational noise rate levels are reached. This measurement also shows that for a given double GEM detector setup the

6.2.3. Uncertainty Calculations

There are two main sources of uncertainty in determining the average rate values for noise rate tests. Namely, these are the uncertainties associated with calculating the rate value and averaging the value over time. Each noise rate calculation is performed by dividing the number of counts above threshold over a 15 minute period. Although this limits the knowledge of more precise noise rate behavior it still gives the necessary information on noise trends and characterization.

Another systematic uncertainty comes from physically starting and stopping the scalers by hand simultaneously with the stop watch. Since the highest precision of measuring time is 1 second, the uncertainty in starting and stopping the scalers by hand simultaneously with the stop watch is 0.5 seconds. The main statistical uncertainty comes from the number of signals counted. Assuming that in each 15 minute period the noise follows a Gaussian distribution, this uncertainty is the square root of the number of noise signals above threshold as given in Equation 6.1. Equation (6.2 is used to calculate the rate uncertainty for each point. Here T stands for the time period which is 15 minutes.

$$\delta N = \sqrt{N} \tag{6.1}$$

$$\delta R = R\left(\frac{0.5}{T * 60} + \frac{\sqrt{N}}{N}\right) \tag{6.2}$$

6.3.Signal Rate as a Function of Gas Flow

Signal rates are a measure of the pulse height for a chosen amount of time as a function of threshold. The claim that maximum signal rate corresponds to maximum chamber gain is based on the assumption that maximum gain occurs once signal rate reaches a maximum level. Conversely, maximum chamber gain may occur some time after maximum signal rate but maximum gain does not occur before signal rate has saturated. This means the rate test serves as an initial but sufficient measurement of turn on time and the initiation of maximum chamber gain.

6.3.1. Measurement of Signal Count

Signal rate is calculated from measurements of the number of signals above threshold as a function of time at the onset of filling the chamber with Ar:CO_2 gas. Signal rate is calculated as the average number of signals divided by the time to count. Each measurement represents the evolution of GEM signal rates and provides characteristic results, namely the background noise, turn-on time, maximum rate, and stability.

Two experiments are performed under different noise environments. The first experiment was performed using the KPiX v7 based double GEM chamber inside a shielded aluminum box but reading signals from a single channel with the QPAO2 preamp card. This noise environment is sensitive to body movement in the room and shows many counts above threshold. The initial noise rate before the chamber turns on suggests that this noise environment is too high so another experiment is performed with the same system except the aluminum box is enclosed in a copper-lined wooden box.

6.3.2. Description of Procedure and Measured Quantities

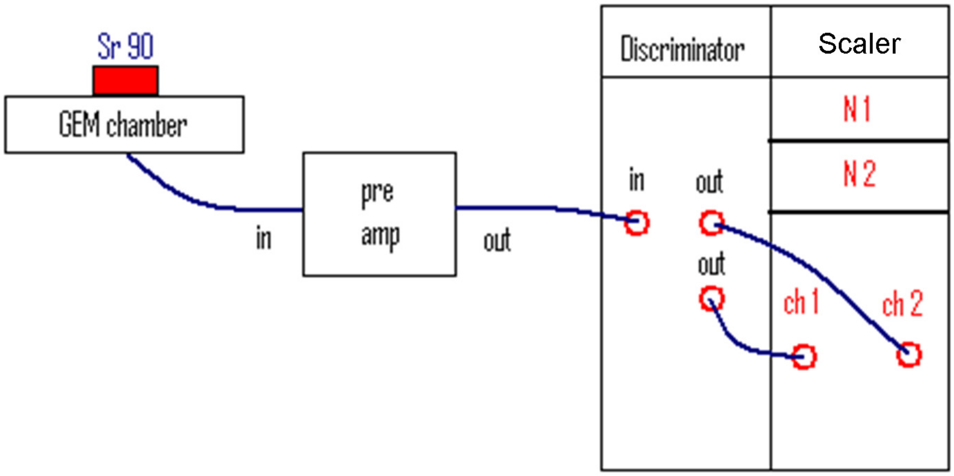

Figure 6.2 Flow chart of data signal in rate tests. The KPiX 7 chamber in conjunction with a Sr-90 radiation source send signals to a preamp. The signals go to a discriminator and then a scaler for counting. The Sr-90 is removed for noise rate tests.

Rate test are performed using a scalar to count pulses from the GEM chamber. These tests did not use KPiX7 electronics but rather the QPAO2 preamp card and NIM electronics. A NIM cable is connected to the back of the KPiX board in the center under the location of the source. This cable goes to the preamp where the negative output goes to a discriminator and scalar. Figure 6.2 illustrates these connections. The readout pad is chosen to be in the center of the chamber under the source window that is built into the chamber. The threshold level on the discriminator is greater than the noise by 50% of the noise fluctuation in order to minimize the number of noise pulses counted as signal.

Test settings that remain constant for the rate tests are the instantaneous count time, time interval, discriminator threshold, gas flow rate, preamp card and channel, and readout pad. The procedure is to continue recording the scalar number, N, for a 5 minute duration every 20 minutes until a maximum signal level is observed. For each 5 minutes counting period, the rate is equal to the number of events divided by 5 minutes. Instantaneous count time is the 5 minute duration used to calculate the rate of signals for a given instant of elapsed time. This time is chosen because it is assumed that the rate does not change dramatically within this time so that the rate calculated represents an instantaneous rate. The time interval is 20 minutes because as qualitative measurements of signal rate show an increase of signal rate within 90 minutes. A 20 minute interval time will show differences in rate between each measurement and provide enough points to observe chamber turn-on and a maximum signal rate level. The final result of the measurement is the total time to reach maximum level of signal rate.

6.3.3. Results

Different GEM chamber designs require a certain amount of time for gas to flow before the chamber operates at peak performance and data can be collected for further measurements such as efficiency and multiplicity. The threshold level also limits the background noise counted as signal. Since pulse height distributions from Sr-90 look like that of Figure 5.6 most signals are in the lower pulse height region. As threshold increases noise rate and signal rate decrease because the discriminator effectively ignores a larger range of pulse heights. Operational gas fill rate is the optimal rate for the chamber to reach maximum gain performance in a minimum time. Operational gas flow rate is the lowest intake gas flow rate that maintains maximum gain and stability.

Figure 6.3 shows the results of signal rate growth as a function of threshold using a 45 ccm gas flow rate. After 90 minutes there is a distinct “turn on” of the chamber as shown by the increase in slope at 90 minutes. After 180 min there is no significant change. The uncertainty bars along the x-axis are due to the assumption that each measurement is the average for that time period. The number of counts recorded after a given 10 minute interval represent the average number of counts in that time period. Therefore, the calculated rate is also an average. It is assumed that the rate of signals above threshold does increase within 10 minutes but at a much lower rate compared to the growth of the average rate over the elapsed time of the measurement. These noise tests reveal a warm up period for the complete electric system that is dependent on the high voltage power supply.

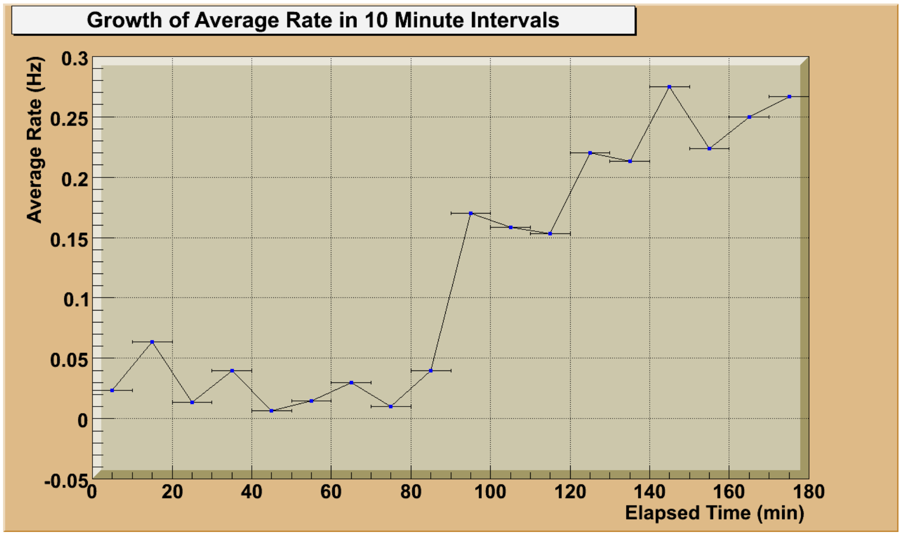

Figure 6.3 Growth of Average Rate (Hz) as calculated by counting signals above threshold in 10 minute intervals

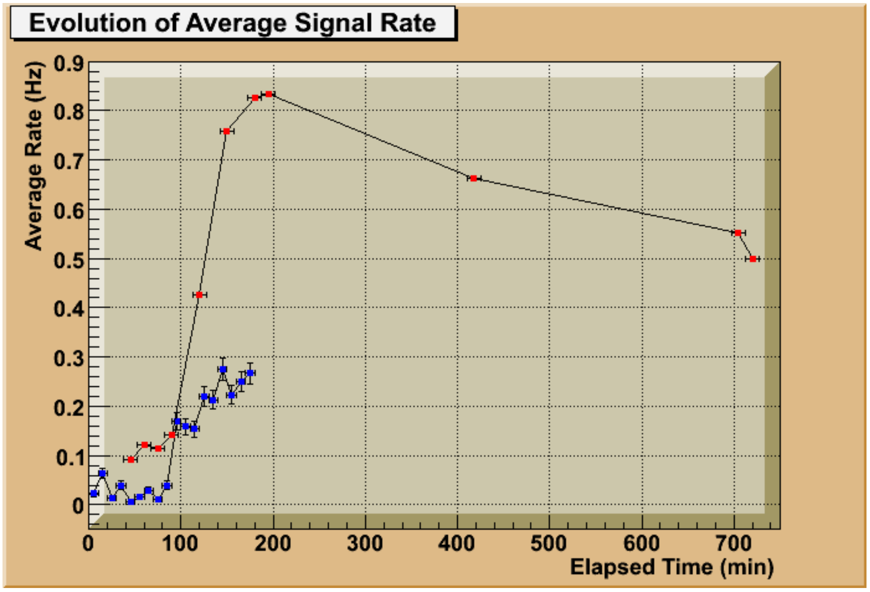

Figure 6.4 Effect of Environmental Noise. Blue is in Al enclosure on top of the table. Red is taken with Al box inside a large copper lined wooden box. The last two points are done with 10ccm input

Figure 6.4 compares data from two signal rate tests having different noise environments. The red line indicates tests performed with the aluminum enclosed chamber inside a copper-lined wooden box. Prior to the start of this experiment, it is assumed this environment is less sensitive to noise fluctuations but the first 4 points show a factor 2 increase in the noise rate compared to the environment without the wood box represented by the blue points. The assumption is that before chamber turn-on (indicated by the increase in signal rate after 90minutes) the signal rate is actually a measure of the noise rate above threshold. Therefore the mean value along the y-axis of the data points before 90 minutes is the average noise rate above threshold. Since the mean value is calculated from multiple measurements of the same quantity the standard deviation is the main uncertainty of the noise rate. This means that smaller standard deviations indicate less sensitivity to the noise environment while larger standard deviations indicate increased sensitivity. The noise environment that has the smallest standard deviation should be used because it provides the most accurate measurement of signal rate. Also, the maximum signal rate is a factor of 3 greater when the Al chamber enclosure is further enclosed in the copper-lined wood box. This measurement shows that the chamber is ready to take data after filling gas for 180 minutes at 45 ccm.

CHAPTER 7

KPIX BASED GEM CHAMBER CHARACTERIZATION

This chapter discusses the GEM chamber characterization using KPiX readout electronics. This chapter provides a description of the available modes that KPiX uses to trigger signal. A 30 x 30 cm2 chamber is constructed for the KPiX version 4 and version 7 electronics. Both are tested for their response to radiation sources. A signal inference method is designed to reconstruct Landau distributions from the KPiX version 4 based GEM chamber data.

7.1.KPiX Trigger Modes

Force trigger mode is a trigger circuit that can receive trigger signals from internal or external sources. For instance, the calibration circuit can provide a trigger source called CalStrobe. The other trigger source used in data taking comes from scintillation counters connected to KPiX via a NIM standard connector on the FPGA board. When taking data using a radiation source the internal CalStrobe trigger is used. For cosmic ray or test beam data the external trigger is used. Forced trigger is currently the chosen mode of operation for all version 4 and version 7. There is another mode of triggering called Self trigger but this is not used to take data and is only in the initial stage of functionality in KPiX version 7.

Data from internal and external force trigger have different characteristics. CalStrobe uses the same trigger frequency as calibration at 30 Hz. Most of the data recorded with this trigger source is characterized as pedestal data unless the source of particles is a test beam tuned to the KPiX trigger frequency. This is an asynchronous mode of triggering because the signals generated by the GEM chamber arrive randomly with respect to KPiX timing. The external force trigger relies on a NIM connector on the FPGA board to provide the signal. In this mode KPiX accepts the percentage of incoming trigger that align with its acquisition cycle. This percentage is called the live time. For both modes all pads are still recorded in parallel. In the case of cosmic rays when only a single pad contains the charge information all other pads are still recorded and contain pedestal data. The amount of pedestal data using periodic internal triggers is many orders of magnitude less compared to using an external trigger. The amount of pedestal data using an external trigger can be estimated. It is roughly equal to 1 divided by the number of pads covered by the number of channel capable of collecting charge for any triggers.

7.2. Source Response

Figure 7.1 illustrates KPiX version 4 based chamber response to radiation sources. The plot in panel (a) is a pulse height density graph for all channels. The y-axis is in units of charge in fC and the x-axis is channel number. The location of the source is indicated by the channels showing a tower of charge values above the lower band near zero fC. The graph in panel (b) is a hits density graph displaying the pad locations with hits greater than 15 fC. Both of these plots are live graphs updated during data taking in order to observe response immediately. The red circle indicates the highest density of hits and therefore the physical location of the source.

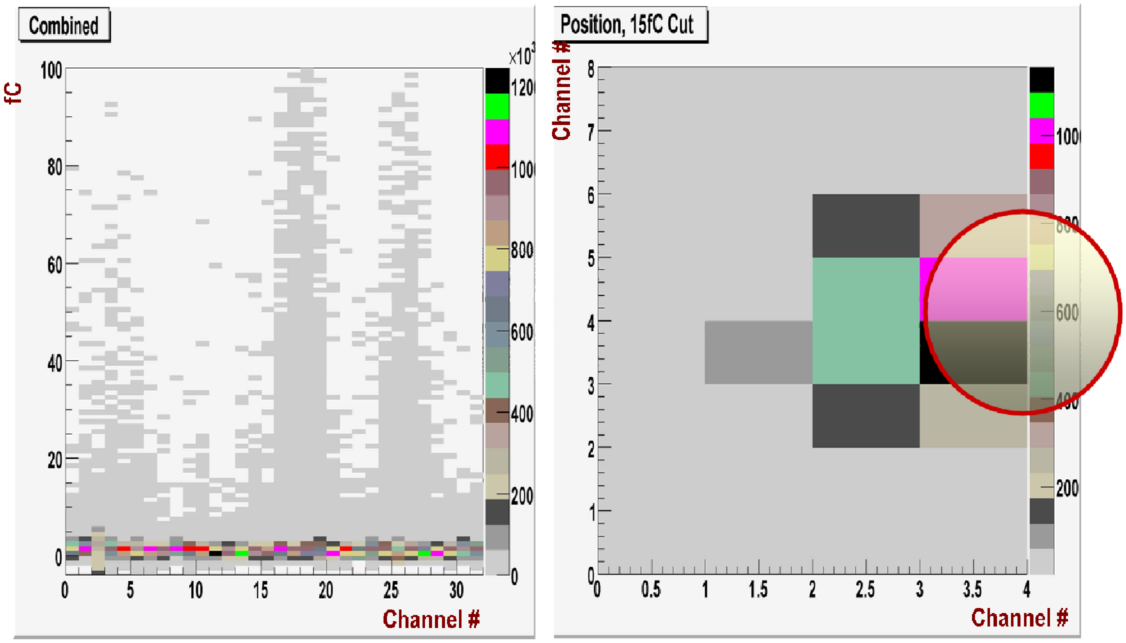

(a) (b)

Figure 7.1 Source response plots from KPiX v4 for all channels pulse height densities (a) and hits density (b).

Figure 7.2 shows the KPiX version 4 pulse height distribution response to Sr90 source from a pad far from the source in panel (a) and a pad directly under the source in panel (b). These histograms are important relative to those just shown because they provide the detailed information about the analog response of GEM detectors to the radiation source. In principle, they can also be fit with Landau functions to find the MPV. It is from these types of histograms that information to characterize gain and efficiency is potentially available.

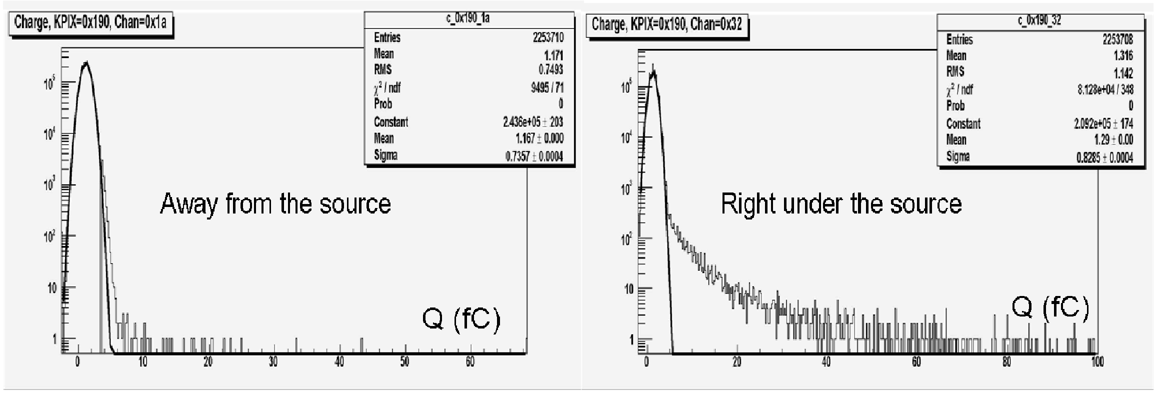

(a) (b)

Figure 7.2 Histograms showing KPiX v4 response to Sr90 source from a pad far from the source, (a), and a pad directly under the source, (b).

Figure 7.3 shows the response to radiation sources using the version 7 GEM chamber. The distribution on the left in panel (a) is a pad far from the source and the one in panel (b) is directly under the source. The first peak is from pedestal while the remaining hits represent a response to the source. The large amount of data in the pad under the source shows that KPiX responds to the source. Although there is evidence, no pure Landau distribution is directly expected from Sr90 source since MIPs do not directly trigger the system.

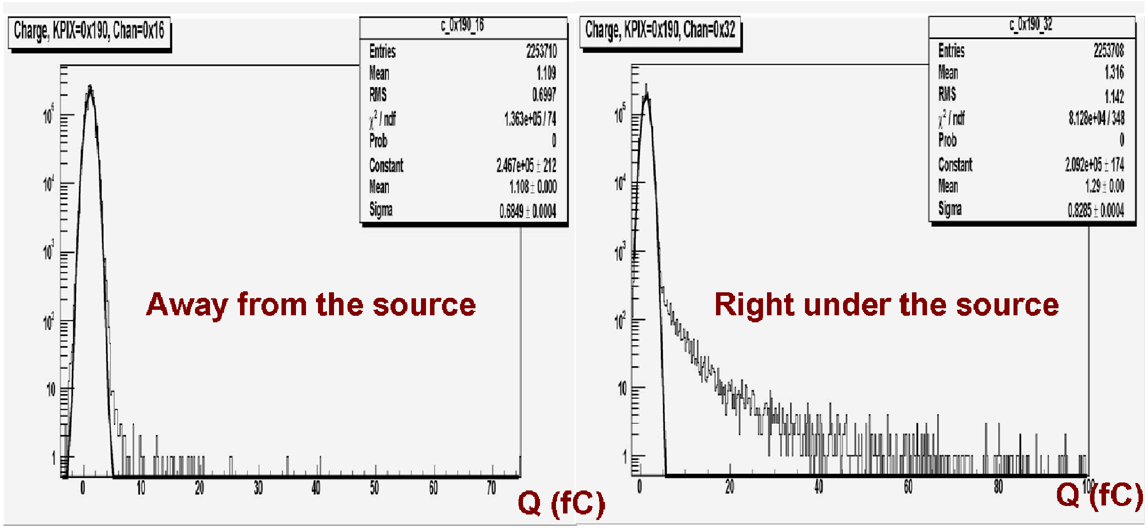

(a) (b)

Figure 7.3 Charge distributions from KPiX v7 using Sr90 radiation source from a pad far from the source (a) and a pad directly underneath the source (b). The first peak is the pedestal and the remaining contributions are from ionization within the chamber.

7.3.KPiX Signal Extraction

An obvious Landau distribution is not expected from a radiation source because its signals are asynchronous with KPiX that inhibit complete integrations of signal and Sr-90 has many non-MIP particles that cause ionization. For KPiX running in asynchronous mode a signal inference method is developed to extract Landau distributions from pedestal dominated data. To extract Landau distributions from KPiX data, Monte Carlo simulations methods are employed to approximate the effect of running with an asynchronous radiation source. The simulation procedure assumes the shape of ionization charges inside GEM is Gaussian, initializes a Landau distribution based on results from test beam data, simulates KPiX timing through random integration of Gaussian, and simulates large Gaussian contribution characteristic of using the CalStrobe as a trigger source. Figure 3.5 is an example of a typical shape from the output of GEM chambers and supports the assumption that the shapes of GEM pulses have a Gaussian behavior. Test beam data is presented later in Chapter 8. If real data and MC data match then the initial Landau represents the real MIP response from the GEM chamber. The assumption that Sr-90 decay products that ionize the chamber gas are not all MIP results in a pulse height distribution peak that is shifted to the left.

7.3.1. Signal Inference Method Procedure

The details of the procedure are given in Appendix C. The procedure assumes a Gaussian shape for the GEM chamber signal pulses and an initial Landau distribution for the inferred pulse height distribution. The integration time that KPiX calculates the charge present in a signal pulse is 330 ns. The area of the pulse Gaussian function of is calculated and another Gaussian function is used to represent the calibration pedestal. Then the data histogram from data Root file is collected and fit using the pedestal. After that a loop is started to pick random numbers from the signal pulse Gaussian and fills another histogram. Then a random number from the assumed Landau is pulled and another histogram is filled. Then a random number is selected between 0 and 330 and put into a histogram to represent the random start time for integrating signal pulses. The signal pulse Gaussian is then integrated in the limited range according to this random number and the result is stored into a histogram. Also the division of this partial area to the total area defines a ratio. These ratios are also put into a histogram and multiplied with a random value selected from the assumed pulse height Landau distribution. This creates a histogram of fractional charge. Then it pulls a random number from pedestal, fills a histogram with this random pedestal value, adds random pedestal value to fractional charge and fill a histogram with the result. This final resulting histogram is should match with the data taken from the Sr-90 radiation source and the initial assumed Landau is the extracted signal pulse height distribution.

7.3.2. Results

The results of the pulse height distribution inference method are represented in Figure 7.4. It highlights the comparison of the inference method to real data. Black points represent real data, the blue line represents simulated data and the red line shows the inferred chamber response. One quality check of the simulation to real data is observation of the blue line over-laid with real data. The simulated data overlaps the real data very well. Another quality test is to calculate the ratio of real to simulated data. The imbedded graph shows that this ratio slightly fluctuates around 1. The MPV of the inferred chamber response is 1.9 fC. The expected MPV value is about 20 fC. This expectation comes from the results of the gas mixture determination that assumes a factor 3 increase in the gain for Ar:CO2::80:20. The factor 10 decrease the KPiX based GEM chamber response to Sr-90 has two sources. The first is that a result of the random integration of signal pulses shifts the MPV to a lower value closer to the noise. The second is that the internal gas flow was determined to be inadequate. This inadequate gas system is determined by observation of an increase signal rate after the gas exhaust was moved from the ionization region to the transfer region between the second GEM foil and the anode board. Its was found that placing the exhaust on the anode side forces gas to flow through this region. Otherwise, impure gas can kill the signal and absorb the electrons from the GEM foil amplification. Without this method the source data is hidden within the large pedestal contributions. Tests performed at SLAC after this measurement revealed an inadequate gas injection system also responsible for low left shifted peaks. A direct forced gas supply system is installed after this measurement.

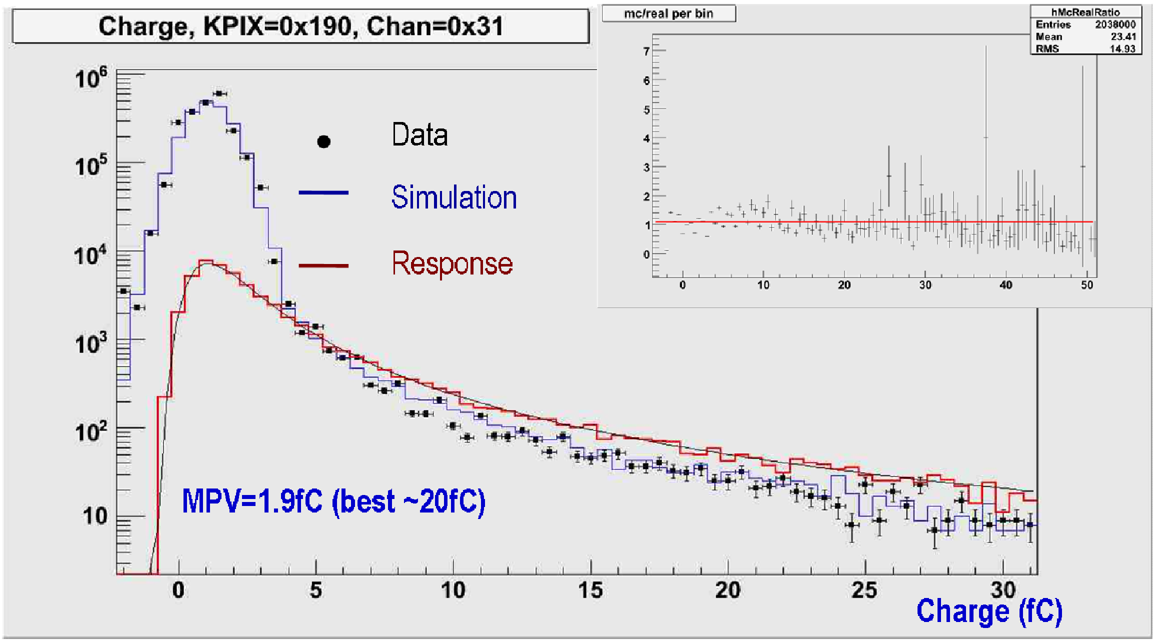

Figure 7.4 Charge distributions of data, simulation, and chamber response.

CHAPTER 8

TEST BEAM AT FERMI NATIONAL ACCELERATOR LABORATORY

8.1.Introduction

Double GEM chamber characterization beam tests performed at Fermi National Accelerator Laboratory, or Fermilab, consist of noise rate, MIP response, chamber gain and absolute efficiency. Other goals were multiplicity and cross-talk measurements. In addition to these tests a new procedure to subtract noise and normalize data is developed to infer absolute efficiency from test beam and source MIP responses. This chapter presents a description of these experiments, procedure and their corresponding results and conclusions.

The QPAO2 preamp based 30 cm x 30 cm double GEM prototype chamber was used in beam tests performed at Fermilab. Chamber responses were recorded from interactions with various beams and with a Strontium 90 radioactive source. Beam tests described in this chapter were performed in the Meson Test Beam Facility [48] using the 120 GeV proton beam. MTBF, including main experiments, associated beams, and the user test beam, are also described throughout this chapter.

8.2.Fermi National Accelerator Laboratory

Fermi National Accelerator Laboratory (FNAL) in Batavia, IL currently hosts the world's most powerful particle accelerator, the Tevatron. There are two large detectors, DZero [49] and CDF [50] that study proton and anti-proton collisions in the Tevatron. FNAL also hosts neutrino experiments such as MINOS [51] and MiniBooNE [52] that use beam lines supported by the Main Injector and the Booster respectively.

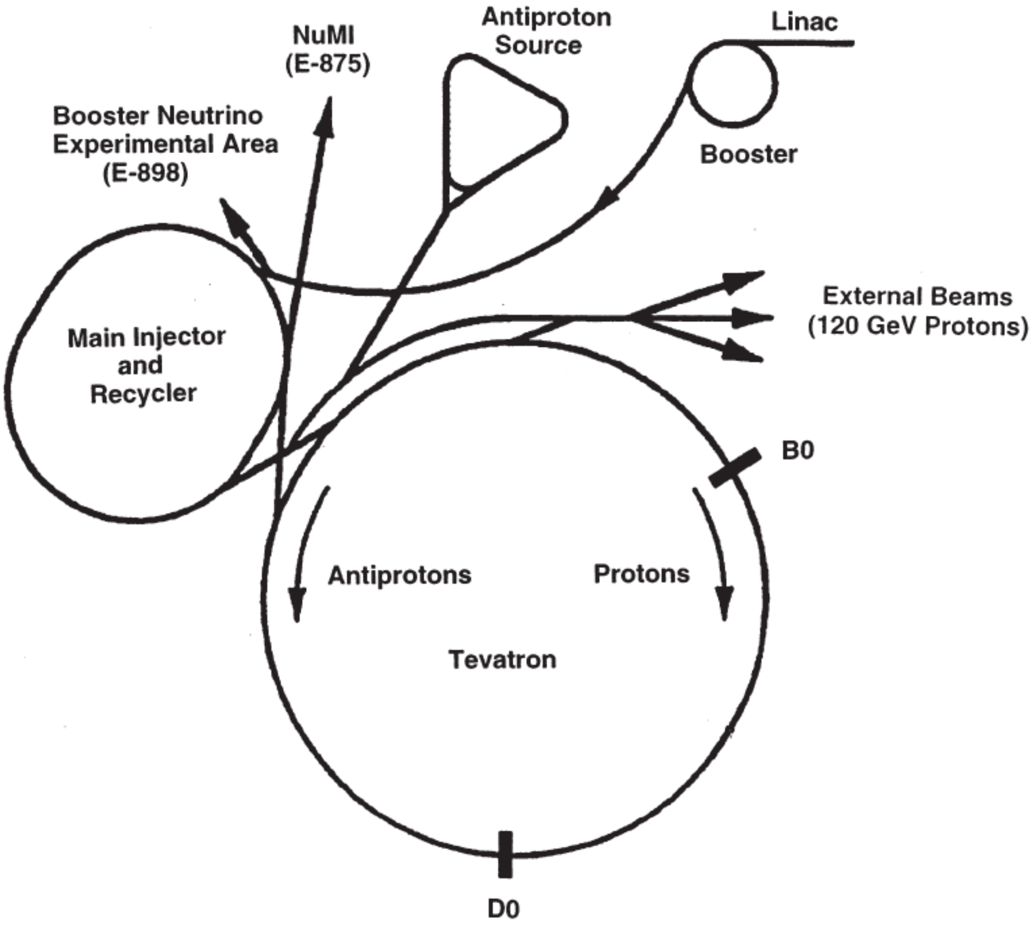

Figure 8.1 Layout of Fermilab's accelerator complex.[53]

The test beam at Fermilab originates from the main injector. A drawing of Fermilab's accelerator chain is shown Figure 8.1. Protons originate from the Preacc [54] that delivers hydrogen ions (H-)of 750 KeV to a linear accelerator, called the Linac. Here in the Linac the beam is accelerated from 750 KeV to 400 MeV into the Booster, a circular (75 m radius) synchrotron accelerator. At this point electrons are stripped from the negatively charged hydrogen ions and accelerated into the Main Injector at 8 GeV. Also a synchrotron, it accelerates 8 GeV protons to 120 GeV. This is now the source of protons provided to the test beam area. For the test beam area, the Main Injector delivers 120 GeV protons to the Switchyard via the P3 line (not shown). The Switchyard allows this beam to split to three fixed target areas one of which is the Meson Test Beam Facility.

8.3. Meson Test Beam Facility

Meson Test Beam Facility (MTBF) is designed as a user experimental area located in the Meson Detector Building at Fermilab. Figure 8.2 shows the available fixed target beam lines after the Switchyard [53]. MTBF is located in the Meson line at the end of the line labeled MT. This facility houses access to a beam of 120 GeV protons and secondary particles from protons on target in the MTest beam line. MTest is divided into one smaller and one larger enclosure section. GEM experiments were performed in the larger of the two, MT6-section2. Figure 8.3 is a rough outline showing the respective locations of the MT6 MTest User Areas. The MTest beam is incident from the left in Figure 8.3.

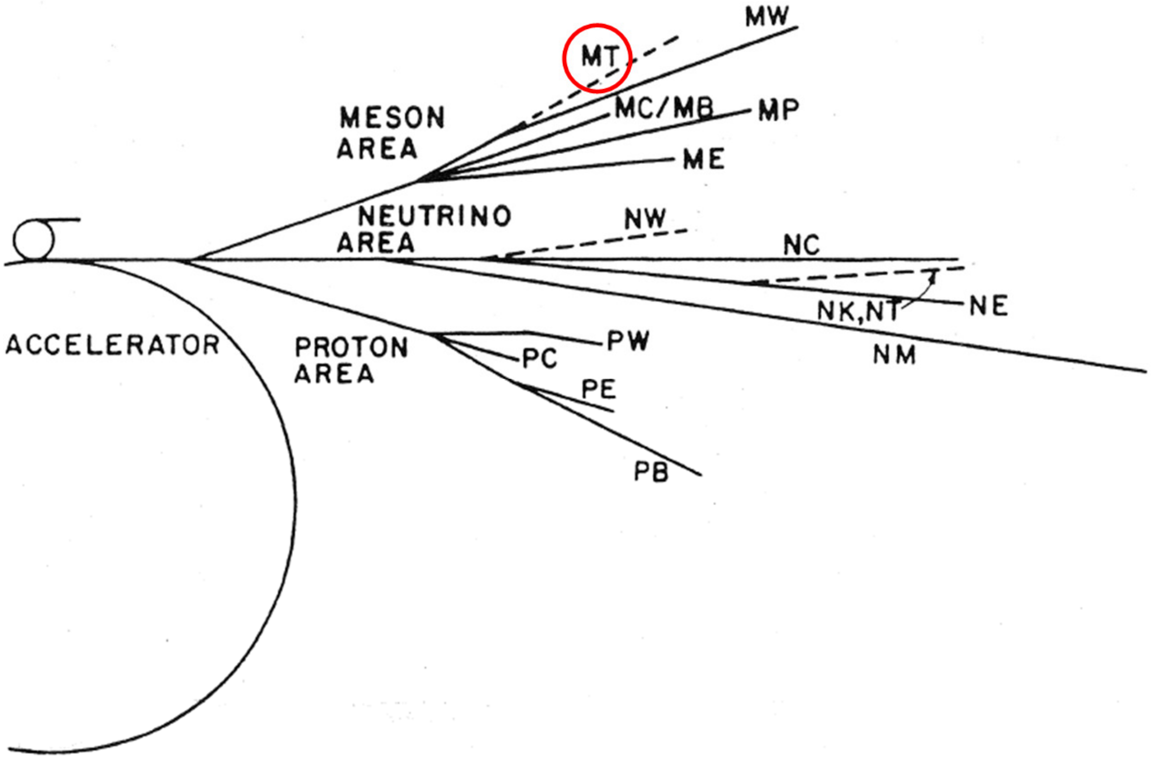

Figure 8.2 Layout of Fermilab's fixed target beams after the Switchyard. MTBF is located at the end of the MT line.

Also seen in Figure 8.3 is the Gas Area, Counting Room and Main Control Room. The user areas are equipped with gas delivery/exhaust systems leading to MT6-2C . The beam enclosure refers to any location inside the boxed red area. The GEM chamber is situated on a movable table located in MT6-2C noted in Figure 8.3. The Counting Room houses the high voltage power supplies, MTest detector electronics (not used), and multiple GEM chamber electronic components. The Main Control Room contains the user control system for the movable table, further GEM electronic components, multiple computer workstations, and beam monitoring stations.

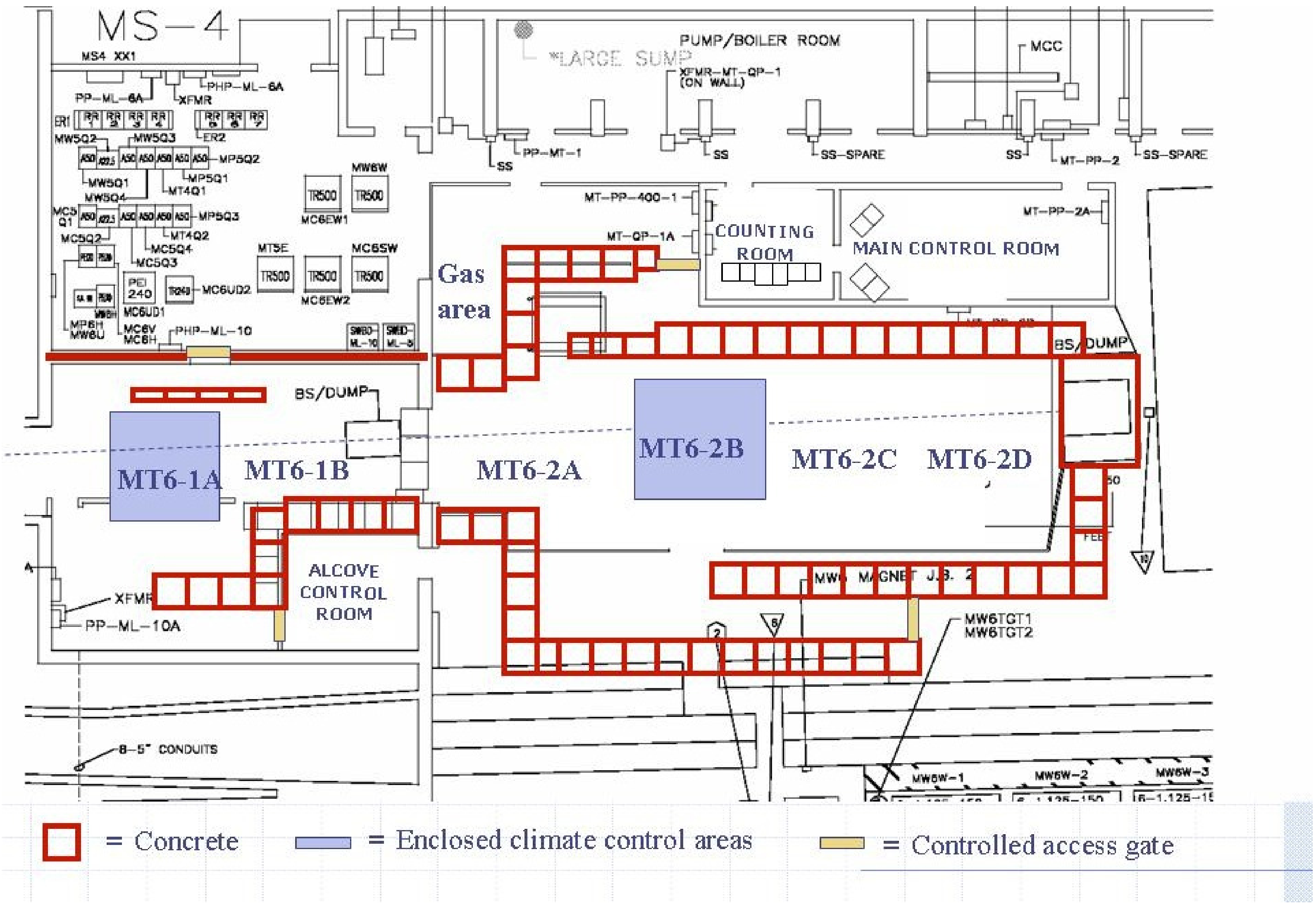

Figure 8.3 GEM chamber experiments were performed within the red boxed area in the section labeled MT6-2C.

8.4. Experimental Setup

The prototype GEM chamber setup consisted of the 30 x 30 cm^2 chamber, readout electronics and beam telescope. The readout electronics was divided into two sections. The first is the QPAO2 preamp card followed by a pulse shaper to lengthen the pulse width for accurate sampling of the pulse height by the ADC. The DAQ computer setup consists of a Windows PC that houses the 100-channel ADLINK ADC and GEMView software [55, 56]. Readout is limited to the center 96 channels using 3 thirty-two channel QPAO2 preamp cards. The anode board connections with the three preamp cards are shown in Figure 8.4. A NIM crate houses the supporting electronic components. It supports the trigger counters, amplifiers, discriminators, logic modules and trigger input to the DAQ computer. All together, the preamp, beam telescope, NIM module electronics, ADLINK ADC, GEMView program, and a Windows PC make up the data acquisition system.

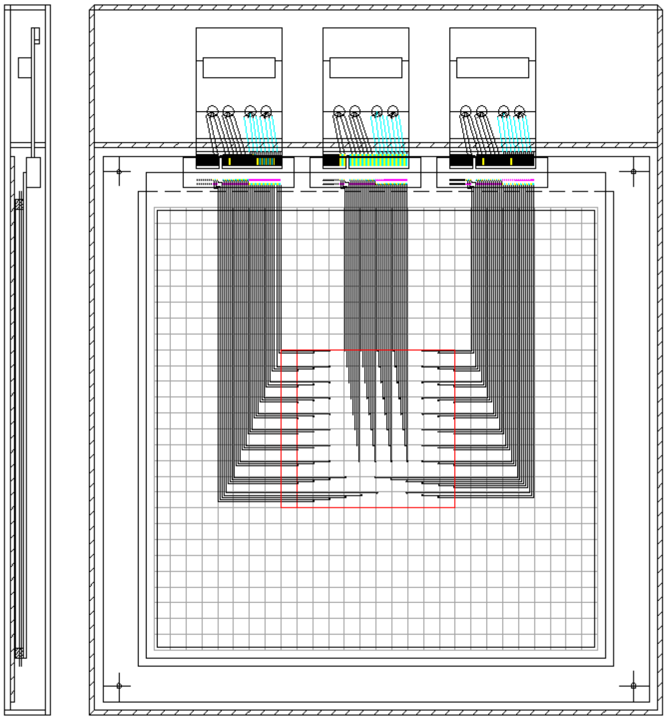

Figure 8.4 Anode pad configuration designed for up to 96 channel readout using three QPAO2 preamp cards.

Figure 8.5 shows a diagram of the setup for these experiments and associated integration into MTBF. With the exception of the gas system, HV power supplies and PC monitoring stations, the equipment is contained within the beam enclosure. The experimental setup within the beam enclosure can be considered as three major sections, the GEM chamber setup, the DAQ computer and beam telescope.

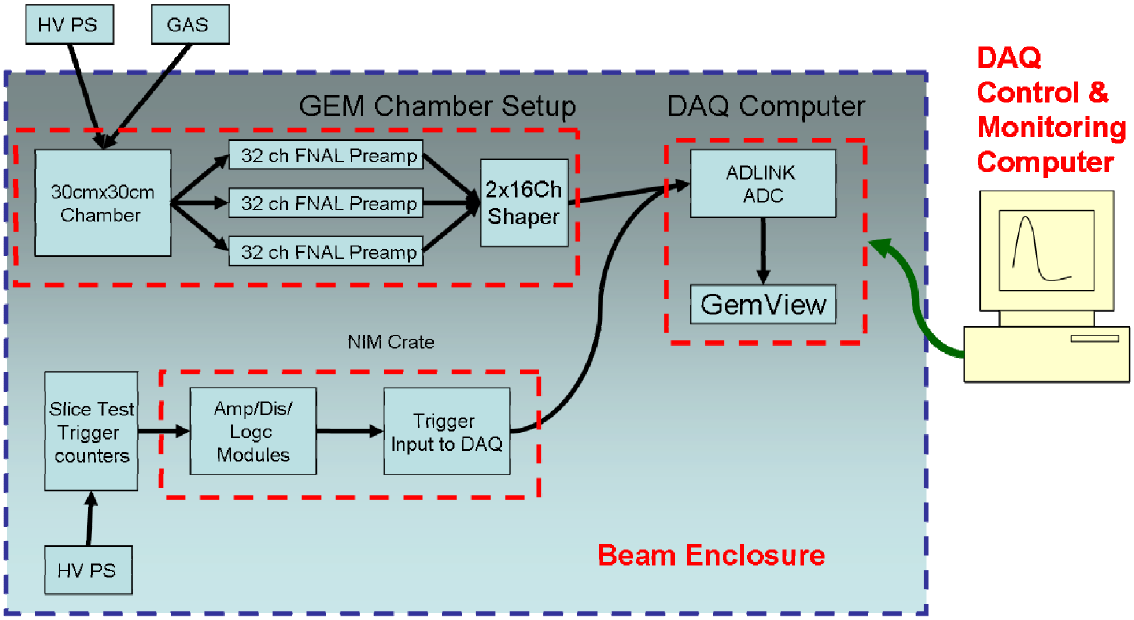

Figure 8.5 A diagram of the experimental setup at MTBF. In this figure the beam telescope is illustrated in the lower left corner and consists of the HV power supply, trigger counters and NIM crate. Also the 2x16 Ch Shaper indicated in the GEM Chamber Setup region is replaced with a single channel commercial shaper.

A beam telescope was set up to trigger the GEM chamber on the incident beam. The beam telescope consists of three finger counters followed by two paddle counters that surround the chamber active area and are in line with the beam. The counter's orientation is presented in panel (a) of Figure 8.6. Before traversing through the chamber, the beam is incident on the three finger counters and one of the paddle counters. The finger counters are separated by 5 cm followed by the first paddle counter another 5 cm away, then the chamber an additional 40 cm and finally the last paddle counter about 2.5 cm behind the chamber. Each finger counter is a 1 cm^3 plastic scintillator connected to a photo multiplier tube using a HV of -870 V. Each paddle counter is a 19 cm x 19 cm x 1 cm plastic scintillator also connected to a photo multiplier tube using a HV of -970 V. The signals from these counters and the chamber are connected with an AND logic coincidence to form a trigger. As a contribution to the trigger signal, the GEM chamber confirms that the beam traversed through the pad read out through the DAQ system. A photograph of the beam telescope and GEM chamber enclosure is shown in panel (b) of Figure 8.6.

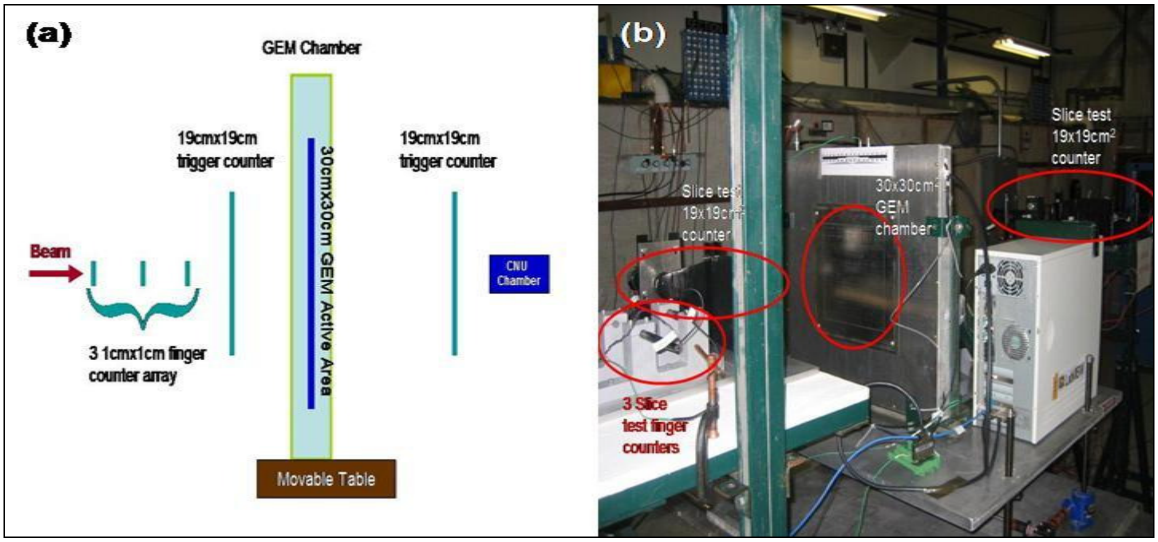

Figure 8.6 A schematic diagram (a) and photograph (b) of the chamber setup in MT6-2C beam enclosure.

Next to the movable table is the NIM crate (not shown in photograph) that houses the beam telescope, power supplies, trigger logic and preamp electronics modules. The first process in creating a trigger to create a beam telescope is to convert the counter and GEM chamber signals to standard NIM signals. Each scintillation counter and the negative output of the preamp card go to a discriminator to create a NIM standard signal. Then the discriminator outputs are grouped together to form 3 coincidence signals. The three finger counters form one group. The large paddle counters form another group and the chamber is its own group. These three signals form a final coincidence that is supplied to the ADC interface card as the trigger in order to indicate an incident beam particle through a specific pad in the chamber.

8.5. Beam Test Data

8.5.1. Introduction

Data taken during experiments at MTBF are from two sources, the Meson line delivering 120 GeV protons and a Sr-90 radioactive source providing electrons with an end-point energy of 2.283 MeV. Test beam data and source data were recorded for three adjacent channels 7, 15 and 23. The positive output from the preamp is used in conjunction with an amplifier and a shaper to lengthen the pulse width for accurate ADC sampling.

8.5.2. 120 GeV Proton Beam

As discussed in section 8.2, protons arriving to MTBF come from the Main Injector. The Main Injector also supplies the Tevatron with protons for use in the collider experiments. As a result the length of beam delivery time at MTBF is approximately 6 seconds every minute. Furthermore, the intensity of protons takes about 1 second to ramp up to maximum and then ramp down providing an effect time of 4 seconds that protons are incident on the GEM chamber, leaving an effective duty factor of the beam to about 6.67%

There is a further structure to the 4 seconds of proton beams. Each proton in the beam is separated by 20 ns from each other theoretically providing a maximum total of 0.2×10^9 protons. Each 20 ns period is not filled with a proton and there is a probability of two or more protons occupying the same period. The double occupancy rate was measured to be up to 35% [57].

It takes less than 20 ns, 16.667ns exactly, for a proton to travel from the first to the last counter in the beam telescope, assuming this distance is 5 m. Therefore, there is insufficient time between two consecutive protons for the trigger. Unfortunately, it is not possible to trigger every 20 ns cycle. Each counter in the beam telescope uses a 32 ns cable to attach to a discriminator. The discriminators then attach to an AND coincidence module that sends the trigger signal to the DAQ. The total time for the trigger to arrive is about 100 ns. Given that protons can be separated by as little as 20ns, only 20% of the incident protons can be triggered by the beam telescope. This means that in 4 seconds the DAQ can potentially record about 800 – 1,400 events. Therefore, the effective proton rate triggered by the beam telescope is 200 – 350 Hz.

There is also a cable path for the data signals. Initially charge that accumulates on the anode pad in the chamber goes to the preamp. The preamp then sends it to an amplifier and then a shaping amplifier. Finally the signal arrives to the DAQ. The anode pad is connected to the preamp via a 0.25 ns cable. Then the signal is carried to the first amplifier, located in the NIM crate, via a 32 ns cable. The shaping amplifier is another NIM module in the same crate so a short 0.5 ns cable is used between these modules. Then another 32 ns cable carries the signal from the shaping amplifier to the DAQ system in the control room. It is at this point that data can be triggered and collected. It is also at this point that the DAQ decides what to do with the incoming charge. It can either ignore it or record it in a data histogram depending on the trigger signal. The timing for this process matches with the timing of the beam telescope so that charge information from a protons ionizing gas in the chamber is correctly associated with its trigger signal.

Recalling from Figure 8.6(b), the DAQ computer is right next to the chamber. The goal of this is to reduce the time to trigger on beam data events. That is, the shorter the length for the signal to arrive to the DAQ the less time required to form a trigger signal. Therefore, the effective trigger rate can be increased to approach the rate of protons within the 4 second spill in the beam.

Data was collected for three channels from the chamber. In each case the anode pad was aligned with the beam telescope by adjusting the movable table. Each anode pad has a unique channel number associated with it. Data was collected for channel numbers 7, 15, and 23. Protons traversing the chamber have energy slightly above the minimum ionizing energy for protons through the each of the detector's materials. Also each trigger from the beam telescope is from a 120 GeV proton traversing the chamber. Therefore the pulse height distributions collected are expected have a Landau distributions. The pulse height is recorded for each event and stored in a data file by the DAQ PC.

8.5.3. Strontium 90 Radioactive Source

Strontium 90, Sr90, data was taken inside the beam enclosure while the test beam was off. Data was recorded for 5 minute periods for two channels, 7 and 15. The beam telescope is not used to trigger Sr90 decays because its decay products would lose too much energy through a single 1 cm depth of scintillation material. Therefore, data was recorded with the DAQ using its self trigger mode.

8.6. Data Analysis

8.6.1. Pedestal Subtraction

A single data-taking run of GEM chambers do not consist entirely of desirable data but also includes noise that contribute to a pedestal distribution within the data's pulse height distributions. The data from pedestal runs provide a reliable distribution representing the pedestal of each channel. A normalization algorithm was used to correctly and accurately subtract pedestal contributions from data.

The process begins by fitting the pedestal with a Gaussian distribution. This fit provides the shape parameters accurately describing the pedestal. Next, as data is fit to Gaussian plus Landau the mean value and sigma of the Gaussian are fixed to the matching parameters from noise. This allows the ROOT fitting functions to find to noise contribution in data based on the known pedestal shape. Allowing the amplitude to float provides the normalization factor. At this point the noise has been normalized to data and has been given an accurate estimate of pedestal contributions. A histogram is created using these final three parameters, amplitude, mean value and sigma. This histogram now represents a noise histogram normalized to data with the same shape as the pedestal. The final step is to subtract this pedestal histogram from the data histogram resulting in noise subtracted data. A detailed procedure is found in Appendix D.

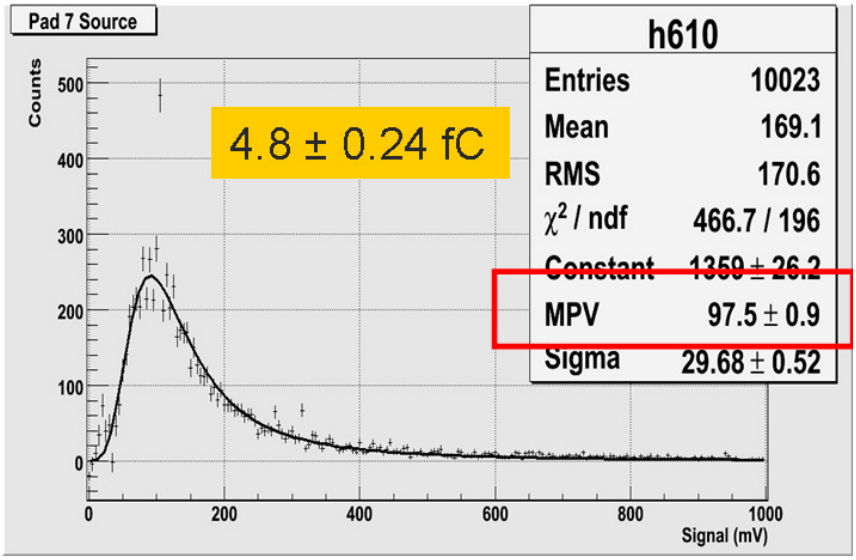

Figure 8.7 Pulse height distribution of normalized source data with pedestal subtracted.

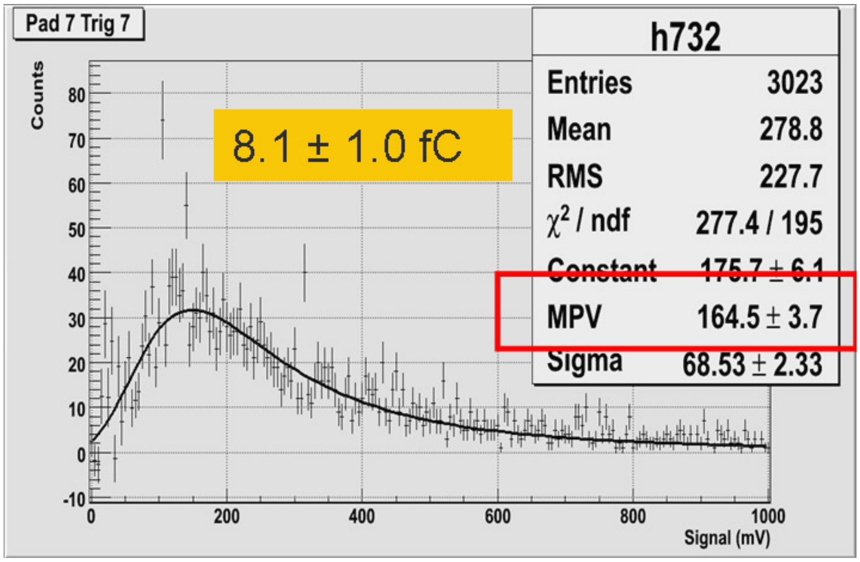

Figure 8.8 Pulse height distribution of test beam data with pedestal subtracted

8.6.2. Chamber Gain

Chamber gain per channel is measured instead of complete chamber gain because the MIP response histograms are only from two of the possible 900 pads in the 30 cm x 30 cm chamber. Chamber gain is the collection of gains from the MIP responses of all active channels. Ionization produced inside the GEM chamber undergoes 3 stages of gain before read out as a voltage in the DAQ system. First, ionization electrons are amplified by the chamber via each GEM foil. Second, the signal pulse goes through the preamp that converts charge to voltage and amplifies the signal. Finally, a NIM module single-channel amplifier amplifies the signal to prepare it to be read by the DAQ system. Equation 8.1 shows the mathematical relationship output voltage has to input charge, chamber gain, preamp gain, and electronics gain. Therefore, the chamber gain can be calculated according to equations 8.1 and 8.2.

$$V_{out} = Q_{in} G_{chamber} G_{preamp} G_{electronics}$$ Equation 8.1

$$Q_{out} = \frac{V_{out}}{G_{preamp} G_{electronics}} = Q_{in} G_{chamber}$$ Equation 8.2

The input charge is taken to be the charge in fC of 30 electrons, namely 4.8X10^{-3} fC. The output voltage is also the MPV for the MIP distribution. The gain for the preamp channel is 10.24

± 0.35 mV/fC and the electronics gain was measured to be 1.985 ± 0.135. Therefore, as seen in Figure 8.9, the effective [31] gain for pad 7 is 1.341 ± 0.259 x 10^3. This result is compared to previous results of GEM chambers that used 70:30 Ar:CO2 gas mixture.

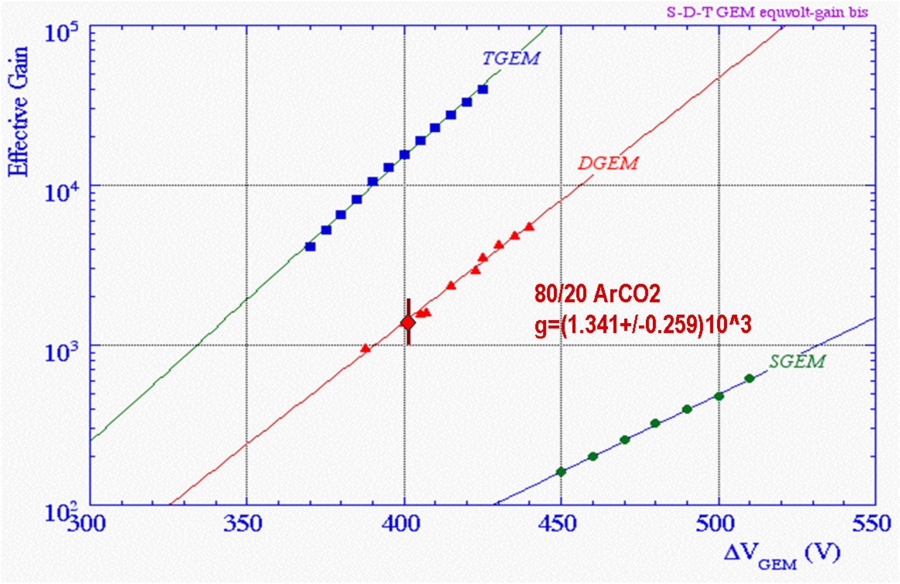

Figure 8.9 Effective Gain versus potential difference across each GEM foil comparing test beam results to previous measurements

8.6.3. Chamber Efficiency

Efficiency is determined from the MIP response histograms. The absolute efficiency is a measure of the chamber's ability to produce signal for each incoming charged particle. That is to say if every signal event in the MIP response distribution is accounted for as a proton that traversed the chamber then the absolute efficiency is 100%. There are two assumptions made for test beam experiments. The first is that protons in the pulse height region above MPV of the distribution always produce signals in the distribution. The second is that the normalization and pedestal subtraction procedure accurately determines the distribution due to possible missed protons in the low pulse height region below threshold.

The efficiency measurement comes from a graph calculated by iterating the integral range of the Landau function and dividing by the total area each time. Efficiency plots shown here are relative to pulse height in mV. Starting at 0 mV the area of the distribution is divided by the total area. The efficiency value for each mV value is then the area in the domain of the distribution starting at that particular mV value up to the end of the x-axis range. Therefore, at 0 fC efficiency is 100% and at 1000 mV the efficiency is 0%. Figure 8.10 through Figure 8.13 show the efficiency plots from source and test beam data taken at Fermilab.

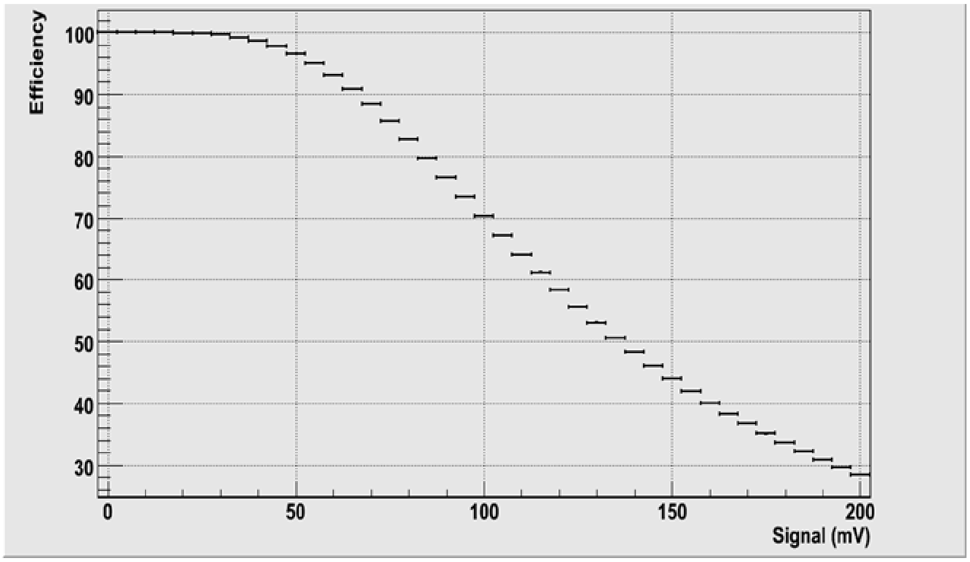

Figure 8.10 Efficiency measured from source data on pad 7

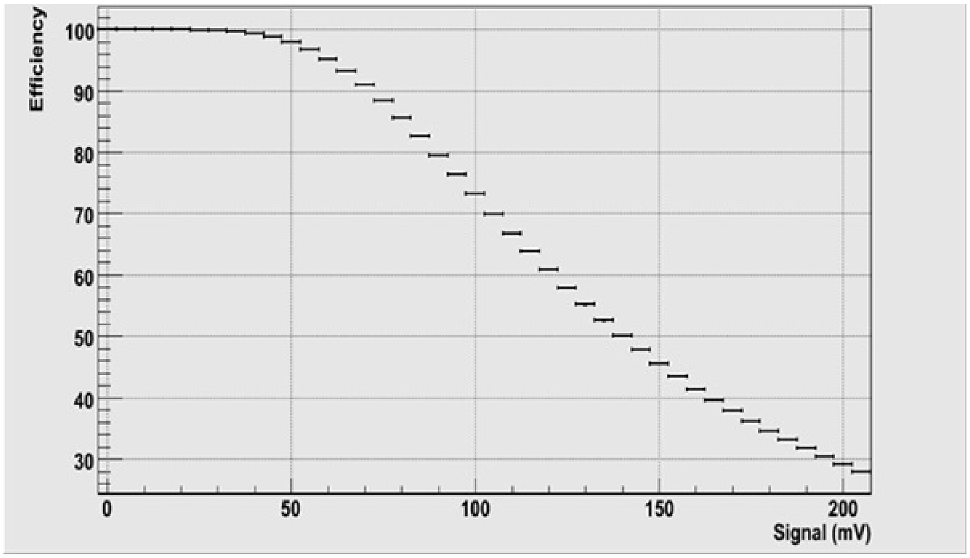

Figure 8.11 Efficiency measured from source data on pad 15.

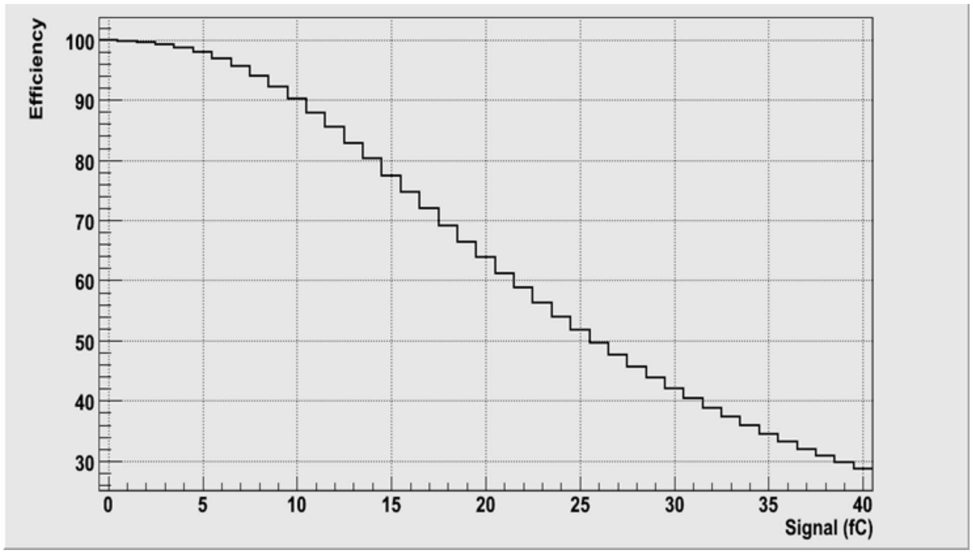

Figure 8.12 Efficiency measured from test beam data on pad 7.

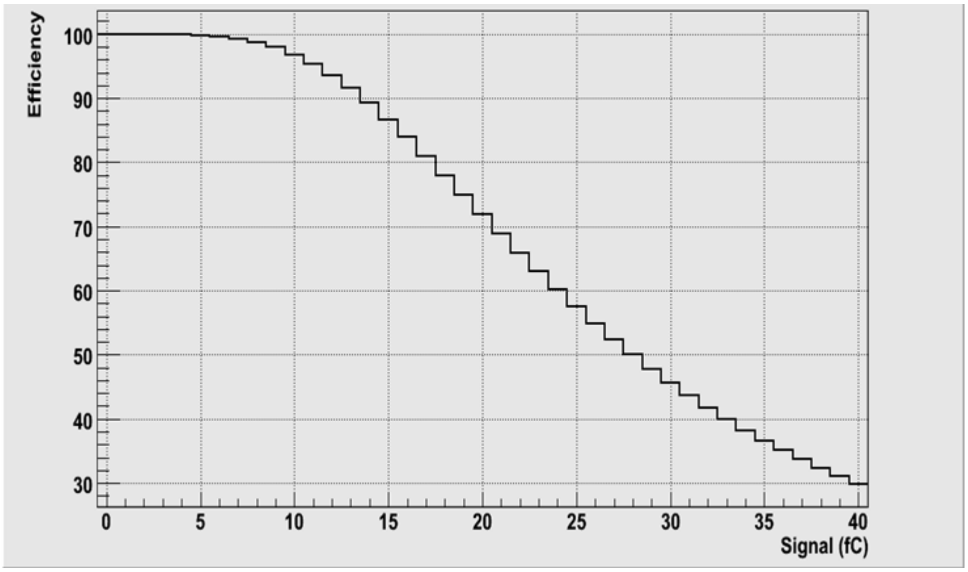

Figure 8.13 Efficiency measured from test beam data on pad 15.

In the MIP response histograms, inefficiency is represented by either a zero event or a low signal event is counted as pedestal. The normalization and subtraction procedure employed for this test beam analysis fit the signal histogram distribution with a Landau probability distribution function. This fit extents over the entire signal range of the ADC. The second assumption is based on the quality of this Landau fit. This fit is done after the pulse height distribution is normalized to pedestal distributions and pedestal is subtracted. Therefore the lower pulse height region accurately describes protons that have lower ionization and could have possibly been counted as inefficiency.

The major objective in the procedure developed to extract the absolute efficiency is the successful inference of signal events below noise threshold which was not recorded to the triggering scheme. It is assumed that some protons trigger the beam telescope but do not trigger the GEM chamber above threshold. Therefore, this procedure infers missed proton events due to high noise levels. Using the chamber as part of the beam telescope does not trigger protons near or below the pedestal threshold. Effectively, this procedure is able to extract efficiency even in the case the trigger is biased by the chamber signal.

Threshold levels to trigger were at an equivalence of 4fC. Therefore at threshold, the UTA double GEM chamber is 99.5 % efficient measuring 120 GeV protons while it is 99% efficient measuring the decay of Sr-90 radiation source.

8.7.Results

In conclusion, successful measurement of large double GEM chamber MIP response, pad gain, and absolute efficiency are attained through test beam experiments. In addition to these measurements, a procedure has been developed to subtract pedestal data from beam and source signals leaving a MIP response that also infers signal events below threshold. This novel procedure provides the ability to measure absolute efficiency even in a biased trigger system.

In conclusion, average MIP response is 6.45 fC giving a pad gain of $1.341 \pm 0.259X10^3$ matching previous results. Large GEM chambers have performed with an efficiency, on average, above 99% with a 4fC pedestal on all measured pads.

CHAPTER 9

CONCLUSIONS AND PROSPECTS

9.1.Summary of Results

Preamplifier cards used in initial GEM chamber studies were successfully tested and all available preamplifier cards 6, and 9 – 18 were certified. Graphs are made for each card and polarity. The positive polarity of all cards has an average of 10.3 ± 1.5 (stat) mV/fC and the negative polarity shows an average of 7.7 ± 0.9 (stat) mV/fC. On average the negative polarity is more consistent but the positive polarity shows higher gain values. In comparing the polarities, each uncertainty represents the accuracy of the average gain. Between cards there is a large fluctuation of gain in the positive output than in negative. Positive polarities are observed to have 25 % increases in gain from negative polarities. Although the uncertainty bars in negative appear large, there is about 20% less fluctuation compared to positive output.

KPiX calibrations provide the pedestal and gain values used to calculate collected charge from data. Pedestals fluctuate from channel to channel less than 1.8% from the mean while gains fluctuate just over 3.3% from the mean in normal gain mode. For double gain mode there is a 4.5% fluctuation of the pedestal and a 2.5% fluctuation of the gain. Although the gain for double gain mode is more consistent than normal gain mode this behavior is less typical. There are more non operational channels in double gain mode than in normal gain. Even still, a 3.3% fluctuation in gain is acceptable although a lower fluctuation is more desirable.

Pedestal values fluctuate between 20 to 130 ADC counts, more than a factor six variation. Gain values go from 5 to 20 ADC/fC, a factor 4 variation. Channel to channel variation of gain is a cause of concern because two adjacent pads with factor 4 variations of gain effect using KPiX as part of a digital detector that uses a single threshold.

Version 7 of KPiX provides the same basic information as version 4 and is also characterized in this study. The variation of pedestal and gain constants between channels is also investigated in version 7. This characterization describes the consistency and percentage acceptance of usable channels. Pedestal values fluctuate between 40 to 120 ADC counts, a factor 3 variation. Gain values go from 3.5 to 6.5 ADC/fC, a factor 2 variation. Recall that version 4 saw a pedestal variation of factor 6 and gain variation factor 4. Therefore KPiX version 7 has a factor 2 improvement in the channel to channel fluctuation of pedestal and gain calibration constants.

Gas flow within GEM chambers is the properties that determines when a chamber is ready to record data. Various chamber designs are investigated in this thesis. More in-depth measurements of the noise rate reveal a dependence on time after turning on the high voltage power supply for the chamber. The time for these measurements starts immediately after HV turn on. These noise tests reveal a warm up period for the complete electric system that is dependent on the high voltage power supply. After 30 minutes of turning the HV on normal operating noise levels are reached. This measurement does not provide the lowest noise level conditions but does provide a time to raise the system to its maximum noise levels. After 30 minutes the noise rates do not fluctuate. Therefore, prior to starting any measurement with this GEM chamber the HV must be on for 30 minutes.

The mean value of the data points before 90 minutes is the average noise rate above threshold. Since the mean value is calculated from multiple measurements of the same quantity the standard deviation is the main uncertainty of the noise rate. This means that smallest standard deviations indicate least sensitivity to the noise environment while largest standard deviations indicate most sensitivity.

When KPiX is used to take data with a radiation source the distribution is hidden in part by the pedestal distributions resulting from the trigger method. A new method is designed called the KPiX Signal Inference Method (KSIM) that infers the distribution shape based on Monte Carlo methods. The MPV of the inferred chamber response is 1.9 fC. Without this method the source data is hidden by the large pedestal contributions resulting from the effect of the Forced Trigger using CalStrobe. This method successfully infers the chamber response to radiation source even if it is hidden within the pedestal distribution.

The main measurements of gain and efficiency are performed and determined as a result of test beam experiments. Characterization test performed at Fermilab test beam facility provided the chamber response and efficiency measurements for large 30 cm x 30 cm Double GEM chambers. At 0 fC absolute efficiency is 100% and at 1000 mV the efficiency is 0%. The input charge is taken to be the charge in fC of 30 electrons, namely 0.004806 fC. The output voltage is also the MPV for the MIP distribution. The gain for the preamp channel is 10.24 ± 0.35 mV/fC and the electronics gain was measured to be 1.985 ± 0.135. Therefore, the effective gain for pad 7 and 15 is 1.341 ± 0.259X10^3. This result is compared to previous results of GEM chambers that used 70:30 Ar:CO2 gas mixture. Another result of the test beam analysis was the development of a pedestal subtraction method.

9.2.Prospects for the Future

9.2.1. GEM Technology in Medical Imaging

Some of the potential applications for GEM technology are for fast x-ray imaging, radiology, and national defense. One group has successfully used GEM chambers to take x-ray images like in Figure 9.1 (a) using the GEM chamber structure shown in Figure 9.1 (a) [58]. There is also potential to use GEM chambers as a replacement for image intensifiers in medical imaging. Currently UTA has started a collaboration with a group from the University of Texas South Western Medical Center to develop GEM technology for this purpose. Current image intensifiers are limited in their field of view. The optical penalty for a large field of view with a small sensor is that images become much dimmer and are inseparable from noise. This requires more efficient optical amplification.

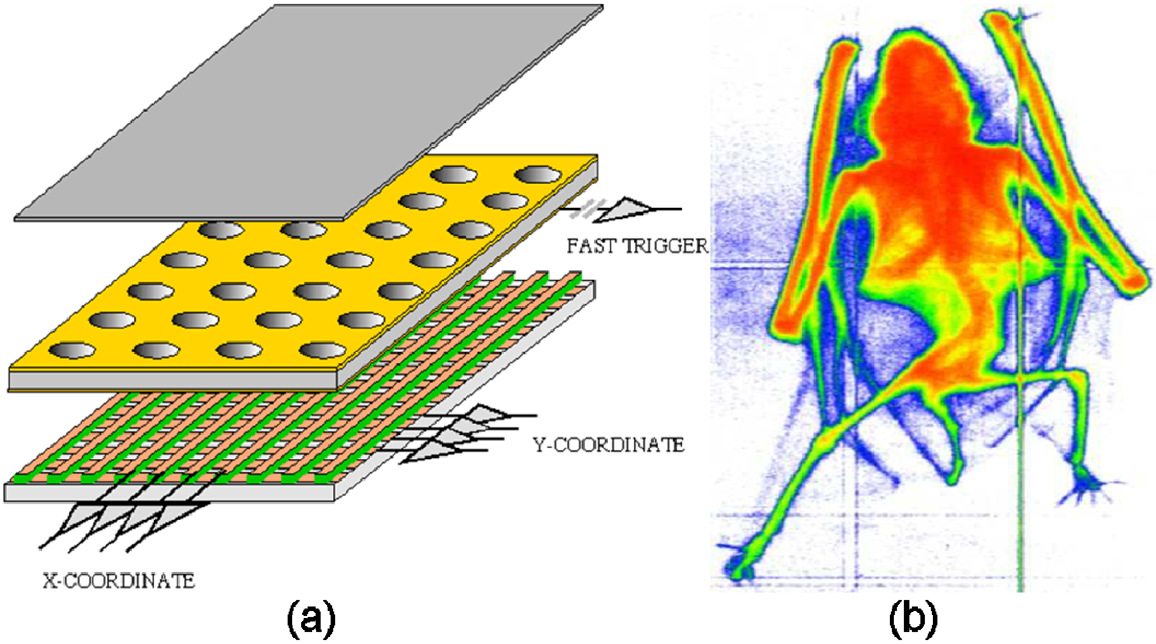

Figure 9.1 A GEM chamber structure (a) and x-ray image of a small bat (b) illustrating potential application of GEM technology.

9.2.2. Future Progress for GEM Technololgy in the ILC

Double GEM chambers will continue to be characterized and developed at UTA for use as a digital hadron calorimeter in the International Linear Collider. Current 30 x 30 cm^2 double GEM chambers using the KPiX version 7 readout will continue to be characterized using new Ru-106 and Fe-55 radiation sources, cosmic-ray muons and test beam at Fermilab. Chamber design has begun for a 1 x 0.3 m^2 area double GEM detector. Multiple chambers are also planned to be integrated into current CALICE test beam studies currently at Fermilab.

APPENDIX A

PREAMP GAIN MEASUREMENT PROCEDURE

1. Connect voltage divider into preamp (PA)
2. Connect output signal ribbon cable (flat gray) from output card (OC) into PA on top side making sure to secure ground connection via the alligator clip.
3. Connect power cable to black and red wires on bottom of PA. Black is ground, red is +5 volts.
4. Connect input signal and ground on top PA. The coated wire is for the signal and soldered wire is for the ground.
5. Turn on power to card using positive 5 volt power supply.
6. Using the oscilloscope to monitor the signal and noise (should be able to read at least 6 mV pulse heights).
7. Set pulse generator (PG) to -490 mV for Vlow and +490 for Vhigh. Use oscilloscope to verify PG output. For an unknown reason the oscilloscope shows this as 500 mV.
8. Connect PA input cable to $\overline{\text{OUTPUT}}$ on the PG.
9. Adjust the signal width on the PG to fit the pulse from within the gate of the discriminator. If testing positive signal connect the trigger output (PG) to discriminator. If testing the negative signal connect the OUTPUT (on PG) to discriminator.
10. Connect output from discriminator to strobe on ADC. This triggers the ADC to collect data.
11. Connect cables from appropriate channels on OC to appropriate channels on ADC.
12. Start the gemtest7 DAQ software on the heppc34 computer.
13. To set pedestal, connect discriminator output to strobe on ADC. Disconnect ADC input channels for this step.
14. Reconnect all channels from OC to ADC input.
15. Allow program to collect data for approximately 3 min or 30,000 iterations.
16. End program and repeat steps 11-15.

APPENDIX B

TABLES AND PROCEDURE FOR GAS RATE TESTS

Table B.1 Table used to record data

Time elapsed (min)	N1 (ch 1)	N2 (ch 2)	Rate (N/min)

Table B.2 Table to record results

Results	
Turn on time	
Maximum Rate	

Include step-by-step instruction of procedure in outline form.

1. turn off all powered electronics and disconnect cables
2. close flow meter input valve and disconnect intake and exhaust gas lines at the flow meter and bubbler, respectively.
3. remove chamber from shielding structure, turn chamber to anode side up and solder signal cable to back of KPiX board
4. cut tape that forms airtight seal
5. lift KPiX board to release Ar:CO_2 gas and to let in air, allow about 10 seconds for remaining gas to diffuse out
6. replace board and reseal with tape
7. place chamber back in the chamber enclosure cathode side up and connect HV leads
8. prior to connecting preamp turn on power for preamp and check noise with scope without input to preamp

9. connect signal cable from chamber to preamp input
10. connect complete cable assembly of negative preamp output to oscilloscope
11. connect gas lines inside chamber enclosure but do not connect gas lines to flow meter and bubbler
12. place source and setup all shielding structures to ensure proper grounding of all systems to minimize noise level
13. turn on HV to GEM chamber to -2100 V
14. connect negative preamp output cable to oscilloscope and using horizontal cursors identify maximum noise level and record on data sheet
15. connect negative preamp output to discriminator and set threshold to 75% higher than maximum noise level
16. connect a discriminator output to scaler channel 1
17. connect another discriminator output to scaler channel 2
18. set gas flow rate on gas flow meter to desired flow rate and record on data sheet
19. connect gas exhaust line to bubbler
20. connect gas intake line to flow meter, reset scalers and start timer
21. occasionally check that bubbles are present in bubbler and gas flow rate in flow meter is maintained
22. after one time interval, switch off N1 and reset scaler ch 2, scaler ch 2 is now counting for next time interval
23. record scaler ch 1 value then switch N1 back to ON position
24. calculate rate as scaler value divided by time interval to get units of N/min
25. after next time interval, switch off N2 and reset scaler ch 1 simultaneously. Scaler ch 1 is now counting for next time interval.
26. record scaler ch 2 value and then switch N2 back to ON position
27. calculate rate as in step 21
28. repeat steps 22 through 27 until 4 “maximum level” points are acquired

APPENDIX C

SIGNAL INFERENCE METHOD PROCEDURE AND CODE

1) Define the Integration Time
    a) This is the amount of time that KPiX electronics integrates the GEM chamber output pulses
2) Define a Gaussian function ,“Pulse”, to represent pulse signal output of double GEM chamber
    a) Parameters: [120, 350+75, 25], amplitude, mean, and sigma respectively
    b) Range: (0,2*mean)
    c) Units: nano-seconds (ns), time
    d) Note: Pulse is output of double GEM chamber and input to KPiX electronics
3) Define a Landau function, Landau Probability Distribution (LPD) to represent charge (pulse height) distribution of Sr-90 radioactive source
    a) Parameters: [200,2.2,0.6], amplitude, most probable value (MPV), and sigma
        i) parameters manually optimized to match final simulated pulse height distribution to data histogram
    b) Range: (-10,100)
    c) Units: femto-Coulombs (fC), charge
    d) Note: Naturally the GEM chamber outputs to the electronics a distribution of pulse heights representing the MIP response that follows a Landau Probability Distribution (LPD). Therefore, this Landau function is defined in such a way that represents previous measurements of GEM MIP responses.
4) Define a Constant function
    a) Parameters: constant
    b) Range: (mean-10*sigma, mean+10*sigma) [mean and sigma from Step 1 Gaussian Parameters]
    c) Units: ns
    d) Note: This represents the starting point of electronic pulse integration period.
5) Integrate Gaussian function of Step 1 (Pulse)
    a) Range: complete range
6) Define another Gaussian (“Pedestal”) to represent calibration pedestal.

    a) Initial Parameters: [999430, 1.3, 0.8]
        i) Manually look at particular channel’s real data Gaussian fit parameters
        ii) the code that fits real data does not store the fit parameters in the root file?
    b) Range: (-100, 100)
    c) Units: fC
7) Get Data histogram from data Root file
8) Fit Data histogram using Pedestal
    a) Range: entire x-axis range
9) Start Loop to pick random numbers
    a) Iteration frequency: 38,000
10) Pull a random number from Pulse
11) Fill a histogram with random Pulse values
    a) Range: (Pulse minimum, Pulse Maximum)
    b) Number of bins : max – min
    c) Units : ns
12) Pull a random number from LPD
13) Fill a histogram with random LPD values
    a) Range: (-100.25,100.25), same as real data
    b) Number of bins: 401
    c) Units: fC
14) Pull a random number form Constant distribution of Step 3
15) Fill a histogram with random Constant values
    a) Range: (0,1000),
    b) Number of bins: 1000
    c) Units: ns
16) Integrate Pulse in limited range (Partial Pulse Area)
    a) Range: (Constant random number, Constant random number + integration Time)

    b) Range: IF the Constant random number falls after the maximum range minus the Integration Time THEN range is (Constant random number, maximum Pulse range)

17) Fill a histogram with Partial Pulse Areas
    a) Range: (0,10000)
    b) Number of bins: 10000
18) Divide the Partial Pulse Integration by the Total Pulse Integration, Ratio
19) Fill a histogram with Ratios
    a) Range: (-0.005, 1.005)
    b) Number of bins: 101
20) Multiply Ratio with random LPD value
21) Fill a histogram with Ratio*LPDvalue, Fractional Charge
    a) Range: (-10.005,100.005)
    b) Number of bins: 1011
    c) Note: This is the fractional of the charge that KPiX will read of the pulse given the randomness of the timing between the integration and arrival of pulse
22) Pull a random number from Pedestal
23) Fill a histogram with random Pedestal value
    a) Range: (-10.005, 100.005)
    b) Number of bins: 1011
24) Add random Pedestal value to Fractional Charge
25) Fill a histogram with the result of Step 24
    a) Range: (-100.25,100.25), same as real data
    b) Number of bins: 401
26) End first Loop
27) Start another Loop
    a) Iteration frequency: 200,000
28) Pull a random number from Pedestal
29) Fill a histogram with random Pedestal value

   a) Range: (-10.005, 100.005)

   b) Number of bins: 1011

30) End second Loop

31) Manipulate histogram plots as desired.

Code in C++ using ROOT Libraries

```
void sim()
{
  gROOT->Reset();
  int width = 5;
  double intTime = 333;
  double gaus1amp = 120; /* ns */
  double gaus1sig = 25;
  double gaus1mean = 333 + 5*gaus1sig;
  double gaus1xlow = 0; /* ns */
  double gaus1xhigh = 2*gaus1mean; /* ns */
  double flat1low = 0;
  double flat1high = gaus1mean + 5*gaus1sig;
  double land1xlow = -10;
  double land1xhigh = 100;
  double land1amp = 200; /* fC */
  double land1mean = 2.2;
  double land1sig = 0.6;
  double gaus2amp = 100000;
  double gaus2mean = 1.3;
  double gaus2sig = 0.8;
  double gaus2xlow = gaus2mean-5*gaus2sig;
  double gaus2xhigh = gaus2mean + 5*gaus2sig;     /* units of fC */
  double randQ = 0;
  double randPulse = 0;
  double IntStart = 0;
  double fracArea = 0;
  double pedCharge = 0;
  double pedestal = 0;
  double Ptot,Pless,Pzero,Pall;
  double par[8], ELGpar[8];
  double GLpar[6];
  double signalFactor = 0.38;
  double pedestalFactor = 2000000;

  // Step 1 Define a gaus function and set parameters
  gaus1 = new TF1("gaus1","gaus(0)",gaus1xlow,gaus1xhigh);
  gaus1->SetParameters(gaus1amp,gaus1mean,gaus1sig);

  // Step 2 Define a gaus function and set parameters
  land1 = new TF1("land1","landau(0)",land1xlow,land1xhigh);
  land1->SetParameters(land1amp,land1mean,land1sig);

  // Step 3 Define a flat function and set parameters
  flat1 = new TF1("flat1","[0]",flat1low,flat1high);
  flat1->SetParameter(0,0.5);
  flat1->SetLineColor(6);
```

```
  flat1->SetLineWidth(4);

  // Step 4 Integrate entire range of gaus1
  Double_t Atot = gaus1->Integral(gaus1xlow,gaus1xhigh);
  cout<<"\n\tTotal Integral of Gaussian Function: " <<Atot<<endl;

  // Step 5 Define a gaus pedestal function and set parameters
  gaus2 = new TF1("gaus2","gaus(0)",gaus2xlow,gaus2xhigh);
  gaus2->SetParameters(gaus2amp,gaus2mean,gaus2sig);
  cCheckPed = new TCanvas("cCheckPed","Check Ped Fit with gaus2",1);
  cCheckPed->cd();
   TFile *inRoot = new TFile("combined.root");
   TH1F *real = (TH1F*)inRoot->Get("c_0x190_31");
   TH1F *real1 = (TH1F*)inRoot->Get("c_0x190_31");
 cCheckPed->SetLogy();
   real->SetMarkerStyle(21);
   real->SetMarkerSize(0.5);
   real1->SetMarkerStyle(21);
   real1->SetMarkerSize(0.5);
   c_0x190_31->SetMarkerStyle(21);
   c_0x190_31->SetMarkerSize(0.5);
   real->Fit("gaus2","q");
   real->Draw();
  cCheckPed->Update();
  TH1F* hLand1  = new TH1F("hLand1","Landau Check",401,-100.25,100.25);
  TH1F* hPulse1 = new TH1F("hPulse1","Pulse Check",gaus1xhigh-
gaus1xlow,gaus1xlow,gaus1xhigh);
  TH1F* hFlatCheck  = new TH1F("hFlatCheck","Flat Check",1000,0,1000);
  TH1F* hFracArea  = new TH1F("hFracArea","a",10000,0,10000);
  TH1F* hAreaRatio  = new TH1F("hAreaRatio","a/A",101,-0.005,1.005);
  TH1F* hFracCharge1  = new TH1F("hFracCharge1","a/A*Q",1011,-10.005,100.005);
  TH1F* hFracCharge2  = new TH1F("hFracCharge2","a/A*Q",1011,-10.005,100.005);
  TH1F* hPedCharge  = new TH1F("hPedCharge","Pedestal Check",1011,-10.005,100.005);
  TH1F* hPedShiftCharge1 = new TH1F("hPedShiftCharge1","p + a/A*Q",1011,-
10.005,100.005);
  TH1F* hPedShiftCharge2  = new TH1F("hPedShiftCharge2","p + a/A*Q with Ped",1011,-
10.005,100.005);
  TH1F* hFinalCharge1  = new TH1F("hFinalCharge1","PedSub(mv) p + a/A*Q",401,-
100.25,100.25);
  TH1F* hFinalCharge2  = new TH1F("hFinalCharge2","PedSub(mv) p + a/A*Q with Ped",401,-
100.25,100.25);
  TH1F* hPedestal  = new TH1F("hPedestal","p",1011,-10.005,100.005);
  TH1F* hMcRealRatio1 = new TH1F("hMcRealRatio1","mc/real per bin",401,-100.25,100.25);
  TH1F* hMcRealRatio2 = new TH1F("hMcRealRatio2","mc/real per bin",401,-100.25,100.25);
  TH1F* hMCsignal1 = new TH1F("hMCsignal1","MC signal without pedestal shift",401,-
100.25,100.25);
  TH1F* hMCsignal2 = new TH1F("hMCsignal2","MC signal with pedestal shift",401,-
100.25,100.25);

  // Set Sumw2
  hMCsignal1->Sumw2();
  hMCsignal2->Sumw2();
  TH1F* htest1 = new TH1F("htest1","kolmo test1",401,-100.25,100.25);
  TH1F* htest2 = new TH1F("htest2","kolmo test2",401,-100.25,100.25);
  htest1->Sumw2();
  htest2->Sumw2();
```

```
  htest1->FillRandom("land1",20000);
  htest2->FillRandom("land1",999);

  // Call Sumw2
  hMcRealRatio1->Sumw2();
  hMcRealRatio2->Sumw2();
  real->Sumw2();

  // Visual Edits
  hFinalCharge2->SetLineColor(4);
  hLand1->SetLineColor(2);
  hLand1->SetStats(1);

  // Step 6 Start Loop
  //for (int i = 0; i < 38000; i++) {
  for (int i = 0; i < 100000; i++) {
    randPulse = gaus1->GetRandom();
    hPulse1->Fill(randPulse);
    randQ = land1->GetRandom();        /* Step 7 -Get a unique random number (using
GetRandom Root Class
                          containing random number generators) from the Landau function(Q)*/
    hLand1->Fill(randQ);        /* Step 8 - Fill a 1D histogram with random number from landau
function */
    // Step 7 - see above
    IntStart = flat1->GetRandom();      /* Step 9 - randomly get a number from flat distribution */
    hFlatCheck->Fill(IntStart);      /* Step 10 - fill a histogram with flat random numbers */
    /* Step 11 - Integrate gaus1 from IntStart to max range */
    if (IntStart >= (flat1high - intTime)) fracArea = gaus1->Integral(IntStart,flat1high);
    if (IntStart < (flat1high - intTime)) fracArea = gaus1->Integral(IntStart,IntStart + intTime);
    hFracArea->Fill(fracArea);      /* Step 12 - fill a hist with fracArea */
    hAreaRatio->Fill(fracArea/Atot);      /* Step 13 - fill a hist with fracArea/Atot */
    hFracCharge1->Fill(fracArea*randQ/Atot);      /* Step 14 - fill a hist with (fracArea/Atot)*randQ
*/
    hFracCharge2->Fill(fracArea*randQ/Atot);      /* Step 14 - fill a hist with (fracArea/Atot)*randQ
*/
    hMCsignal2->Fill(fracArea*randQ/Atot);      /* Step 14 - fill a hist with (fracArea/Atot)*randQ */
    pedCharge = gaus2->GetRandom();
    hPedCharge->Fill(pedCharge);
    hPedShiftCharge1->Fill(pedCharge + (fracArea*randQ/Atot));
    hPedShiftCharge2->Fill(pedCharge + (fracArea*randQ/Atot));
    hMCsignal1->Fill(pedCharge + (fracArea*randQ/Atot));
    //hFinalCharge1->Fill((pedCharge + (fracArea*randQ/Atot)) - gaus2mean);
    //hFinalCharge2->Fill((pedCharge + (fracArea*randQ/Atot)) - gaus2mean);
    hFinalCharge1->Fill((pedCharge + (fracArea*randQ/Atot)));
    hFinalCharge2->Fill((pedCharge + (fracArea*randQ/Atot)));
  }

  ctemp = new TCanvas("ctemp","FracCharge before and after Ped fill",1);
  ctemp->cd();
  ctemp->SetLogy();
  hPedShiftCharge1->SetLineColor(9);
  hFinalCharge1->SetLineColor(2);
  hFracCharge1->Draw();
  hPedShiftCharge1->Draw("same");
  hFinalCharge1->Draw("hist same");
  ctemp->Update();
```

```
  for (int i = 0; i < 100000; i++) {
    pedestal = gaus2->GetRandom();
    hPedestal->Fill(pedestal);
    //hPedShiftCharge2->Fill(pedestal);
    //hFinalCharge2->Fill(pedestal - gaus2mean);
    //hFinalCharge2->Fill(pedestal);
    //hFinalCharge1->Fill(pedestal);
  }

  hPedShiftCharge2->Scale(signalFactor);
  hPedestal->Scale(pedestalFactor);
  hFracCharge2->Scale(signalFactor);
  hMCsignal1->Scale(signalFactor);
  hMCsignal2->Scale(signalFactor);

  //hMCsignal1->Add(hPedShiftCharge2,hPedestal,signalFactor,pedestalFactor);
  hMCsignal1->Add(hPedestal,1);
  //hMCsignal2->Add(hFracCharge2,hPedestal,signalFactor,pedestalFactor);
  hMCsignal2->Add(hPedestal,1);

  Ptot = (hAreaRatio->Integral(1,100));
  Pzero = (hAreaRatio->Integral(1,1))/1000;
  Pless = (hAreaRatio->Integral(2,100))/1000;
  Pall = (hAreaRatio->Integral(100,100))/1000;
  cout<<"\n\ta/A Hist Total Area: " <<Ptot<<endl;
  cout<<"\n\ta/A Hist Percentage of zeros: " <<Pzero<<endl;
  cout<<"\n\ta/A Hist Percentage less than 1: " <<Pless<<endl;
  cout<<"\n\ta/A Hist Percentage approximately 1: " <<Pall<<endl;
  TF1 *f2 = new TF1("f2","gaus");
  f2->SetLineColor(2);
  f2->SetLineWidth(.6);
  hFinalCharge1->Fit("f2","q");
cout<<"\nFLAG"<<endl;
  TF1 *fexpo = new TF1("fexpo","expo",gaus2mean+3*gaus2sig,10);
  TF1 *fland = new TF1("fland","landau",-5,100);
  TF1 *fgaus = new TF1("fgaus","gaus",-5,8);
  TF1 *f1 = new TF1("f1","expo(0)+landau(2)",-5,100);
  TF1 *f3 = new TF1("f3","expo(0)+landau(2)+gaus(5)",gaus2mean-3*gaus2sig,100);
  TF1 *f2 = new TF1("f2","gaus(0) + landau(3)",gaus2mean-5*gaus2sig,100);
  f1->SetLineColor(2);
cout<<"\nFLAG"<<endl;
  hFinalCharge1->Fit("fgaus","qR");
  fgaus->GetParameters(&GLpar[0]);
  hFinalCharge1->Fit("fland","qR+");
  fland->GetParameters(&GLpar[3]);
cout<<"\nFLAG"<<endl;
  f2->SetParameters(GLpar);
  hFinalCharge1->Fit("f2","R+");
  cout<<"\n\n\tThe above fit parameters are from expo + landau + gaus"<<endl<<endl;
  cout<<endl;
  cout<<"lpar0 "<<GLpar[3]<<endl;
  cout<<"lpar1 "<<GLpar[4]<<endl;
  cout<<"lpar2 "<<GLpar[5]<<endl;
  cout<<endl;
  TF1 *landfinal = new TF1("landfinal","landau");
```

```
  landfinal->SetLineWidth(.6);
  c3 = new TCanvas("c3","landau check",1);
  c3->SetFillColor(18);
  c3->cd();
  c3->SetLogy();
   hLand1->Fit("landfinal","q");
   cout<<"\n\nFinal Landau MPV: "<<landfinal->GetParameter(1)<<endl;
   cout<<"\n\nFinal        Landau        Red-Chi2:        "<<((landfinal->GetChisquare())/(landfinal-
>GetNDF()))<<endl<<endl;
  hLand1->Draw();
  c3->Update();
  c32 = new TCanvas("c32","real and mc1(ped shifted)",1);
  c32->SetFillColor(18);
  c32->cd();
  c32->SetLogy();
   real1->SetMarkerStyle(21);
   real1->SetMarkerSize(0.6);
   real1->Draw("e1");
  hMCsignal1->Draw("same");
  c32->Update();
  c12 = new TCanvas("c12","real and mc2(NOT ped shifted)",1);
  c12->SetFillColor(18);
  c12->cd();
  c12->SetLogy();
  real1->Draw("e1");
  hMCsignal2->Draw("same");
  c12->Update();
  hMcRealRatio1->Divide(hMCsignal1,real,1,1);
  cRatio1 = new TCanvas("cRatio1","mc(ped) / real",1);
  cRatio1->cd();
  cRatio1->SetFillColor(18);
  hMcRealRatio1->Draw();
  cRatio1->Update();
  hMcRealRatio2->Divide(hMCsignal2,real,1,1);
  cRatio2 = new TCanvas("cRatio2","mc(no ped) / real",1);
  cRatio2->cd();
  cRatio2->SetFillColor(18);
  hMcRealRatio2->Draw();
  cRatio2->Update();
  TFile myfile("sim_kpix_5sig.root","RECREATE");
//Write objects
  hMcRealRatio1->Write();
  hMcRealRatio2->Write();
  hLand1->Write();
  hPulse1->Write();
  hFlatCheck->Write();
  hFracArea->Write();
  hAreaRatio->Write();
  hPedCharge->Write();
  hFracCharge1->Write();
  hFracCharge2->Write();
  hFinalCharge1->Write();
  hFinalCharge2->Write();
  hPedShiftCharge1->Write();
  hPedShiftCharge2->Write();
  hPedestal->Write();
```

```
  hMCsignal1->Write();
  hMCsignal2->Write();

  //inRoot.Close();
  myfile.Close();
  gBenchmark->Show("fillrandom");

}
```

APPENDIX D

PEDESTAL SUBRACTION PROCEDURE

1. Fit pedestal histogram with a Gaussian function, fgausA
2. Fit data with Gaussian plus Landau function, fgausLandA, fixing mean and sigma for Gaussain part to fgausA and allow all other parameters to float
3. Define a new Gaussian function, fgausB, with the amplitude taken fgausLandA but mean and sigma taken from fgausA
4. Subtract fgausB from data histogram at each x-axis value of the bin center

REFERENCES

1. Sauli, F., *GEM: A new concept for electron amplification in gas detectors.* Nuclear Instruments and Methods in Physics Research Section A: Accelerators, Spectrometers, Detectors and Associated Equipment, 1997. **386**(2-3): p. 531-534.
2. Heusch, C.A., *ELECTRON-ELECTRON COLLISIONS AT THE INTERNATIONAL LINEAR COLLIDER.* International Journal of Modern Physics A: Particles & Fields; Gravitation; Cosmology; Nuclear Physics, 2003. **18**(16): p. 2733.
3. Gunion, J.F., *UNIQUE PHYSICS PROBES USING e-e-, e-Î³ and Î³Î³ COLLIDERS.* International Journal of Modern Physics A: Particles & Fields; Gravitation; Cosmology; Nuclear Physics, 2003. **18**(16): p. 2739.
4. *Welcome to CALICE*. CALICE Web 2009 [cited 2009 16 Apr 2009]; Available from: https://twiki.cern.ch/twiki/bin/view/CALICE/CaliceCollaboration.
5. J-C Brient, P.D., E.Garutti, I.Laktineh, R.Poeschl, J.Repond, F.Sefkow, T.Takeshita, D.Ward, J.Yu, *CALICE Report to the Calorimeter R&D Review Panel*. 2007. p. 77 pages.
6. Kaushik, V., *Performance of novel digital hadron calorimeter using gas electron multiplier (GEM) and the energy flow algorithm development*, in *Physics*. 2004, The University of Texas at Arlington: Arlington, TX. unpublished.
7. Xia, L. *Development of a Particle Flow Algorithm at Argonne*. in *CALORIMETRY IN HIGH ENERGY PHYSICS: XII International Conference*. 2006. Chicago, Illinois (USA): AIP.
8. Repond, J., *Calorimetry at the International Linear Collider.* Nuclear Instruments and Methods in Physics Research Section A: Accelerators, Spectrometers, Detectors and Associated Equipment, 2007. **572**(1): p. 211-214.
9. University, S. *SLAC National Accelerator Laboratory*. Available from: http://www.slac.stanford.edu/.
10. Managed by Fermi Research Alliance, L. *Fermilab*. Available from: http://www.fnal.gov/.
11. Glashow, S.L., *Partial-symmetries of weak interactions.* Nuclear Physics, 1961. **22**(4): p. 579-588.
12. Salam, A. and J.C. Ward, *Electromagnetic and weak interactions.* Physics Letters, 1964. **13**(2): p. 168-171.
13. Weinberg, S., *A Model of Leptons.* Physical Review Letters, 1967. **19**(21): p. 1264.
14. Georgi, H. and S.L. Glashow, *Unity of All Elementary-Particle Forces.* Physical Review Letters, 1974. **32**(8): p. 438.
15. Ashok Das, T.F., *Introduction to Nuclear and Particle Physics*. 1994, New York: John Wiley & Sons, Inc.
16. Griffiths, D., *Introduction to Elementary Particles*. 1987, New York: John Wiley & Sons, Inc.
17. Group, L.E.W. *w09_show_pull_18*. [eps, jpg, pdf] 2009 13-Mar-2009 15:23; Available from: http://lost-contact.mit.edu/afs/net/project/afs32/cern.ch/l3/lepewwg/plots/winter2009/.
18. Martin, B.R., *Nuclear and Particle Physics*. 2006, England: John Wiley & Sons, Ltd.
19. Zeller, G.P., et al., *Precise Determination of Electroweak Parameters in Neutrino-Nucleon Scattering.* Physical Review Letters, 2002. **88**(9): p. 091802.
20. Heidenreich, K. *Silicon Detector Design Study*. 2006; Available from: http://silicondetector.org/display/SiD/home.
21. University, C.N. *Home*. 2009; Available from: http://www.changwon.ac.kr/english/.
22. Institute, K.A.E.R. *Home*. 2002; Available from: http://www.kaeri.re.kr/engnew/.
23. G. Drake, J.R., D. Underwood, A.B. Wicklund, L. Xia, *A digital hadron calorimeter with resistive plate chambers for the linear collider.* International Journal of Modern Physics A (IJMPA), 2005. **20** (16): p. 3830 - 3833.

24. Repond, J., *A digital hadron calorimeter with Resistive Plate Chambers.* Nuclear Instruments and Methods in Physics Research Section A: Accelerators, Spectrometers, Detectors and Associated Equipment, 2004. **533**(1-2): p. 126-129.
25. Repond, J., *A digital hadron calorimeter for the Linear Collider.* Nuclear Instruments and Methods in Physics Research Section A: Accelerators, Spectrometers, Detectors and Associated Equipment, 2004. **518**(1-2): p. 54-58.
26. J. E. Brau, R.E.F., D. Strom, M. Breidenbach, D. Freytag, N. Graf, G. Haller, R. Herbst, J. Jaros, T. Nelsen, V. Radeka, B. Holbook, R. Lander, M. Tripathi and Y. Karyotakis, *An electromagnetic calorimeter for the silicon detector concept* Pramana, 2007. **69**(6): p. 1025-1030.
27. R. Frey, D.M.S.O.U., M. Breidenbach, D. Freytag, G. Haller, M. Huffer, J.J. Russell (SLAC) *A silicon / tungsten electromagnetic calorimeter with integrated electronics.* Aug 2002: p. Pages: 5.
28. Strom, D., et al., *Fine Grained Silicon-Tungsten Calorimetry for a Linear Collider Detector.* Nuclear Science, IEEE Transactions on Aug. 2005 **52** (4): p. 868 - 873
29. Brau, J.E., et al., *Silicon detectors at the ILC.* Nuclear Instruments and Methods in Physics Research Section A: Accelerators, Spectrometers, Detectors and Associated Equipment, 2007. **579**(2): p. 567-571.
30. Ramberg, E. *Meson Test Beam Facility*. 2001; Available from: http://www-ppd.fnal.gov/mtbf-w/.
31. GROUP, G.D.D. *WELCOME TO THE GAS DETECTORS DEVELOPMENT GROUP INVENTORS OF THE GAS ELECTRON MULTIPLIER (GEM)*. 2003; Available from: http://gdd.web.cern.ch/GDD/.
32. CERN. *Welcome*. 2008; Available from: http://public.web.cern.ch/public/.
33. Heidenreich, K. *Silicon Detector Letter of Intent and Supporting Materials*. 2006; Available from: http://silicondetector.org/display/SiD/LOI.
34. White, D.A. *HCal_Summary_SiD_Workshop_Oct_2006_v3*. [pdf, ppt] 2006 09 October 2007 21:27; Available from: http://ilcagenda.linearcollider.org/materialDisplay.py?contribId=22&sessionId=7&materialId=slides&confId=1199.
35. Shekhtman, L., *Micro-pattern gaseous detectors.* Nuclear Instruments and Methods in Physics Research Section A: Accelerators, Spectrometers, Detectors and Associated Equipment, 2002. **494**(1-3): p. 128-141.
36. Sauli, F., *Development and applications of gas electron multiplier detectors.* Nuclear Instruments and Methods in Physics Research Section A: Accelerators, Spectrometers, Detectors and Associated Equipment, 2003. **505**(1-2): p. 195-198.
37. Bachmann, S., et al., *Discharge studies and prevention in the gas electron multiplier (GEM).* Nuclear Instruments and Methods in Physics Research Section A: Accelerators, Spectrometers, Detectors and Associated Equipment, 2002. **479**(2-3): p. 294-308.
38. Buzulutskov, A., *Physics of multi-GEM structures.* Nuclear Instruments and Methods in Physics Research Section A: Accelerators, Spectrometers, Detectors and Associated Equipment, 2002. **494**(1-3): p. 148-155.
39. Berger, M.J., Coursey, J.S., Zucker, M.A., and Chang, J. *ESTAR, PSTAR, and ASTAR: Computer Programs for Calculating Stopping-Power and Range Tables for Electrons, Protons, and Helium Ions*. [Online] 2005 2009, May 4; Stopping Powers and Ranges for Electrons]. Available from: http://physics.nist.gov/PhysRefData/Star/Text/contents.html.
40. Jensen, E.N. and L.J. Laslett, *Shape of the Beta-Spectra of Sr90 and Y90.* Physical Review, 1949. **75**(12): p. 1949.
41. Amsler, C., Physics Letters, 2008. **B**(667).
42. Zimmerman, T., *A high speed, low noise ASIC preamplifier for silicon strip detectors.* Nuclear Science, IEEE Transactions on, 1990. **37**(2): p. 439-443.
43. Büttner, C., et al., *Progress with the gas electron multiplier.* Nuclear Instruments and Methods in Physics Research Section A: Accelerators, Spectrometers, Detectors and Associated Equipment, 1998. **409**(1-3): p. 79-83.
44. Behnke, M. *Equipment Logistics Services: AD811 Octal ADC*. 2006; Available from: http://www-css.fnal.gov/els/prep/catalog/hardware_info/egg_ortec/ad811.html.

45. *DAQ-2208 Datasheet*. [Online] 2009 Feb. 21, 2008; Available from: http://www.adlinktech.com/PD/marketing/Datasheet/DAQ-2208/DAQ-2208_Datasheet_5.pdf.
46. Team, T.R. *ROOT: A Data Analysis Framework*. 1995; Available from: http://root.cern.ch/drupal/.
47. Benlloch, J., et al., *Further developments and beam tests of the gas electron multiplier (GEM)*. Nuclear Instruments and Methods in Physics Research Section A: Accelerators, Spectrometers, Detectors and Associated Equipment, 1998. **419**(2-3): p. 410-417.
48. *Description of Meson Test Beam Facility and its Capabilities*. Available from: http://www-ppd.fnal.gov/mtbf-w/description.doc.
49. Laboratory, F.N.A. *The D0 Experiment, Fermilab*. Available from: http://www-d0.fnal.gov/.
50. Laboratory, F.N.A. *The Collider Detector at Fermilab*. Available from: http://www-cdf.fnal.gov/.
51. Laboratory, F.N.A. *The MINOS Experiment and NuMI Beamline*. Available from: http://www-numi.fnal.gov/.
52. Laboratory, F.N.A. *BOONE Booster Neutrino Experiment*. Available from: http://www-boone.fnal.gov/.
53. R. Rubinstein, e., *Fermilab research program 2007: Workbook*. 2007. p. Size: 257 pages.
54. Evanger, B.M. and B.W. Worthel, *Concepts Rookie Book*, in *Training Docs*. 2004, Fermi National Accelerator Laboratory.
55. Kim, S., *GemView and Plotter Menu*, in *UTA-HEP/LC-0014*. 2006, University of Texas at Arlington: Arlington, TX.
56. Soomin, K., *GemView, The UTA GEM DAQ Program*, in *UTA-HEP/LC-0015*. 2006, University of Texas at Arlington: Arlington, TX.
57. Brice, S., et al., *Accelerator/Experiment Operations - FY 2007*. 2007. p. Size: 25 pages.
58. Bachmann, S., et al., *High rate X-ray imaging using multi-GEM detectors with a novel readout design.* Nuclear Instruments and Methods in Physics Research Section A: Accelerators, Spectrometers, Detectors and Associated Equipment, 2002. **478**(1-2): p. 104-108.

BIOGRAPHICAL INFORMATION

Jacob Smith is the proud son of Russell and Janet Smith. He was born in Austin, TX and is an older brother to Taryn and Jeremy Smith. In a family of five, Jacob has always received support, encouragement, and motivation from his family to seek excellence and pursue success in all areas of life. Throughout his career as a Master student Jacob has also received much encouragement and support from close friends and family in his local church.

Jacob's interests in physics began growing before college while attending Lawrence. D. Bell High School. Initially, this interest led Jacob to start at UTA as an electrical engineering major. The switch to physics came during his sophomore year and later in his senior year Jacob was approached by Dr. Jaehoon Yu to join research with the GEM team. After graduating with a Bachelor of Science in Physics from UTA, Jacob continued studies in pursuit of a Master of Science degree in Physics with the GEM project.

Currently, Jacob is finalizing plans to continue research in High Energy Physics in pursuit of a Doctor of Philosophy. Specifically he is interested in experimental HEP related to detector development of future particle accelerators, understanding the Standard Model, top quark physics, QCD physics and exploring supersymmetry.